AD-A084 435 AEROSPACE CORP EL SEGUNDO CA AEROPHYSICS LAB F/G 20/4

NUMERICAL SOLUTIONS FOR LAMINAR BOUNDARY LAYER BEHIND BLAST WAV--ETC(U)

MAY 80 S W LIU, H MIRELS F04701-79-C-0080

UNCLASSIFIED TR-0080(5940-02)-2 SD-TR-80-23 NL

1 of 2

AD A084435

LEVEL IV

REPORT SD-TR-80-23

AD A084435

Numerical Solutions for Laminar Boundary Layer Behind Blast Waves

S. W. LIU and H. MIRELS
Aerophysics Laboratory
Laboratory Operations
The Aerospace Corporation
El Segundo, Calif. 90245

1 May 1980

Interim Report

THE AEROSPACE CORPORATION

Prepared for

SPACE DIVISION
AIR FORCE SYSTEMS COMMAND
Los Angeles Air Force Station
P.O. Box 92960, Worldway Postal Center
Los Angeles, Calif. 90009

This final report was submitted by The Aerospace Corporation, El Segundo, CA 90245, under Contract No. F04701-79-C-0080 with the Space Division, Contracts Management Office, P.O. Box 92960, Worldway Postal Center, Los Angeles, CA 90009. It was reviewed and approved for The Aerospace Corporation by W. R. Warren, Jr., Director, Aerophysics Laboratory. Gerhard E. Aichinger was the project officer for Mission-Oriented Investigation and Experimentation (MOIE) Programs.

This report has been reviewed by the Public Affairs Office (PAS) and is releasable to the National Technical Information Service (NTIS). At NTIS, it will be available to the general public, including foreign nations.

This technical report has been reviewed and is approved for publication. Publication of this report does not constitute Air Force approval of the report's findings or conclusions. It is published only for the exchange and stimulation of ideas.

Gerhard E. Aichinger
Project Officer

FOR THE COMMANDER

Evan R. Brossman, Chief
Contracts Management Office

UNCLASSIFIED

SECURITY CLASSIFICATION OF THIS PAGE (When Data Entered)

REPORT DOCUMENTATION PAGE

19

READ INSTRUCTIONS BEFORE COMPLETING FORM

1. REPORT NUMBER

18 SD-TR-80-23

2. GOVT ACCESSION NO.

AD-A084 435

3. RECIPIENT'S CATALOG NUMBER

4. TITLE (and Subtitle)

6 NUMERICAL SOLUTIONS FOR LAMINAR BOUNDARY LAYER BEHIND BLAST WAVES,

5. TYPE OF REPORT & PERIOD COVERED

9 Interim Report,

6. PERFORMING ORG. REPORT NUMBER

14 TR-0080(5940-02)-2

7. AUTHOR(s)

10 Shaowen W. Liu [redacted] Harold Mirels

8. CONTRACT OR GRANT NUMBER(s)

15 F04701-79-C-0080

9. PERFORMING ORGANIZATION NAME AND ADDRESS

The Aerospace Corporation
El Segundo, Calif. 90245

10. PROGRAM ELEMENT, PROJECT, TASK AREA & WORK UNIT NUMBERS

12 110

11. CONTROLLING OFFICE NAME AND ADDRESS

Space Division
Los Angeles Air Force Station
Los Angeles, Calif. 90009

12. REPORT DATE

11 1 May [redacted]80

13. NUMBER OF PAGES

112

14. MONITORING AGENCY NAME & ADDRESS(if different from Controlling Office)

15. SECURITY CLASS. (of this report)

Unclassified

15a. DECLASSIFICATION/DOWNGRADING SCHEDULE

16. DISTRIBUTION STATEMENT (of this Report)

Approved for public release; distribution unlimited.

17. DISTRIBUTION STATEMENT (of the abstract entered in Block 20, if different from Report)

18. SUPPLEMENTARY NOTES

19. KEY WORDS (Continue on reverse side if necessary and identify by block number)

Blast Waves
Heat Transfer
Laminar Boundary Layer
Skin Fraction

20. ABSTRACT (Continue on reverse side if necessary and identify by block number)

Numerical solutions are obtained for plane ($\sigma = 0$) and axisymmetric ($\sigma = 1$) laminar boundary layers induced by blast waves of the form $x_s \sim t^{2/(\bar{\sigma}+3)}$, where x_s is the distance of the blast wave from the blast origin; t is time; $\bar{\sigma}$ is 0, 1, or 2 for plane, cylindrical, and spherical waves, respectively. Explicit dependence on time is eliminated by a similarity transformation. The entire region between the shock ($x = x_s$) and the blast origin ($x = 0$) is considered, except for a small region near $x = 0$ where the equations are singular. Numerical results are presented for ideal air with $\bar{\sigma} = 0$, $\sigma = 0$; $\bar{\sigma} = 1$, $\sigma = 0$; $\bar{\sigma} = 1$,

DD FORM 1473 (FACSIMILE)

UNCLASSIFIED 409367

SECURITY CLASSIFICATION OF THIS PAGE (When Data Entered)

19. KEY WORDS (Continued)

sigma subs xi-square
sigma-bar

20. ABSTRACT (Continued)

$\sigma = 1$ and $\bar{\sigma} = 2$, $\sigma = 1$. Wall shear and heat transfer are found to increase with $\xi = 1 - x/x_s$ at a rate faster than that indicated by previous solutions for the flow directly behind the shock ($\xi^2 \ll 1$). The results are applicable in the laminar-boundary-layer region, $p_\infty x_s \lesssim 0(10^{-3} - 10^{-2})$ atm/ft, where p_∞ is ambient pressure.

subs < or = .001 - .01

Accession For	
NTIS GRA&I	X
DDC TAB	☐
Unannounced	☐
Justification ________	
By ________	
Distribution/	
Availability Codes	
Dist.	Avail and/or special
A	

CONTENTS

FIGURES

TABLES

NOMENCLATURE

A	constant, Eqs. (10) and (17)
B	conversion factor, Eq. (40)
C	constant, Eq. (7)
C_f	friction coefficient, $\tau_w/\frac{1}{2}\rho_e u_e^2$, Eq. (36)
C_2	conversion factor, Eq. (40)
D_1, D_2, D_3, D_4	conversion factors, Eq. (40)
f	velocity function, Eq. (11)
F	inviscid flow function, Eq. (8)
F_1, F_2	conversion factors, Eqs. (22) and (23)
g	enthalpy function, Eq. (12)
h	enthalpy, Eqs. (3) and (4)
H	total enthalpy
m	exponent of power law shock, Eq. (7)
$\mathcal{M}$	normalized lateral flux, Eq. (39)
M	Mach number, Eq. (32)
p	pressure
Pr	Prandtl number
q_w	surface heat transfer, Eq. (35)
R	inviscid flow function, Eq. (8)
Re	Reynolds number, Eq. (33)
S	function defined in Eq. (23)

S_0, S_1, S_2, S_3	integral functions, Eqs. (28), (29), (30), and (31)
St	Stanton number, $q_w/\rho_e u_e H_e$, Eq. (37)
t	time
u	velocity component in x-direction
v	velocity component in y-direction
V	transformed lateral velocity
x, y, z	coordinate axes
α	(m-1)/m
γ	ratio of specific heats
δ^*	displacement thickness, Eq. (25)
δ^{**}	integral thickness defined by Eq. (26)
η	transformed coordinate, Eq. (10)
θ	momentum thickness, Eq. (27)
μ	viscosity
ν	kinematic viscosity, μ/ρ
ξ	transformed coordinate, $= 1 - (x/x_s)$, Eq. (10)
ρ	density
σ	= 0, two dimensional; = 1, axisymmetric
$\bar{\sigma}$	= 0, plane wave; = 1, axisymmetric; = 2, spherical
τ	transformed coordinate, Eq. (10)
τ_w	surface shear, Eq. (34)
φ	inviscid flow function, Eq. (8)
ψ	stream function, Eqs. (9) and (12)

Subscripts

e	outer edge of boundary layer
0	initial value
w	wall or surface
s	shock front
$(\ )_{\xi,\ \eta,\ \xi\eta}$	partial derivative
$(\ )'$	$\partial(\ )/\partial\eta$, alternative notation for partial derivation of η

I. INTRODUCTION

The solution for the wall boundary layer behind a shock wave moving with nonuniform velocity is, in general, complicated because of the addition of the temporal dimension to the problem. However, for a large class of flow problems of practical importance, similarity solutions exist so that the analysis is tractable. Such is the case with the boundary-layer flow behind a strong shock moving with power-law velocity. The formulation of the problem and the transformation devised to reduce the independent variables from three (x, y, t) of the original problem to two normalized spatial variables (ξ, η) in the transformed frame have been detailed in Ref. 1. Numerical solutions were also obtained in Ref. 1 by series expansions of both the inviscid and boundary-layer flow in powers of the normalized distance from the shock wave, ξ. Two terms in each expansion were used, and the results are limited to the region directly behind the shock wave ($\xi^2 \ll 1$). The effort involved in extending the series to higher order terms increases very rapidly. Chen and Chang,[2] apparently unaware of the existence of Ref. 1, reformulated the problem using essentially the same approach, but they carried the expansion to the next term. Unfortunately, some of their coefficients appear to be in error.

Numerical finite difference methods are available for evaluating boundary-layer flows in two coordinate variables.[3] We have, therefore, reexamined the shock-induced boundary-layer problem in the light of a direct application of finite difference methods to the transformed boundary-layer equations. In this report similarity (ξ, η) solutions are obtained for the laminar boundary layer behind a power-law shock associated with a blast wave. A finite difference method based upon Blottner's numerical scheme[3] is used. The results are valid, at all times, in the entire flow region between the shock front and the immediate vicinity of the blast-wave

origin provided the boundary layer remains laminar. The method of analysis is described in Section II. Results and discussions are given in Section III. The relation between blast-wave strength and the energy of the disturbed flow is discussed in Appendix A. The extent of the laminar boundary layer, behind blast waves, is discussed in Appendix B.

II. ANALYSIS

Similarity properties of the inviscid flow associated with strong power-law shocks and the corresponding similarity transformation devised for the shock-induced laminar boundary layer have already been detailed in Ref. 1. For completeness, the governing equations and basic assumptions are briefly repeated here.

With the assumption that the fluid Prandtl number and specific heats are constant and that the viscosity is proportional to temperature, the unsteady, compressible laminar boundary-layer equations for a perfect gas are:

Continuity

$$\frac{\partial \rho}{\partial t} + \frac{1}{x^{\sigma}} \frac{\partial(\rho u x^{\sigma})}{\partial x} + \frac{\partial(\rho v)}{\partial y} = 0 \tag{1}$$

Momentum

$$\rho \frac{Du}{Dt} = - \frac{\partial p_e}{\partial x} + \frac{\partial}{\partial y} \left(\mu \frac{\partial u}{\partial y}\right) \tag{2}$$

Energy

$$\rho \frac{Dh}{Dt} - \frac{Dp_e}{Dt} = \frac{1}{Pr} \frac{\partial}{\partial y} \left(\mu \frac{\partial h}{\partial y}\right) + \mu \left(\frac{\partial u}{\partial y}\right)^2 \tag{3}$$

State

$$p = [(\gamma - 1)/\gamma]\rho h \tag{4}$$

where

$$\frac{D}{Dt} = \frac{\partial}{\partial t} + u\frac{\partial}{\partial x} + v\frac{\partial}{\partial y}$$

Symbols are defined in the Nomenclature section, and the orientation of coordinates is indicated in Fig. 1. Both two-dimensional and axisymmetric boundary layers corresponding to $\sigma = 0$ and 1, respectively, are included. The choice of σ is determined by the geometry of the propagating shock and the surface on which the boundary layer develops (Fig. 2). The boundary conditions are:

$$\begin{aligned} \text{at } y = 0 \qquad & u(x,0,t) = 0 \\ & v(x,0,t) = v_w(x,t) \\ & h_w(x,0,t) = h_w(x,t) \end{aligned} \tag{5}$$

$$\begin{aligned} \text{at } y = \infty \qquad & u(x,\infty,t) = u_e(x,t) \\ & h(x,\infty,t) = h_e(x,t) \end{aligned} \tag{6}$$

We confined our attention to a strong shock that moves according to the power law (Appendix A)

$$x_s = Ct^m, \qquad u_s = \frac{dx_s}{dt} = Cmt^{m-1} \tag{7}$$

The disturbed flow for constant specific heats is similar at successive instants in time.[4] If the independent variable x is replaced by $\xi = 1 - (x/x_s)$, the disturbed flow can be expressed as

$$p_e/p_\infty = u_s^2 F(\xi), \qquad \rho_e/\rho_\infty = R(\xi)$$

$$u_e = u_s \varphi(\xi), \quad h_e \cong \frac{\gamma}{\gamma - 1} \frac{p_e}{\rho_e} = \frac{\gamma}{\gamma - 1} u_s^2 \frac{F(\xi)}{R(\xi)} \tag{8}$$

The functions F, R, and φ depend on the geometry of the shock wave as well as the parameters γ, m, and the coordinate ξ. Analytical and numerical solutions for F, R, and φ are given in Ref. 4 for plane, cylindrical, and spherical shocks (corresponding to $\overline{\sigma}$ = 0, 1, 2 respectively) and γ = 1,4. When $m = 2/(3 + \overline{\sigma})$, the flows correspond to constant energy blast waves. These cases are discussed in Appendix A.

Four combinations of shock and surface orientation are of practical interest. These are shown schematically in Fig. 2.

Equation (1) is satisfied by a scalar stream function ψ such that

$$u = \frac{\rho_\infty}{\rho x^\sigma} \frac{\partial \psi}{\partial y}, \qquad v = -\frac{\rho_\infty}{\rho x^\sigma}\left[\frac{\partial \psi}{\partial x} + \frac{\partial}{\partial t}\left(x^\sigma \int_0^y \frac{\rho}{\rho_\infty} d\overline{y}\right)\right] \tag{9}$$

The following independent variables are introduced:

$$\xi = 1 - x/Ct^m$$

$$\eta = \frac{x^\sigma \int_0^y \left(\frac{\rho}{\rho_\infty}\right) d\overline{y}}{[At^{2m(\sigma+1) - 1}(1 - x/Ct^m)]^{1/2}} \tag{10}$$

$$\tau = t$$

where A is a constant to be defined later. Next, the following form is assumed for the dependent variables

$$\psi = u_e \left[A\tau^{2m(\sigma+1) - 1}\xi\right]^{1/2} f(\xi, \eta) \tag{11}$$

$$h/h_e = \rho_e/\rho = g(\xi, \eta) \tag{12}$$

which, by Eq. (9), gives $f_\eta = u/u_e$. For the present, the surface is assumed impermeable. The boundary conditions on $f(\xi, \eta)$ are then

$$f(\xi, 0) = f_\eta(\xi, 0) = 0, \qquad f_\eta(\xi, \infty) = 1 \tag{13}$$

Wall temperature is assumed negligible compared with the free-stream temperature.[1] The boundary conditions on $g(\xi, \eta)$ are then

$$g(\xi, 0) = 0, \qquad g(\xi, \infty) = 1 \tag{14}$$

When Eqs. (10), (11), and (12) are introduced into Eqs. (1), (2), and (3), they become

$$\begin{aligned}(1 - \xi)^{2\sigma}(F/F_o) f_{\eta\eta\eta} &+ (\eta - \varphi f) f_{\eta\eta} \\ = 2\xi \Bigg\{ &\left[f\varphi_\xi + \varphi f_\xi - \frac{1}{2}(2\sigma + \alpha)\eta\right] f_{\eta\eta} \\ &+ \left[\alpha + (1 - \xi - \varphi f_\eta)\left(\frac{\varphi_\xi}{\varphi} + \frac{f_{\eta\xi}}{f_\eta}\right)\right] f_\eta - \frac{F_\xi g}{R\varphi}\Bigg\}\end{aligned} \tag{15}$$

$$\begin{aligned}(1 - \xi)^{2\sigma}&\left(\frac{1}{Pr}\frac{F}{F_o} g_{\eta\eta} + \frac{\gamma - 1}{\gamma}\frac{R\varphi^2}{F_o} f_{\eta\eta}^2\right) \\ &+ (\eta - \varphi f) g_\eta = 2\xi \Bigg\{\left[f\varphi_\xi + \varphi f_\xi - \frac{1}{2}(2\sigma + \alpha)\eta\right] g_\eta \\ &+ \left[\frac{2\alpha}{\gamma} + (1 - \xi - \varphi f_\eta)\left(\frac{g_\xi}{g} + \frac{F_\xi}{\gamma F} - \frac{R_\xi}{R}\right)\right] g\Bigg\}\end{aligned} \tag{16}$$

where $\alpha = (m-1)/m$. In deriving Eqs. (15) and (16) the constant A was chosen as follows to simplify the coefficients of $f_{\eta\eta\eta}$ and $g_{\eta\eta}$

$$A = 2mF_o C^{2(\sigma+1)} \nu_\infty \rho_\infty / p_\infty \tag{17}$$

The explicit dependence of the flow on the independent variable τ has now been eliminated.

The development up to here is the same as that presented in Ref. 1. Equations (15) and (16) are two simultaneous equations for f and g in terms of the two independent transformed variables ξ and η. Functionally, they are analogous to the steady-state boundary layer equations successfully treated by Blottner.[3] Blottner's derivation, however, made use of a transformed lateral velocity component that reduced the order of the differential equation for f by one. The lateral velocity component is, in turn, defined by an additional differential equation arising from the continuity equation.

The transformed lateral velocity component is defined by

$$V \equiv -2 \frac{\xi^{1/2}}{\varphi} \frac{\partial(\varphi \xi^{1/2} f)}{\partial \xi} \tag{18}$$

which is motivated by the expanded form for ψ_x. The relation between V and v is found with the use of Eq. (9). Eqs. (15), (16), and (18) now become

$$2\xi \left[\frac{(1-\xi)}{f'} - \varphi\right] \frac{\partial f'}{\partial \xi} - \left[\varphi V + \eta \left\{2\xi\left(\sigma + \frac{\alpha}{2}\right) + 1\right\}\right] \frac{1}{f'} f'_\eta$$

$$+ 2\xi \left[\alpha + (1-\xi)\frac{\varphi_\xi}{\varphi} - \varphi_\xi f' - \frac{F_\xi}{R\varphi} \frac{g}{f'}\right] - (1-\xi)^{2\sigma}\left(\frac{F}{F_o}\right) \frac{1}{f'} f'_{\eta\eta} = 0$$

(19)

$$2\xi\,(1-\xi-\varphi f')\,\frac{\partial g}{\partial \xi} - \left[\varphi V + \eta\left\{2\xi\left(\sigma + \frac{\alpha}{2}\right) + 1\right\}\right] g_\eta$$

$$- (1-\xi)^{2\sigma}\,\frac{\gamma - 1}{\gamma}\,\varphi^2\,\frac{R}{F_o}\left(f'_\eta\right)^2 + 2\xi\left[(1-\xi-\varphi f')\left(\frac{F_\xi}{\gamma F} - \frac{R_\xi}{R}\right) + \frac{2\alpha}{\gamma}\right] g$$

$$- (1-\xi)^{2\sigma}\,\frac{F}{F_o}\,\frac{1}{Pr}\,g_{\eta\eta} = 0 \qquad (20)$$

$$\frac{\partial V}{\partial \eta} + \left(2\xi\,\frac{\varphi_\xi}{\varphi} + 1\right) f' + 2\xi\,\frac{\partial f'}{\partial \xi} = 0 \qquad (21)$$

Note that f' $(\equiv \partial f/\partial \eta)$ is now the lowest order of the function f appearing in the above equations, which, termwise, are now directly comparable to Blottner's equations of Ref. 3.

A computer program has been written based on the numerical scheme outlined in Ref. 3, and Eqs. (19), (20), and (21) have been integrated for the four cases of practical interest shown in Fig. 2. The results are presented in Section III. Quantities of interest are noted below.

Physical coordinates are obtained from [e.g., Eqs. (10) and (17)]

$$x = x_s\,(1 - \xi)$$

$$y = F_1 \cdot F_2 \cdot S \qquad (22)$$

where

$$F_1(\tau) = \left[F_0 \frac{\mu_\infty}{p_\infty} u_s x_s\right]^{1/2}$$

$$F_2(\xi) = \frac{(2\xi)^{1/2}}{(1-\xi)^{\sigma} R}$$

$$S(\xi, \eta) = \int_0^{\eta} g \, d\eta \tag{23}$$

Boundary-layer integral lengths are expressible as:

$$y_e = F_1 \cdot F_2 \cdot S_0 (\xi) \tag{24}$$

$$\delta^* = \int_0^{\infty} \left(1 - \frac{\rho u}{\rho_e u_e}\right) dy = F_1 \cdot F_2 \cdot S_1 (\xi) \tag{25}$$

$$\delta^{**} = \int_0^{\infty} \left(1 - \frac{\rho}{\rho_e}\right) dy = F_1 \cdot F_2 \cdot S_2 (\xi) \tag{26}$$

$$\theta = \int_0^{\infty} \frac{\rho u}{\rho_e u_e} \left(1 - \frac{u}{u_e}\right) dy = F_1 \cdot F_2 \cdot S_3(\xi) \tag{27}$$

where

$$S_0 = \int_0^{\eta_e} g \, d\eta \tag{28}$$

$$S_1 = \int_0^{\eta_e} (g - f') \, d\eta \tag{29}$$

$$S_2 = \int_0^{\eta_e} (g-1)\, d\eta \tag{30}$$

$$S_3 = \int_0^{\eta_e} f'(1-f')\, d\eta \tag{31}$$

Here η_e is the value of η at the outer edge of the boundary layer, where the edge boundary conditions ($y = \infty$) are satisfied in the present numerical code. The choice for η_e is discussed later. The quantity y_e is the value of y corresponding to η_e and is a rough measure of boundary layer thickness. The quantity δ^* is the familiar displacement thickness. The use of δ^{**} will be discussed later; θ is the momentum thickness. Note that these integral lengths are dominated by the factor F_2, which is singular at $\xi = 1$.

Local Mach number M and Reynolds number Re can be expressed in the form

$$M = \frac{u_e}{(\gamma p_e/\rho_e)^{1/2}} = \frac{\varphi}{(\gamma F/R)^{1/2}} \tag{32}$$

$$Re = \frac{\rho_e\, u_e\, (x_s - x)}{\mu_e} = \left(\frac{p_\infty\, x_s}{\mu_\infty\, u_s}\right)\left(\frac{R^2 \varphi \xi}{F}\right) \tag{33}$$

The shear and heat transfer at the wall can be found from

$$\tau_w = \mu_w \left(\frac{\partial u}{\partial y}\right)_w = \left[\frac{\mu_\infty}{2F_o\, p_\infty\, u_s\, x_s}\right]^{1/2} \left[\frac{(1-\xi)^\sigma}{(2\xi)^{1/2}}\right] p_e u_e f_{\eta\eta}(\xi, 0) \tag{34}$$

$$q_w = - k_w \left(\frac{\partial T}{\partial y}\right)_w = - \frac{1}{Pr} \left[\frac{\mu_\infty}{2F_o p_\infty u_s x_s}\right]^{1/2} \left[\frac{(1-\xi)^\sigma}{(2\xi)^{1/2}}\right] p_e h_e g_\eta (\xi, 0) \tag{35}$$

Normalized expressions for the above are

$$C_f (Re)^{1/2} = \frac{\tau_w}{\frac{1}{2} \rho_e u_e^2} (Re)^{1/2} = \left(\frac{2F}{\varphi F_o}\right)^{1/2} (1-\xi)^\sigma f_{\eta\eta}(\xi, 0) \tag{36}$$

$$St (Re)^{1/2} = \frac{q_w}{\rho_e u_e H_e} (Re)^{1/2} = - \frac{1}{Pr} \left(\frac{F}{2F_o}\right)^{1/2} \frac{(1-\xi)^\sigma}{\varphi\left(1 + \frac{\gamma-1}{2} \frac{\varphi^2}{\gamma F/R}\right)} g_\eta (\xi, 0) \tag{37}$$

where C_f and St represent the friction coefficient and Stanton number, respectively. These are functions only of ξ.

Integration of the continuity equation [Eq. (1)] across the boundary layer provides an expression for net mass flux in the lateral direction, namely

$$(\rho v)_e - (\rho v)_w = \frac{\partial}{\partial t} (\rho_e \delta^{**}) + \frac{\sigma}{x} \rho_e u_e \delta^* + \frac{\partial}{\partial x} [\rho_e u_e \delta^*] \tag{38}$$

which can be expressed in the form

$$\begin{aligned} \mathcal{M} &\equiv (2\xi)^{1/2} [(\rho v)_e - (\rho v)_w]/B \\ &= C_2 \left[D_1 S_2 + D_2 \xi \frac{dS_2}{d\xi} - D_3 S_1 - D_4 \frac{dS_1}{d\xi}\right] \end{aligned} \tag{39}$$

where

$$
\begin{aligned}
B &= \rho_\infty \left[F_o \mu_\infty u_s^3 / p_\infty x_s\right]^{1/2} \\
C_2 &= 1/(1-\xi)^\sigma \\
D_1 &= 1 + 2\xi\left(\frac{\alpha}{2} + \sigma\right) \\
D_2 &= 2\xi\,(1-\xi) \\
D_3 &= 2\xi\varphi_\xi + \varphi \\
D_4 &= 2\xi\varphi
\end{aligned}
\tag{40}
$$

The normalized lateral mass flux $\mathcal{M}$ is a function only of ξ. The present computing program provides S_1 and S_2 versus ξ in appropriate tables such that the derivatives $dS_1/d\xi$, $dS_2/d\xi$ and the corresponding values of $\mathcal{M}$ can be subsequently calculated.

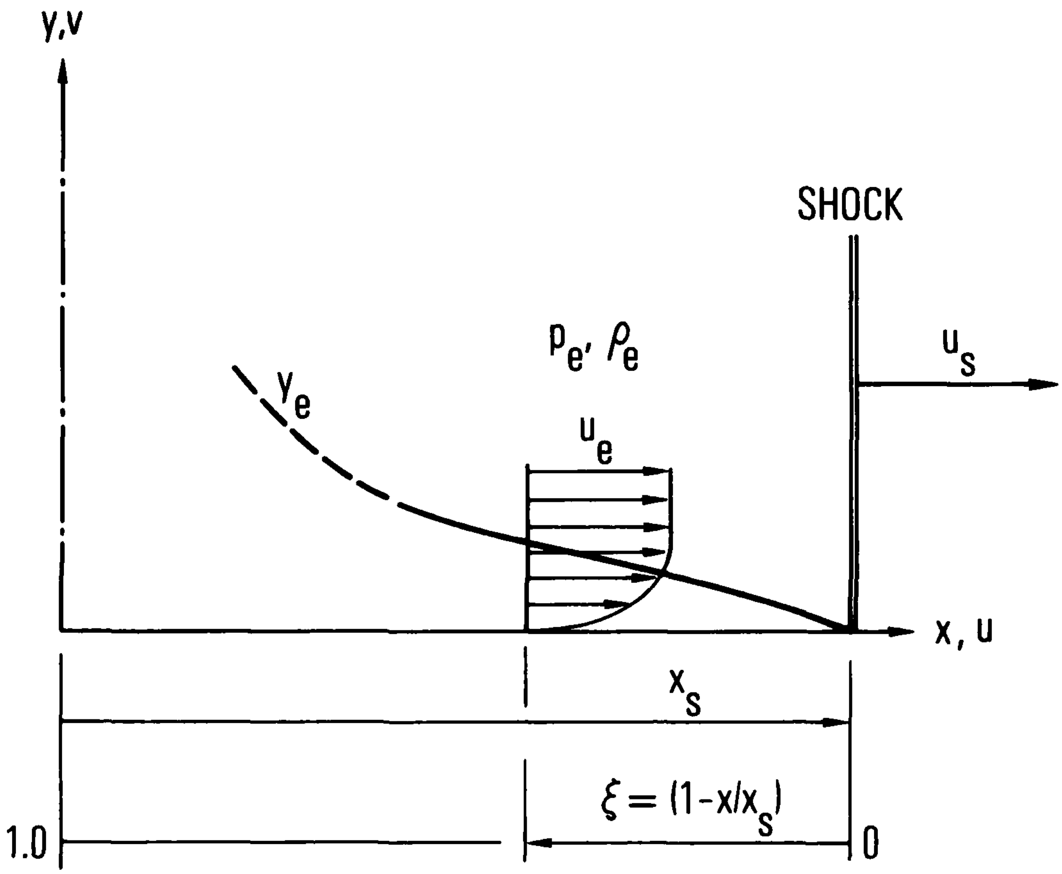

Fig. 1. Boundary layer behind moving shock

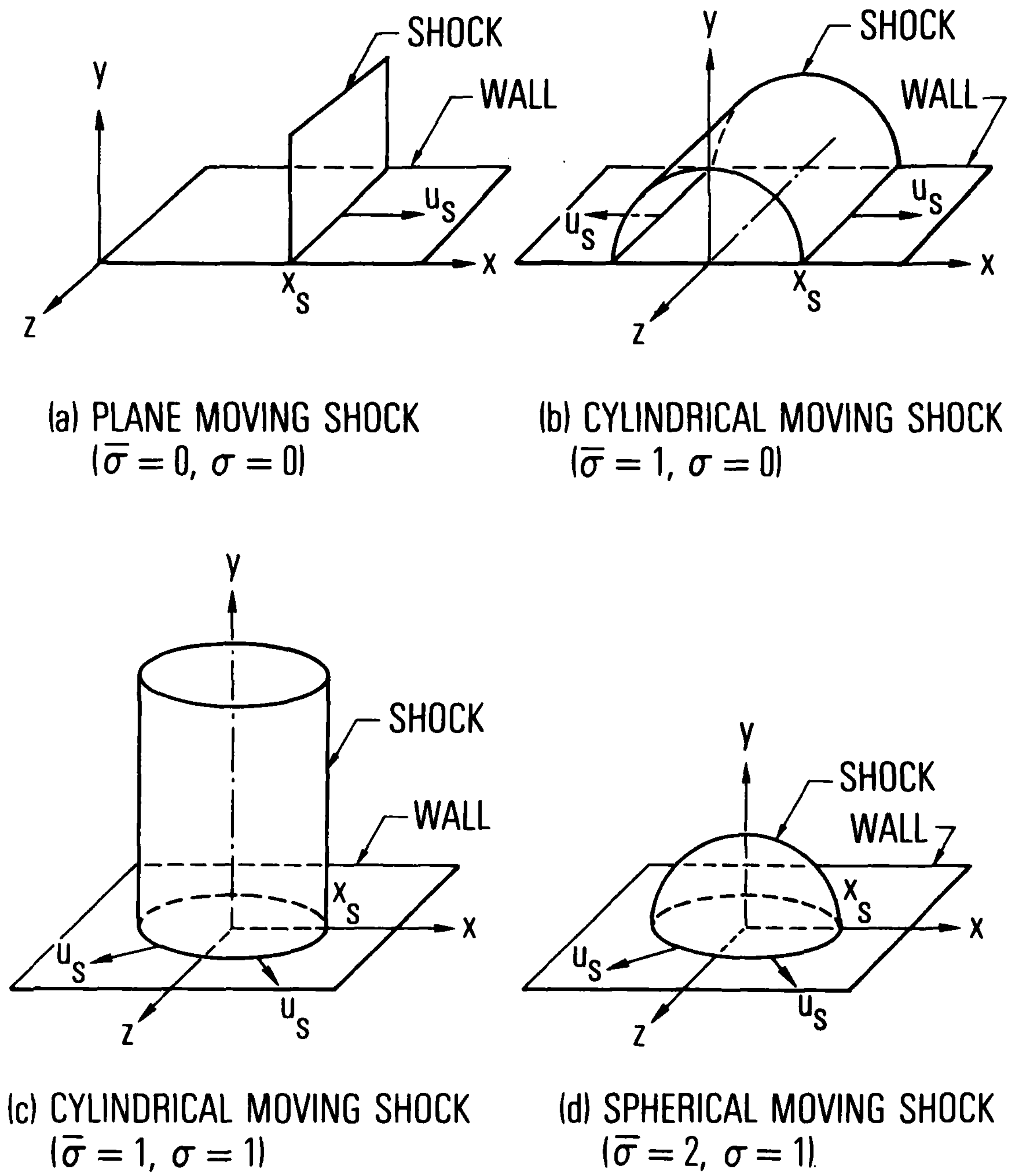

Fig. 2. Moving shock-plane wall orientation

III. RESULTS AND DISCUSSIONS

Inviscid and viscid flow-field solutions have been obtained; the results are discussed herein. The inviscid flow functions F, R, and φ associated with blast waves are discussed in Ref. 4. Both analytical expressions and numerical tables for the cases $\bar{\sigma} = 0, 1, 2$, and $\gamma = 1.4$ are given. For the present applications, however, it has been found necessary to refine the tabular results to minimize the interpolation errors in coefficients appearing in the boundary-layer equations. To this end, it was found more convenient to recalculate the inviscid flow functions and their derivatives to the degree of accuracy desired by starting from the basic equations governing a power-law shock, such as those given in Ref. 5. The results for $\gamma = 1.4$ are given here as Tables 1, 2, and 3, for the cases $\bar{\sigma} = 0$, 1, and 2, respectively.* They are also presented as Figs. 3, 4, and 5. The variation of Mach number M with ξ for the three inviscid blast-wave flows are plotted as Fig. 6. The variation of $Re/(\rho_\infty x_s/\mu_\infty u_s)$ with ξ for the same cases are plotted as Fig. 7.

Boundary-layer solutions have been obtained for $\gamma = 1.4$, $Pr = 0.72$ for the four cases noted in Fig. 2. In each, the integration has been successfully carried out from the shock to the immediate vicinity of the blast origin. At the blast origin ($\xi = 1.0$), both the inviscid flow and the boundary-layer equations are singular. Results have been obtained for all cases to well beyond $\xi = 0.9$. Divergence did set in, however, as the integration approached $\xi = 1$. The refinement of the inviscid-flow functions discussed earlier contributed noticeably to extending the range of integration closer to the singularity. The numerical techniques and the results are discussed in the following paragraphs.

---

*The authors are indebted to Heather Bagwell of The Aerospace Corporation for providing these results.

The boundary-layer equations were programmed using Blottner's numerical technique.[3] At each streamwise station ξ the present computing program allowed up to 100 mesh points distributed, either uniformly or nonuniformly, in the interval $0 \leq \eta \leq \eta_e$, where, as previously noted, η_e denotes the value of η at which the freestream boundary conditions ($y = \infty$) are applied. For the results herewith presented, 98 mesh points were used. A graduated grid size was used so that the mesh network was finest near the surface where the definition of the profiles is of the greatest interest. The calculation is most accurate when the value of η_e at each streamwise station is just sufficient for the profiles to approach the outer edge asymptotically within an acceptable tolerance.

The boundary-layer solution at $\xi = 0$ was obtained by iteration, using reasonable profiles for f_η and g as first estimates. For $\xi = 0$, Eqs. (19) and (20) reduce to the zero-order equations of Ref. 1; the two results are, therefore, directly comparable. As has been noted in Ref. 1, they do not depend on σ or $\overline{\sigma}$. The wall gradients of the present calculation are listed in Table 4 and are shown to compare very favorably with those of Ref. 1.

A first estimate of the boundary-layer solution for $\xi > 0$ was obtained by satisfying outer-edge boundary conditions at $\eta_e = 6$ for all values of ξ. The choice $\eta_e = 6$ was based on the $\xi = 0$ solution. The resulting velocity and enthalpy profiles at successive values of ξ are given in Fig. 8 in the form of composite profile summary plots. Note that the velocity profiles develop overshoot with increase in ξ. It is also seen from Fig. 8 that, in terms of η, the boundary-layer thickness decreases significantly with increase in ξ. That is, the physical edge of the boundary layer occurs at significantly smaller values of η as ξ increases. (This is a consequence of the definition of η. In the physical variable, y, the boundary-layer thickness increases with increase in ξ.) In order to maintain computational accuracy, it is desirable to decrease η_e with increase in ξ. The present approach was to let the second choice for η_e correspond to the values of η,

at which $u/u_e \equiv f_\eta = 1 \pm 0.0005$ in the preceding $\eta_e = 6$ solution. The + and - signs refer to velocity profiles with and without overshoot. The resulting values of η_e are given in Fig. 9. The boundary-layer profiles were recalculated using the new η_e-distribution. These calculations not only provided a more detailed description of the profiles by utilizing more fully the effective η-thickness of the boundary, but also improved the stability of the numerical process at large ξ where the η-thickness can be as much as two orders of magnitude smaller than that at $\xi = 0$. It was found, however, that the results for wall shear and heat transfer and for the boundary layer thicknesses δ^*, δ^{**}, and θ from the second calculation did not differ significantly from the first $\eta_e = 6$ calculation (i.e., were within computational accuracy). Hence further iterations of η_e were not needed.

The results from the variable η_e solution are given in Figs. 10 to 13 and in Tables 4 and 5. Sample velocity and enthalpy profiles are given in Fig. 10. These figures provide somewhat more detail than Fig. 8. Note that the velocity overshoot is least severe for the case $\sigma = \overline{\sigma} = 0$ and is most severe for the case $\overline{\sigma} = 1$, $\sigma = 0$. A maximum overshoot velocity of about $u/u_e = 1.09$ is achieved at $\xi = 0.5$ in the latter case. Velocity and enthalpy gradients, evaluated at the wall, are given in Fig. 11 and Table 5. The derivative of $f_{\eta\eta}(\xi, 0)$ and $g_\eta(\xi, 0)$ with ξ at $\xi = 0$ has been obtained numerically in this study, and a comparison is made in Table 4 with the corresponding values from Ref. 1. Agreement is to within about three significant figures, which is about the accuracy of some of the present computer code subroutines. Wall shear and wall heat transfer coefficients, referenced to local flow properties [Eqs. (36) and (37)], are given in Fig. 10. It is seen that the shear and heat transfer coefficients increase by about an order of magnitude, as ξ increases from 0 to about 0.9. The results for normalized lateral mass flux and boundary-layer lengths are given in Table 5 and Fig. 13. These quantities have been normalized to remain of order one as ξ varies. The value of S_0 in Table 5 is based on the variable η_e solution (Fig. 9). Hence the corresponding value y_e provides a rough estimate of

local boundary-layer thickness. Equations (22) to (31) indicate that in physical variables the characteristic boundary-layer lengths (e.g., $y_e, \delta^*, \ldots$) are proportional to $1/(1-\xi)^{\sigma}R$. Because $R \rightarrow 0$ as $\xi \rightarrow 1$, these lengths tend to become infinite as $\xi \rightarrow 1$, for $\sigma = 0$ as well as $\sigma = 1$ cases.

Because both the inviscid and the boundary-layer flow fields near the blast origin are more or less idealized, the solution in this regime is more of analytical, than practical, interest in that it serves as a test for the functional self-consistency of the equations and the method of calculation used.

Table 1. Inviscid flow functions, $\tilde{\sigma} = 0$, $\gamma = 1.4$

ξ	φ	$\frac{d\varphi}{d\xi}$	F	$\frac{dF}{d\xi}$	R	$\frac{dR}{d\xi}$
0.00	.833333E+00	-.125000E+01	.833333E+00	-.375000E+01	.600000E+01	-.450000E+02
.01	.820896E+00	-.123732E+01	.797345E+00	-.345263E+01	.557160E+01	-.407670E+02
.02	.808588E+00	-.122429E+01	.764188E+00	-.318318E+01	.518304E+01	-.370193E+02
.03	.796412E+00	-.121095E+01	.733599E+00	-.293852E+01	.482981E+01	-.336927E+02
.04	.784370E+00	-.119733E+01	.705344E+00	-.271593E+01	.450797E+01	-.307324E+02
.05	.772466E+00	-.118347E+01	.679215E+00	-.251303E+01	.421410E+01	-.280919E+02
.06	.760701E+00	-.116941E+01	.655025E+00	-.232776E+01	.394520E+01	-.257311E+02
.07	.749078E+00	-.115519E+01	.632607E+00	-.215831E+01	.369866E+01	-.236160E+02
.08	.737598E+00	-.114084E+01	.611811E+00	-.200306E+01	.347216E+01	-.217168E+02
.09	.726262E+00	-.112642E+01	.592503E+00	-.186062E+01	.326369E+01	-.200082E+02
.10	.715070E+00	-.111196E+01	.574560E+00	-.172974E+01	.307144E+01	-.184681E+02
.11	.704022E+00	-.109750E+01	.557873E+00	-.160932E+01	.289383E+01	-.170772E+02
.12	.693120E+00	-.108308E+01	.542342E+00	-.149838E+01	.272945E+01	-.158187E+02
.13	.682361E+00	-.106874E+01	.527877E+00	-.139604E+01	.257706E+01	-.146782E+02
.14	.671744E+00	-.105452E+01	.514395E+00	-.130153E+01	.243554E+01	-.136427E+02
.15	.661270E+00	-.104045E+01	.501823E+00	-.121415E+01	.230389E+01	-.127011E+02
.16	.650935E+00	-.102656E+01	.490091E+00	-.113327E+01	.218124E+01	-.118434E+02
.17	.640738E+00	-.101289E+01	.479137E+00	-.105833E+01	.206677E+01	-.110609E+02
.18	.630676E+00	-.999463E+00	.468906E+00	-.988833E+00	.195979E+01	-.103460E+02
.19	.620748E+00	-.986300E+00	.459344E+00	-.924309E+00	.185965E+01	-.969169E+01
.20	.610949E+00	-.973428E+00	.450404E+00	-.864351E+00	.176578E+01	-.909203E+01
.21	.601278E+00	-.960864E+00	.442043E+00	-.808584E+00	.167765E+01	-.854162E+01
.22	.591731E+00	-.948627E+00	.434220E+00	-.756671E+00	.159480E+01	-.803565E+01
.23	.582304E+00	-.936730E+00	.426898E+00	-.708304E+00	.151680E+01	-.756987E+01
.24	.572995E+00	-.925186E+00	.420043E+00	-.663203E+00	.144328E+01	-.714045E+01
.25	.563799E+00	-.914005E+00	.413624E+00	-.621115E+00	.137388E+01	-.674398E+01
.26	.554714E+00	-.903193E+00	.407611E+00	-.581808E+00	.130830E+01	-.637740E+01
.27	.545734E+00	-.892756E+00	.401979E+00	-.545071E+00	.124624E+01	-.603797E+01
.28	.536857E+00	-.882697E+00	.396702E+00	-.510711E+00	.118746E+01	-.572321E+01
.29	.528079E+00	-.873018E+00	.391758E+00	-.478552E+00	.113170E+01	-.543092E+01
.30	.519396E+00	-.863719E+00	.387124E+00	-.448433E+00	.107877E+01	-.515905E+01
.31	.510803E+00	-.854797E+00	.382783E+00	-.420206E+00	.102846E+01	-.490592E+01
.32	.502298E+00	-.846250E+00	.378714E+00	-.393737E+00	.980595E+00	-.466979E+01
.33	.493877E+00	-.838074E+00	.374902E+00	-.368902E+00	.935012E+00	-.444922E+01
.34	.485536E+00	-.830263E+00	.371331E+00	-.345587E+00	.891563E+00	-.424289E+01
.35	.477271E+00	-.822811E+00	.367986E+00	-.323687E+00	.850111E+00	-.404958E+01
.36	.469078E+00	-.815711E+00	.364853E+00	-.303108E+00	.810531E+00	-.386820E+01

Table 1. Inviscid flow functions, $\bar{\sigma} = 0$, $\gamma = 1.4$ (Continued)

ξ	φ	$\frac{d\varphi}{d\xi}$	F	$\frac{dF}{d\xi}$	R	$\frac{dR}{d\xi}$
.37	.460955E+00	-.808956E+00	.361920E+00	-.283760E+00	.772710E+00	-.369777E+01
.38	.452898E+00	-.802536E+00	.359174E+00	-.265564E+00	.736542E+00	-.353738E+01
.39	.444904E+00	-.796444E+00	.356605E+00	-.248443E+00	.701932E+00	-.338620E+01
.40	.436968E+00	-.790669E+00	.354202E+00	-.232330E+00	.668790E+00	-.324349E+01
.41	.429089E+00	-.785203E+00	.351955E+00	-.217161E+00	.637036E+00	-.310857E+01
.42	.421263E+00	-.780035E+00	.349856E+00	-.202877E+00	.606595E+00	-.298082E+01
.43	.413487E+00	-.775156E+00	.347895E+00	-.189424E+00	.577398E+00	-.285967E+01
.44	.405759E+00	-.770556E+00	.346065E+00	-.176753E+00	.549381E+00	-.274460E+01
.45	.398075E+00	-.766224E+00	.344357E+00	-.164817E+00	.522487E+00	-.263514E+01
.46	.390434E+00	-.762151E+00	.342766E+00	-.153572E+00	.496661E+00	-.253086E+01
.47	.382832E+00	-.758326E+00	.341284E+00	-.142980E+00	.471854E+00	-.243136E+01
.48	.375266E+00	-.754738E+00	.339904E+00	-.133003E+00	.448019E+00	-.233628E+01
.49	.367736E+00	-.751379E+00	.338622E+00	-.123607E+00	.425115E+00	-.224528E+01
.50	.360238E+00	-.748238E+00	.337430E+00	-.114761E+00	.403101E+00	-.215807E+01
.51	.352771E+00	-.745305E+00	.336325E+00	-.106433E+00	.381942E+00	-.207436E+01
.52	.345331E+00	-.742572E+00	.335300E+00	-.985972E-01	.361603E+00	-.199390E+01
.53	.337919E+00	-.740027E+00	.334351E+00	-.912268E-01	.342054E+00	-.191646E+01
.54	.330530E+00	-.737663E+00	.333474E+00	-.842978E-01	.323265E+00	-.184182E+01
.55	.323165E+00	-.735470E+00	.332664E+00	-.777873E-01	.305209E+00	-.176979E+01
.56	.315820E+00	-.733440E+00	.331917E+00	-.716740E-01	.287861E+00	-.170018E+01
.57	.308495E+00	-.731563E+00	.331229E+00	-.659378E-01	.271197E+00	-.163284E+01
.58	.301189E+00	-.729832E+00	.330597E+00	-.605599E-01	.255197E+00	-.156762E+01
.59	.293898E+00	-.728238E+00	.330017E+00	-.555223E-01	.239839E+00	-.150437E+01
.60	.286623E+00	-.726774E+00	.329485E+00	-.508083E-01	.225103E+00	-.144297E+01
.61	.279352E+00	-.725432E+00	.329000E+00	-.464017E-01	.210973E+00	-.138332E+01
.62	.272114E+00	-.724204E+00	.328556E+00	-.422875E-01	.197432E+00	-.132530E+01
.63	.264878E+00	-.723084E+00	.328153E+00	-.384513E-01	.184462E+00	-.126883E+01
.64	.257652E+00	-.722065E+00	.327786E+00	-.348793E-01	.172050E+00	-.121382E+01
.65	.250436E+00	-.721140E+00	.327454E+00	-.315585E-01	.160181E+00	-.116019E+01
.66	.243229E+00	-.720302E+00	.327155E+00	-.284762E-01	.148842E+00	-.110789E+01
.67	.236030E+00	-.719547E+00	.326884E+00	-.256206E-01	.138019E+00	-.105684E+01
.68	.228838E+00	-.718867E+00	.326641E+00	-.229801E-01	.127701E+00	-.100700E+01
.69	.221652E+00	-.718257E+00	-.326424E+00	-.205436E-01	.117875E+00	-.958316E+00
.70	.214473E+00	-.717713E+00	.326230E+00	-.183065E-01	.108531E+00	-.910751E+00
.71	.207298E+00	-.717228E+00	.326057E+00	-.162406E-01	.996568E-01	-.864268E+00

Table 1. Inviscid flow functions, $\bar{\sigma} = 0$, $\gamma = 1.4$ (Continued)

ξ	φ	$\frac{d\varphi}{d\xi}$	F	$\frac{dF}{d\xi}$	R	$\frac{dR}{d\xi}$
.72	.200128E+00	-.716798E+00	.325904E+00	-.143539E-01	.912421E-01	-.818837E+00
.73	.192962E+00	-.716419E+00	.325770E+00	-.126308E-01	.832766E-01	-.774435E+00
.74	.185799E+00	-.716086E+00	.325651E+00	-.110621E-01	.757501E-01	-.731040E+00
.75	.178640E+00	-.715795E+00	.325548E+00	-.963675E-02	.686525E-01	-.688637E+00
.76	.171483E+00	-.715542E+00	.325458E+00	-.835213E-02	.619741E-01	-.647216E+00
.77	.164329E+00	-.715323E+00	.325380E+00	-.719376E-02	.557049E-01	-.606768E+00
.78	.157177E+00	-.715135E+00	.325314E+00	-.615545E-02	.498355E-01	-.567292E+00
.79	.150026E+00	-.714974E+00	.325257E+00	-.522924E-02	.443559E-01	-.528787E+00
.80	.142877E+00	-.714839E+00	.325209E+00	-.440741E-02	.392565E-01	-.491259E+00
.81	.135729E+00	-.714725E+00	.325169E+00	-.368246E-02	.345274E-01	-.454715E+00
.82	.128583E+00	-.714630E+00	.325135E+00	-.304712E-02	.301588E-01	-.419167E+00
.83	.121437E+00	-.714552E+00	.325107E+00	-.249433E-02	.261407E-01	-.384631E+00
.84	.114292E+00	-.714488E+00	.325085E+00	-.201725E-02	.224628E-01	-.351126E+00
.85	.107147E+00	-.714437E+00	.325067E+00	-.160925E-02	.191147E-01	-.318676E+00
.86	.100003E+00	-.714397E+00	.325052E+00	-.126394E-02	.160857E-01	-.287309E+00
.87	.928592E-01	-.714365E+00	.325041E+00	-.975117E-03	.133648E-01	-.257057E+00
.88	.857155E-01	-.714341E+00	.325033E+00	-.736840E-03	.109407E-01	-.227957E+00
.89	.785722E-01	-.714323E+00	.325026E+00	-.543376E-03	.880165E-02	-.200053E+00
.90	.714290E-01	-.714310E+00	.325022E+00	-.389240E-03	.693547E-02	-.173396E+00
.91	.642860E-01	-.714301E+00	.325018E+00	-.269191E-03	.532939E-02	-.148043E+00
.92	.571430E-01	-.714295E+00	.325016E+00	-.178247E-03	.397003E-02	-.124066E+00
.93	.500001E-01	-.714291E+00	.325015E+00	-.111698E-03	.284323E-02	-.101545E+00
.94	.428572E-01	-.714288E+00	.325014E+00	-.651225E-04	.193394E-02	-.805813E-01
.95	.357143E-01	-.714287E+00	.325013E+00	-.344330E-04	.122600E-02	-.613000E-01
.96	.285714E-01	-.714286E+00	.325013E+00	-.157547E-04	.701800E-03	-.438626E-01
.97	.214286E-01	-.714286E+00	.325013E+00	-.575604E-05	.341874E-03	-.284896E-01
.98	.142857E-01	-.714286E+00	.325013E+00	-.139253E-05	.124061E-03	-.155077E-01
.99	.714287E-02	-.714286E+00	.325013E+00	-.123082E-06	.219310E-04	-.546279E-02
1.00	0.	-.714286E+00	.325013E+00	0.	0.	0.

Table 2. Inviscid flow functions, $\bar{\sigma} = 1$, $\gamma = 1.4$

ξ	φ	$\frac{d\varphi}{d\xi}$	F	$\frac{dF}{d\xi}$	R	$\frac{dR}{d\xi}$
0.00	.833333E+00	-.152778E+01	.833333E+00	-.652778E+01	.600000E+01	-.850000E+02
.01	.818225E+00	-.149375E+01	.772759E+00	-.561583E+01	.522493E+01	-.705753E+02
.02	.803461E+00	-.145895E+01	.720504E+00	-.485809E+01	.457368E+01	-.591028E+02
.03	.789048E+00	-.142366E+01	.675187E+00	-.422367E+01	.403537E+01	-.498892E+02
.04	.774989E+00	-.138813E+01	.635699E+00	-.368881E+01	.357509E+01	-.424232E+02
.05	.761285E+00	-.135262E+01	.601141E+00	-.323501E+01	.318236E+01	-.363231E+02
.06	.747935E+00	-.131737E+01	.570777E+00	-.284776E+01	.284504E+01	-.313004E+02
.07	.734936E+00	-.128260E+01	.544003E+00	-.251552E+01	.255350E+01	-.271348E+02
.08	.722281E+00	-.124851E+01	.520315E+00	-.222907E+01	.230006E+01	-.236568E+02
.09	.709963E+00	-.121529E+01	.499294E+00	-.198096E+01	.207852E+01	-.207342E+02
.10	.697972E+00	-.118307E+01	.480588E+00	-.176516E+01	.188387E+01	-.182635E+02
.11	.686298E+00	-.115198E+01	.463900E+00	-.157670E+01	.171202E+01	-.161627E+02
.12	.674928E+00	-.112211E+01	.448976E+00	-.141150E+01	.155960E+01	-.143667E+02
.13	.663851E+00	-.109354E+01	.435603E+00	-.126620E+01	.142384E+01	-.128232E+02
.14	.653053E+00	-.106632E+01	.423596E+00	-.113797E+01	.130244E+01	-.114900E+02
.15	.642520E+00	-.104046E+01	.412795E+00	-.102446E+01	.119345E+01	-.103330E+02
.16	.632239E+00	-.101599E+01	.403064E+00	-.923675E+00	.109528E+01	-.932405E+01
.17	.622196E+00	-.992887E+00	.394285E+00	-.833954E+00	.100656E+01	-.844037E+01
.18	.612377E+00	-.971146E+00	.386353E+00	-.753871E+00	.926121E+00	-.766304E+01
.19	.602768E+00	-.950734E+00	.379179E+00	-.682216E+00	.852994E+00	-.697641E+01
.20	.593358E+00	-.931616E+00	.372684E+00	-.617956E+00	.786334E+00	-.636745E+01
.21	.584132E+00	-.913748E+00	.366798E+00	-.560203E+00	.725422E+00	-.582526E+01
.22	.575079E+00	-.897083E+00	.361461E+00	-.508194E+00	.669637E+00	-.534073E+01
.23	.566186E+00	-.881568E+00	.356617E+00	-.461272E+00	.618441E+00	-.490616E+01
.24	.557444E+00	-.867152E+00	.352220E+00	-.418865E+00	.571369E+00	-.451505E+01
.25	.548840E+00	-.853779E+00	.348227E+00	-.380480E+00	.528014E+00	-.416186E+01
.26	.540365E+00	-.841394E+00	.344599E+00	-.345683E+00	.488021E+00	-.384192E+01
.27	.532009E+00	-.829943E+00	.341302E+00	-.314099E+00	.451078E+00	-.355120E+01
.28	.523763E+00	-.819371E+00	.338307E+00	-.285398E+00	.416911E+00	-.328626E+01
.29	.515619E+00	-.809625E+00	.335586E+00	-.259289E+00	.385277E+00	-.304416E+01
.30	.507568E+00	-.800655E+00	.333114E+00	-.235518E+00	.355961E+00	-.282233E+01
.31	.499603E+00	-.792411E+00	.330868E+00	-.213857E+00	.328770E+00	-.261859E+01
.32	.491717E+00	-.784845E+00	.328830E+00	-.194108E+00	.303535E+00	-.243102E+01
.33	.483904E+00	-.777912E+00	.326980E+00	-.176091E+00	.280101E+00	-.225796E+01
.34	.476157E+00	-.771568E+00	.325303E+00	-.159650E+00	.258332E+00	-.209796E+01
.35	.468471E+00	-.765771E+00	.323783E+00	-.144643E+00	.238103E+00	-.194977E+01

Table 2. Inviscid flow functions, $\bar{\sigma} = 1$, $\gamma = 1.4$ (Continued)

ξ	φ	$\frac{d\varphi}{d\xi}$	F	$\frac{dF}{d\xi}$	R	$\frac{dR}{d\xi}$
.36	.460840E+00	-.760483E+00	.322406E+00	-.130942E+00	.219301E+00	-.181227E+01
.37	.453260E+00	-.755666E+00	.321160E+00	-.118434E+00	.201825E+00	-.168449E+01
.38	.445725E+00	-.751285E+00	.320033E+00	-.107017E+00	.185582E+00	-.156559E+01
.39	.438233E+00	-.747307E+00	.319016E [illegible]	-.965969E-01	.170486E+00	-.145479E [illegible]
.40	.430778E+00	-.743781E+00	.318098E+00	-.870908E-01	.156461E+00	-.135144E+01
.41	.423358E+00	-.740438E+00	.317272E+00	-.784224E-01	.143435E+00	-.125494E+01
.42	.415968E+00	-.737489E+00	.316527E+00	-.705224E-01	.131341E+00	-.116477E+01
.43	.408607E+00	-.734838E+00	.315859E+00	-.633276E-01	.120128E+00	-.108044E+01
.44	.401271E+00	-.732437E+00	.315259E+00	-.567804E-01	.109714E+00	-.100155E+01
.45	.393957E+00	-.730286E+00	.314721E+00	-.508279E-01	.100072E+00	-.927704E+00
.46	.386664E+00	-.728358E+00	.314240E+00	-.454217E-01	.911445E-01	-.858569E+00
.47	.379389E+00	-.726632E+00	.313811E+00	-.405178E-01	.828861E-01	-.793835E+00
.48	.372131E+00	-.725091E+00	.313428E+00	-.360730E-01	.752541E-01	-.733221E+00
.49	.364887E+00	-.723718E+00	.313088E+00	-.320518E-01	.682088E-01	-.676472E+00
.50	.357656E+00	-.722497E+00	.312786E+00	-.284186E-01	.617126E-01	-.623356E+00
.51	.350437E+00	-.721414E+00	.312519E+00	-.251410E-01	.557303E-01	-.573658E+00
.52	.343227E+00	-.720456E+00	.312282E+00	-.221893E-01	.502287E-01	-.527181E+00
.53	.336027E+00	-.719611E+00	.312074E+00	-.195359E-01	.451765E-01	-.483743E+00
.54	.328835E+00	-.718866E+00	.311891E+00	-.171553E-01	.405442E-01	-.443176E+00
.55	.321649E+00	-.718213E+00	.311730E+00	-.150238E-01	.363039E-01	-.405321E+00
.56	.314470E+00	-.717642E+00	.311589E+00	-.131194E-01	.324293E-01	-.370032E+00
.57	.307296E+00	-.717143E+00	.311467E+00	-.114221E-01	.288952E-01	-.337168E+00
.58	.300127E+00	-.716709E+00	.311360E+00	-.991286E-02	.256782E-01	-.306602E+00
.59	.292962E+00	-.716333E+00	.311268E+00	-.857445E-02	.227560E-01	-.278208E+00
.60	.285800E+00	-.716008E+00	.311188E+00	-.739078E-02	.201072E-01	-.251871E+00
.61	.278642E+00	-.715728E+00	.311120E+00	-.634701E-02	.177121E-01	-.227479E+00
.62	.271486E+00	-.715488E+00	.311061E+00	-.542944E-02	.155515E-01	-.204927E+00
.63	.264332E+00	-.715284E+00	.311011E+00	-.462546E-02	.136077E-01	-.184113E+00
.64	.257180E+00	-.715109E+00	.310968E+00	-.392344E-02	.118638E-01	-.164941E+00
.65	.250030E+00	-.714962E+00	.310932E+00	-.331270E-02	.103037E-01	-.147318E+00
.66	.242881E+00	-.714838E+00	.310902E+00	-.278344E-02	.891255E-02	-.131156E+00
.67	.235733E+00	-.714734E+00	.310876E+00	-.232668E-02	.767604E-02	-.116368E+00
.68	.228586E+00	-.714647E+00	.310855E+00	-.193422E-02	.658089E-02	-.102872E+00
.69	.221440E+00	-.714575E+00	.310837E+00	-.159859E-02	.561456E-02	-.905895E-01
.70	.214294E+00	-.714516E+00	.310823E+00	-.131300E-02	.476531E-02	-.794442E-01
.71	.207149E+00	-.714467E+00	.310811E+00	-.107127E-02	.402213E-02	-.693625E-01

Table 2. Inviscid flow functions, $\bar{\sigma} = 1$, $\gamma = 1.4$ (Continued)

ξ	φ	$\frac{d\varphi}{d\xi}$	F	$\frac{dF}{d\xi}$	R	$\frac{dR}{d\xi}$
.72	.200005E+00	-.714428E+00	.310801E+00	-.867836E-03	.337475E-02	-.602739E-01
.73	.192861E+00	-.714396E+00	.310793E+00	-.697678E-03	.281357E-02	-.521102E-01
.74	.185717E+00	-.714370E+00	.310787E+00	-.556287E-03	.232968E-02	-.448062E-01
.75	.178573E+00	-.714350E+00	.310782E+00	-.439631E-03	.191479E-02	-.382989E-01
.76	.171430E+00	-.714334E+00	.310778E+00	-.344118E-03	.156125E-02	-.325279E-01
.77	.164287E+00	-.714322E+00	.310775E+00	-.266563E-03	.126197E-02	-.274354E-01
.78	.157144E+00	-.714312E+00	.310773E+00	-.204157E-03	.101046E-02	-.229658E-01
.79	.150000E+00	-.714302E+00	.310771E+00	-.154433E-03	.800758E-03	-.190661E-01
.80	.142857E+00	-.714299E+00	.310770E+00	-.115239E-03	.627412E-03	-.156856E-01
.81	.135715E+00	-.714295E+00	.310769E+00	-.847111E-04	.485477E-03	-.127759E-01
.82	.128572E+00	-.714292E+00	.310768E+00	-.612424E-04	.370478E-03	-.102911E-01
.83	.121429E+00	-.714290E+00	.310767E+00	-.434620E-04	.278384E-03	-.818780E-02
.84	.114286E+00	-.714289E+00	.310767E+00	-.302089E-04	.205588E-03	-.642466E-02
.85	.107143E+00	-.714288E+00	.310767E+00	-.205098E-04	.148886E-03	-.496288E-02
.86	.100000E+00	-.714287E+00	.310767E+00	-.135576E-04	.105448E-03	-.376600E-02
.87	.928572E-01	-.714286E+00	.310767E+00	-.869109E-05	.727972E-04	-.279989E-02
.88	.857143E-01	-.714286E+00	.310766E+00	-.537652E-05	.487870E-04	-.203279E-02
.89	.785714E-01	-.714286E+00	.310766E+00	-.318985E-05	.315763E-04	-.143529E-02
.90	.714286E-01	-.714286E+00	.310766E+00	-.180059E-05	.196064E-04	-.980319E-03
.91	.642857E-01	-.714286E+00	.310766E+00	-.956905E-06	.115774E-04	-.643188E-03
.92	.571429E-01	-.714286E+00	.310766E+00	-.472013E-06	.642462E-05	-.401539E-03
.93	.500000E-01	-.714286E+00	.310766E+00	-.211837E-06	.329525E-05	-.235375E-03
.94	.428571E-01	-.714286E+00	.310766E+00	-.840082E-07	.152459E-05	-.127049E-03
.95	.357143E-01	-.714286E+00	.310766E+00	-.281342E-07	.612700E-06	-.612700E-04
.96	.285714E-01	-.714286E+00	.310766E+00	-.737520E-08	.200769E-06	-.250962E-04
.97	.214286E-01	-.714286E+00	.310766E+00	-.131263E-08	.476435E-07	-.794059E-05
.98	.142857E-01	-.714286E+00	.310766E+00	-.115238E-09	.627404E-08	-.156851E-05
.99	.714286E-02	-.714286E+00	.310766E+00	-.180059E-11	.196064E-09	-.980319E-07
1.00	0.	-.714286E+00	.310766E+00	0.	0.	0.

Table 3. Inviscid flow functions, $\bar{\sigma} = 2$, $\gamma = 1.4$

ξ	φ	$\frac{d\varphi}{d\xi}$	F	$\frac{dF}{d\xi}$	R	$\frac{dR}{d\xi}$
0.00	.833333E+00	-.180556E+01	.833333E+00	-.930556E+01	.600000E+01	-.125000E+03
.01	.815605E+00	-.173992E+01	.749763E+00	-.749201E+01	.490687E+01	-.953153E+02
.02	.798538E+00	-.167328E+01	.682078E+00	-.610478E+01	.406594E+01	-.740079E+02
.03	.782139E+00	-.160658E+01	.626641E+00	-.502662E+01	.340783E+01	-.583975E+02
.04	.766404E+00	-.154068E+01	.580787E+00	-.417689E+01	.288484E+01	-.467508E+02
.05	.751320E+00	-.147635E+01	.542532E+00	-.349887E+01	.246347E+01	-.379178E+02
.06	.736870E+00	-.141424E+01	.510374E+00	-.295189E+01	.211973E+01	-.311186E+02
.07	.723027E+00	-.135483E+01	.483158E+00	-.250624E+01	.183614E+01	-.258133E+02
.08	.709763E+00	-.129850E+01	.459985E+00	-.213990E+01	.159976E+01	-.216216E+02
.09	.697046E+00	-.124549E+01	.440151E+00	-.183631E+01	.140091E+01	-.182714E+02
.10	.684841E+00	-.119595E+01	.423092E+00	-.158286E+01	.123220E+01	-.155647E+02
.11	.673115E+00	-.114990E+01	.408359E+00	-.136981E+01	.108796E+01	-.133560E+02
.12	.661832E+00	-.110733E+01	.395587E+00	-.118963E+01	.963783E+00	-.115365E+02
.13	.650957E+00	-.106814E+01	.384477E+00	-.103635E+01	.856205E+00	-.100246E+02
.14	.640458E+00	-.103220E+01	.374786E+00	-.905287E+00	.762475E+00	-.875774E+01
.15	.630303E+00	-.999369E+00	.366310E+00	-.792668E+00	.680394E+00	-.768801E+01
.16	.620461E+00	-.969457E+00	.358881E+00	-.695473E+00	.608183E+00	-.677815E+01
.17	.610905E+00	-.942281E+00	.352357E+00	-.611251E+00	.544396E+00	-.599901E+01
.18	.601607E+00	-.917650E+00	.346619E+00	-.538004E+00	.487845E+00	-.532756E+01
.19	.592544E+00	-.895378E+00	.341566E+00	-.474092E+00	.437547E+00	-.474547E+01
.20	.583692E+00	-.875279E+00	.337111E+00	-.418159E+00	.392686E+00	-.423808E+01
.21	.575031E+00	-.857176E+00	.333180E+00	-.369082E+00	.352576E+00	-.379354E+01
.22	.566542E+00	-.840901E+00	.329710E+00	-.325919E+00	.316638E+00	-.340224E+01
.23	.558208E+00	-.826295E+00	.326645E+00	-.287883E+00	.284381E+00	-.305631E+01
.24	.550012E+00	-.813209E+00	.323937E+00	-.254305E+00	.255383E+00	-.274929E+01
.25	.541939E+00	-.801504E+00	.321546E+00	-.224622E+00	.229283E+00	-.247583E+01
.26	.533977E+00	-.791052E+00	.319433E+00	-.198349E+00	.205769E+00	-.223148E+01
.27	.526114E+00	-.781735E+00	.317569E+00	-.175074E+00	.184569E+00	-.201251E+01
.28	.518339E+00	-.773442E+00	.315923E+00	-.154440E+00	.165445E+00	-.181579E+01
.29	.510642E+00	-.766074E+00	.314472E+00	-.136138E+00	.148188E+00	-.163866E+01
.30	.503015E+00	-.759538E+00	.313194E+00	-.119901E+00	.132614E+00	-.147887E+01
.31	.495449E+00	-.753751E+00	.312068E+00	-.105496E+00	.118559E+00	-.133448E+01
.32	.487938E+00	-.748635E+00	.311078E+00	-.927166E-01	.105878E+00	-.120383E+01
.33	.480474E+00	-.744121E+00	.310209E+00	-.813840E-01	.944413E-01	-.108549E+01
.34	.473053E+00	-.740146E+00	.309446E+00	-.713392E-01	.841316E-01	-.978204E+00
.35	.465670E+00	-.736652E+00	.308778E+00	-.624418E-01	.748440E-01	-.880880E+00

Table 3. Inviscid flow functions, $\sigma = 2$, $\gamma = 1.4$ (Continued)

ξ	φ	$\frac{d\varphi}{d\xi}$	F	$\frac{dF}{d\xi}$	R	$\frac{dR}{d\xi}$
.36	.458319E+00	-.733587E+00	.308194E+00	-.545672E-01	.664839E-01	-.792560E+00
.37	.450997E+00	-.730904E+00	.307684E+00	-.476047E-01	.589656E-01	-.712397E+00
.38	.443700E+00	-.728559E+00	.307239E+00	-.414555E-01	.522113E-01	-.639639E+00
.39	.436425E+00	-.726515E+00	.306852E+00	-.360316E-01	.461504E-01	-.573616E+00
.40	.429169E+00	-.724737E+00	.306516E+00	-.312540E-01	.407186E-01	-.513727E+00
.41	.421929E+00	-.723194E+00	.306225E+00	-.270522E-01	.358572E-01	-.459432E+00
.42	.414704E+00	-.721859E+00	.305974E+00	-.233629E-01	.315129E-01	-.410244E+00
.43	.407491E+00	-.720705E+00	.305757E+00	-.201295E-01	.276368E-01	-.365721E+00
.44	.400289E+00	-.719711E+00	.305570E+00	-.173009E-01	.241843E-01	-.325461E+00
.45	.393097E+00	-.718858E+00	.305409E+00	-.148316E-01	.211146E-01	-.289098E+00
.46	.385912E+00	-.718126E+00	.305272E+00	-.126806E-01	.183904E-01	-.256296E+00
.47	.378734E+00	-.717501E+00	.305155E+00	-.108111E-01	.159778E-01	-.226748E+00
.48	.371561E+00	-.716969E+00	.305055E+00	-.919025E-02	.138456E-01	-.200173E+00
.49	.364394E+00	-.716517E+00	.304970E+00	-.778847E-02	.119653E-01	-.176310E+00
.50	.357231E+00	-.716134E+00	.304899E+00	-.657941E-02	.103111E-01	-.154921E+00
.51	.350071E+00	-.715811E+00	.304838E+00	-.553950E-02	.885939E-02	-.135787E+00
.52	.342914E+00	-.715540E+00	.304787E+00	-.464771E-02	.758856E-02	-.118704E+00
.53	.335760E+00	-.715313E+00	.304745E+00	-.388528E-02	.647910E-02	-.103484E+00
.54	.328608E+00	-.715123E+00	.304709E+00	-.323557E-02	.551324E-02	-.899567E-01
.55	.321458E+00	-.714965E+00	.304680E+00	-.268379E-02	.467486E-02	-.779615E-01
.56	.314309E+00	-.714834E+00	.304655E+00	-.221684E-02	.394939E-02	-.673520E-01
.57	.307161E+00	-.714727E+00	.304635E+00	-.182315E-02	.332365E-02	-.579935E-01
.58	.300014E+00	-.714638E+00	.304619E+00	-.149253E-02	.278577E-02	-.497615E-01
.59	.292868E+00	-.714566E+00	.304605E+00	-.121600E-02	.232505E-02	-.425420E-01
.60	.285723E+00	-.714508E+00	.304594E+00	-.985727E-03	.193190E-02	-.362303E-01
.61	.278578E+00	-.714460E+00	.304585E+00	-.794833E-03	.159774E-02	-.307305E-01
.62	.271434E+00	-.714422E+00	.304578E+00	-.637339E-03	.131488E-02	-.259547E-01
.63	.264289E+00	-.714392E+00	.304572E+00	-.508056E-03	.107650E-02	-.218230E-01
.64	.257146E+00	-.714367E+00	.304568E+00	-.402493E-03	.876520E-03	-.182621E-01
.65	.250002E+00	-.714348E+00	.304564E+00	-.316779E-03	.709573E-03	-.152060E-01
.66	.242859E+00	-.714333E+00	.304561E+00	-.247596E-03	.570919E-03	-.125943E-01
.67	.235715E+00	-.714321E+00	.304559E+00	-.192104E-03	.456387E-03	-.103728E-01
.68	.228572E+00	-.714312E+00	.304558E+00	-.147890E-03	.362327E-03	-.849225E-02
.69	.221429E+00	-.714305E+00	.304556E+00	-.112911E-03	.285553E-03	-.690866E-02
.70	.214286E+00	-.714300E+00	.304555E+00	-.854454E-04	.223296E-03	-.558248E-02
.71	.207143E+00	-.714296E+00	.304555E+00	-.640530E-04	.173163E-03	-.447841E-02

Table 3. Inviscid flow functions, $\bar{\sigma} = 2$, $\gamma = 1.4$ (Continued)

ξ	φ	$\frac{d\varphi}{d\xi}$	F	$\frac{dF}{d\xi}$	R	$\frac{dR}{d\xi}$
.72	.200000E+00	-.714293E+00	.304554E+00	-.475334E-04	.133093E-03	-.356502E-02
.73	.192857E+00	-.714291E+00	.304554E+00	-.348936E-04	.101321E-03	-.281448E-02
.74	.185714E+00	-.714289E+00	.304553E+00	-.253179E-04	.763430E-04	-.220221E-02
.75	.178571E+00	-.714288E+00	.304553E+00	-.181402E-04	.568878E-04	-.170664E-02
.76	.171429E+00	-.714287E+00	.304553E+00	-.128218E-04	.418845E-04	-.130889E-02
.77	.164286E+00	-.714287E+00	.304553E+00	-.892975E-05	.304388E-04	-.992570E-03
.78	.157143E+00	-.714286E+00	.304553E+00	-.611991E-05	.218091E-04	-.743494E-03
.79	.150000E+00	-.714286E+00	.304553E+00	-.412113E-05	.153855E-04	-.549484E-03
.80	.142857E+00	-.714286E+00	.304553E+00	-.272212E-05	.106707E-04	-.400152E-03
.81	.135714E+00	-.714286E+00	.304553E+00	-.176018E-05	.726307E-05	-.286700E-03
.82	.128571E+00	-.714286E+00	.304553E+00	-.111165E-05	.484186E-05	-.201744E-03
.83	.121429E+00	-.714286E+00	.304553E+00	-.683861E-06	.315381E-05	-.139139E-03
.84	.114286E+00	-.714286E+00	.304553E+00	-.408481E-06	.200156E-05	-.938230E-04
.85	.107143E+00	-.714286E+00	.304553E+00	-.236009E-06	.123354E-05	-.616769E-04
.86	.100000E+00	-.714286E+00	.304553E+00	-.131293E-06	.735239E-06	-.393878E-04
.87	.928571E-01	-.714286E+00	.304553E+00	-.699311E-07	.421738E-06	-.243311E-04
.88	.857143E-01	-.714286E+00	.304553E+00	-.354154E-07	.231381E-06	-.144613E-04
.89	.785714E-01	-.714286E+00	.304553E+00	-.169040E-07	.120480E-06	-.821451E-05
.90	.714286E-01	-.714286E+00	.304553E+00	-.751886E-08	.589479E-07	-.442109E-05
.91	.642857E-01	-.714286E+00	.304553E+00	-.307053E-08	.267477E-07	-.222898E-05
.92	.571429E-01	-.714286E+00	.304553E+00	-.112828E-08	.110571E-07	-.103661E-05
.93	.500000E-01	-.714286E+00	.304553E+00	-.362648E-09	.406166E-08	-.435178E-06
.94	.428571E-01	-.714286E+00	.304553E+00	-.978222E-10	.127821E-08	-.159776E-06
.95	.357143E-01	-.714286E+00	.304553E+00	-.207681E-10	.325644E-09	-.488466E-07
.96	.285714E-01	-.714286E+00	.304553E+00	-.311646E-11	.610827E-10	-.114530E-07
.97	.214286E-01	-.714286E+00	.304553E+00	-.270198E-12	.706118E-11	-.176530E-08
.98	.142857E-01	-.714286E+00	.304553E+00	-.860809E-14	.337437E-12	-.126539E-09
.99	.714286E-02	-.714286E+00	.304553E+00	-.237767E-16	.186410E-14	-.139807E-11
1.00	0.	-.714286E+00	.304553E+00	0.	0.	0.

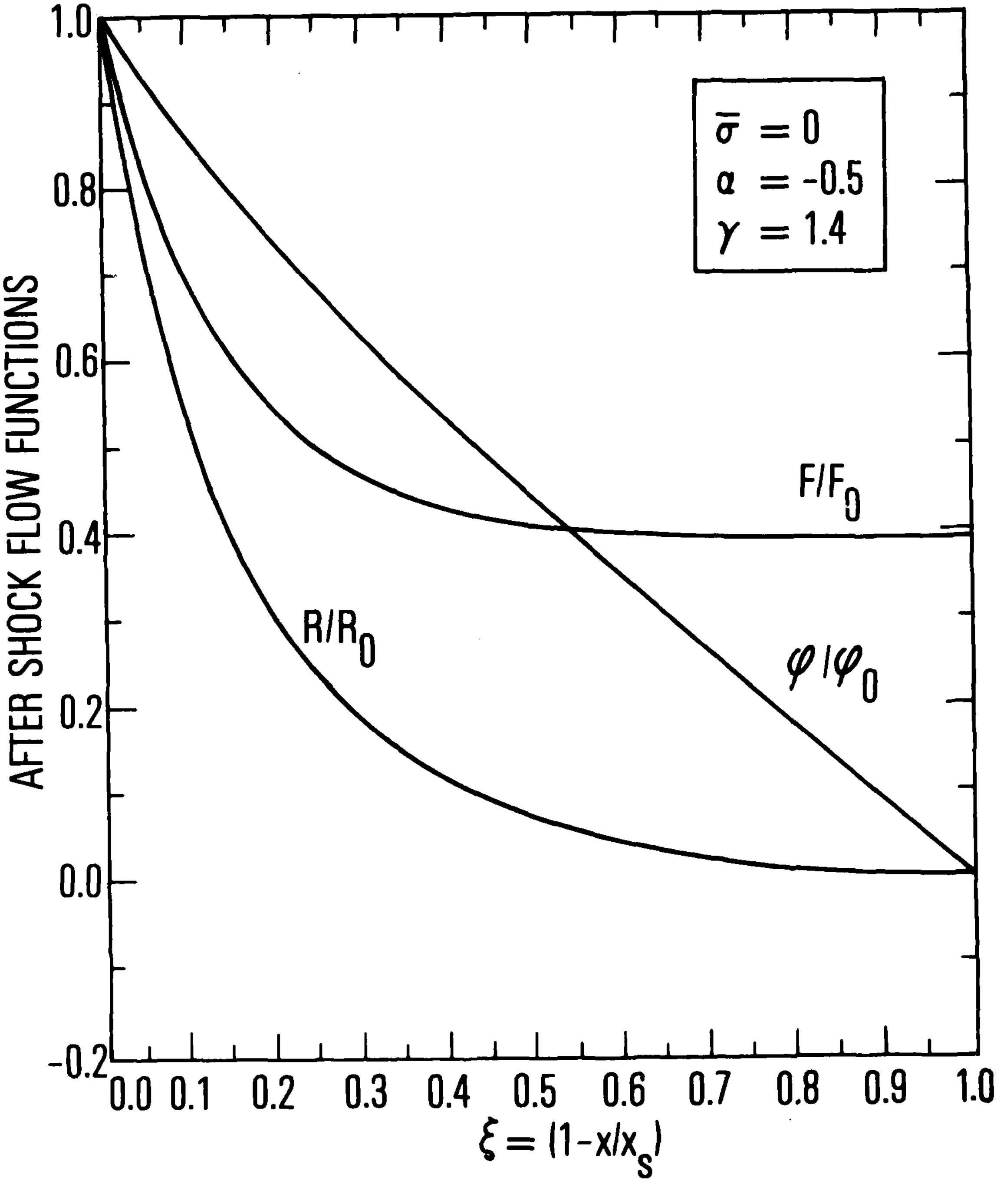

Fig. 3. Inviscid flow field, $\overline{\sigma} = 0$

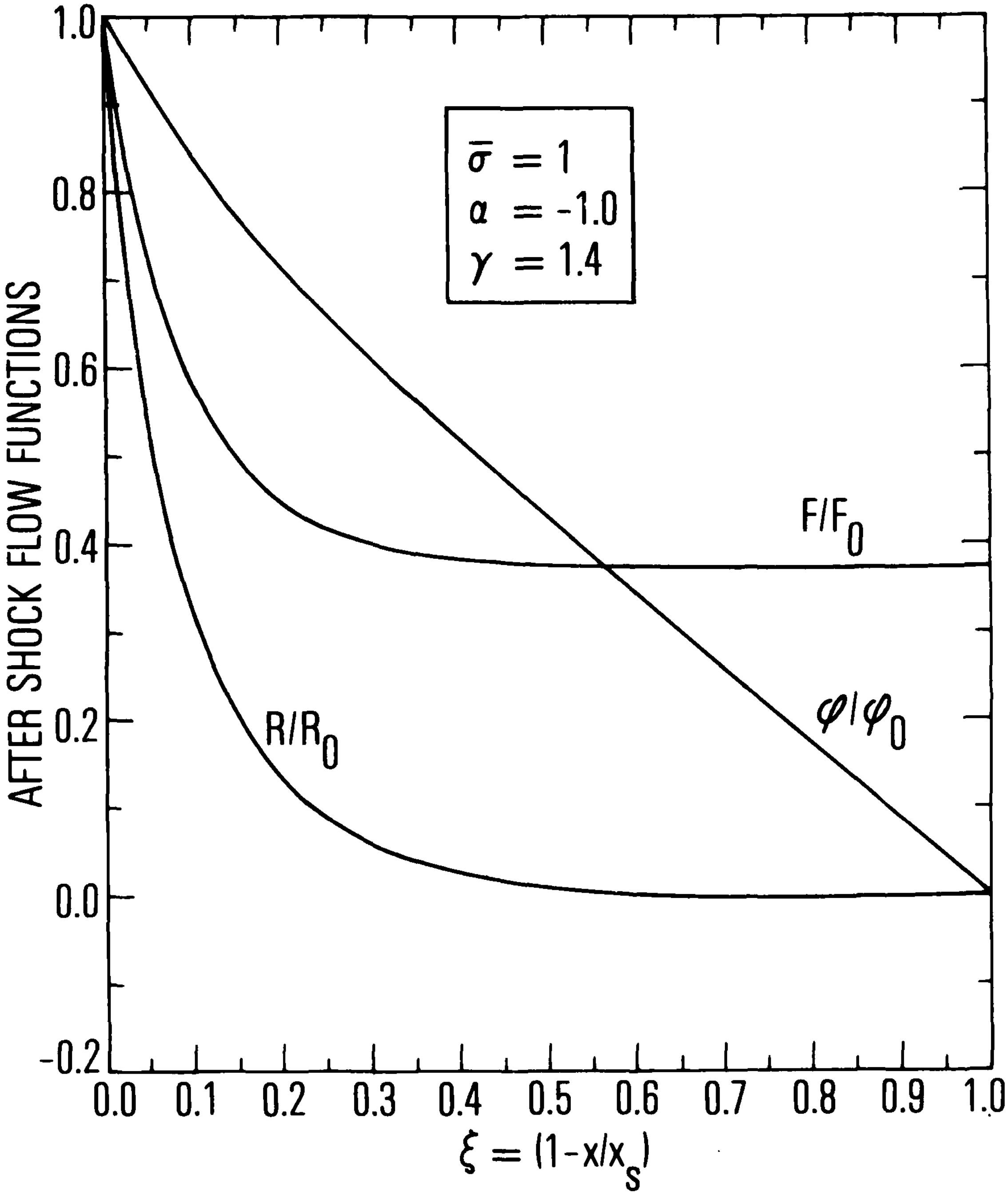

Fig. 4. Inviscid flow field, $\bar{\sigma}$ = 1

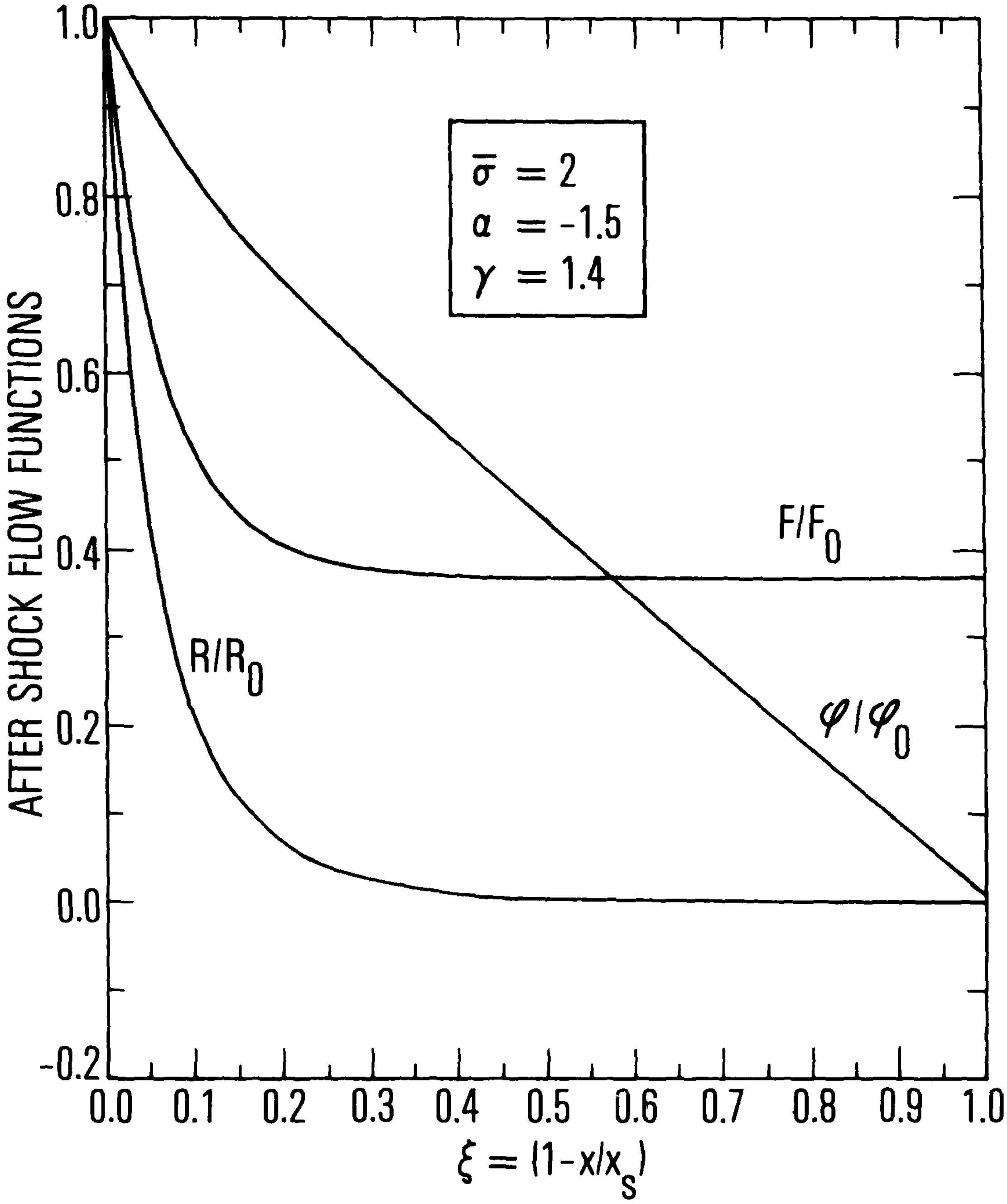

Fig. 5. Inviscid flow field, $\overline{\sigma} = 2$

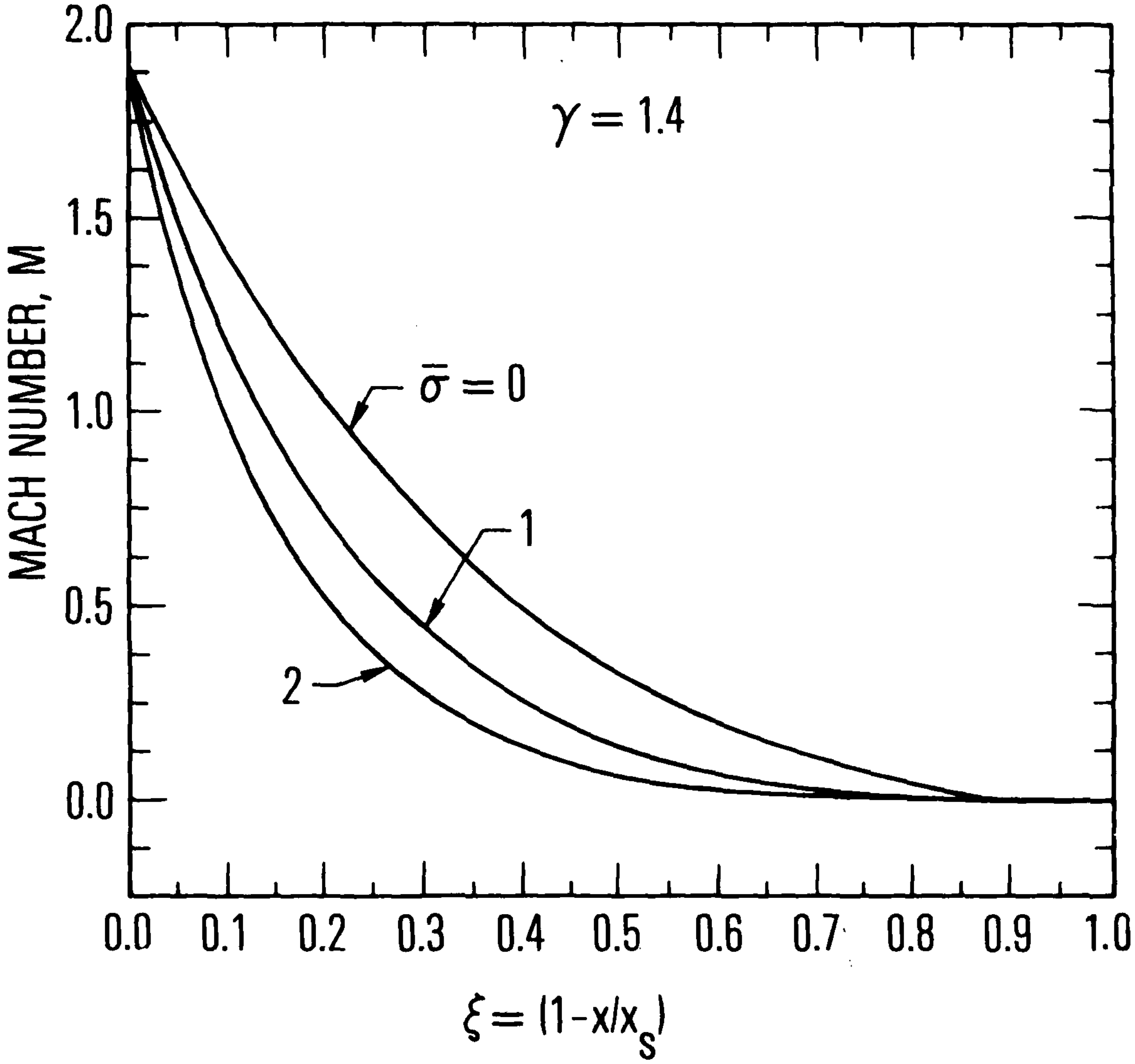

Fig. 6. Local Mach number

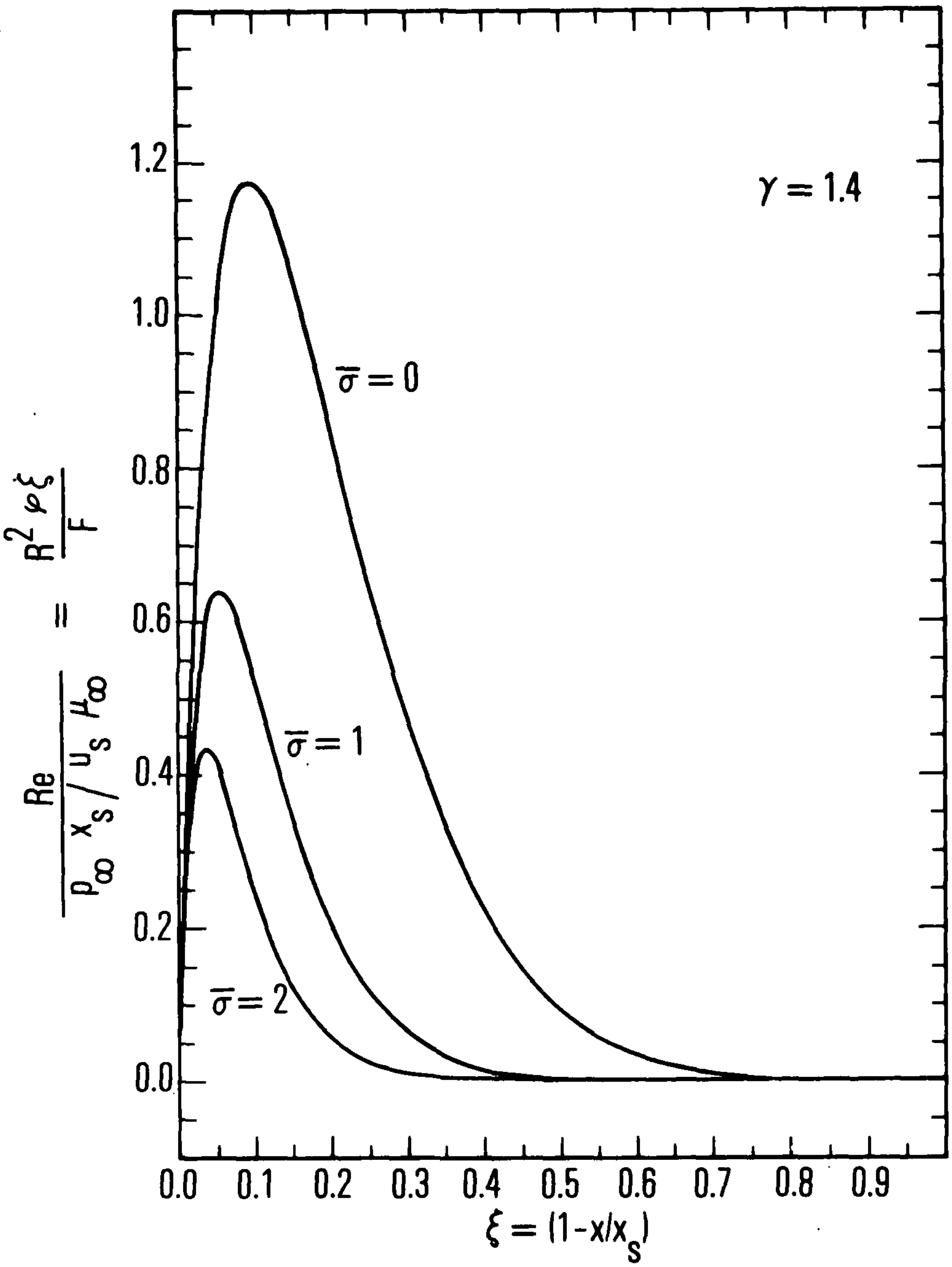

Fig. 7. Local Reynolds number

Table 4. Comparison with wall gradients of Reference 1

$\gamma = 1.4$, $Pr = 0.72$	$f'' = (0,0)$		$g'(0,0)$	
	Present	Ref. 1	Present	Ref. 1
	0.66198	0.66141	0.89864	0.89693

$\bar{\sigma}$	σ	α	$[\partial \bar{f}''/\partial \xi]_{\xi=0}$		$[\partial \bar{g}'/\partial \xi]_{\xi=0}$	
			Present	Ref. 1	Present	Ref. 1
0	0	-1/2	1.785	1.787	-1.435	-1.437
1	0	-1	2.597	2.601	-3.025	-3.040
1	1	-1	3.775	3.788	-1.814	-1.816
2	1	-3/2	4.576	4.601	-3.405	-3.419

$$\bar{f}'' = \frac{f''(\xi,0)}{f''(0,0)} \qquad \bar{g}' = \frac{g'(\xi,0)}{g'(0,0)}$$

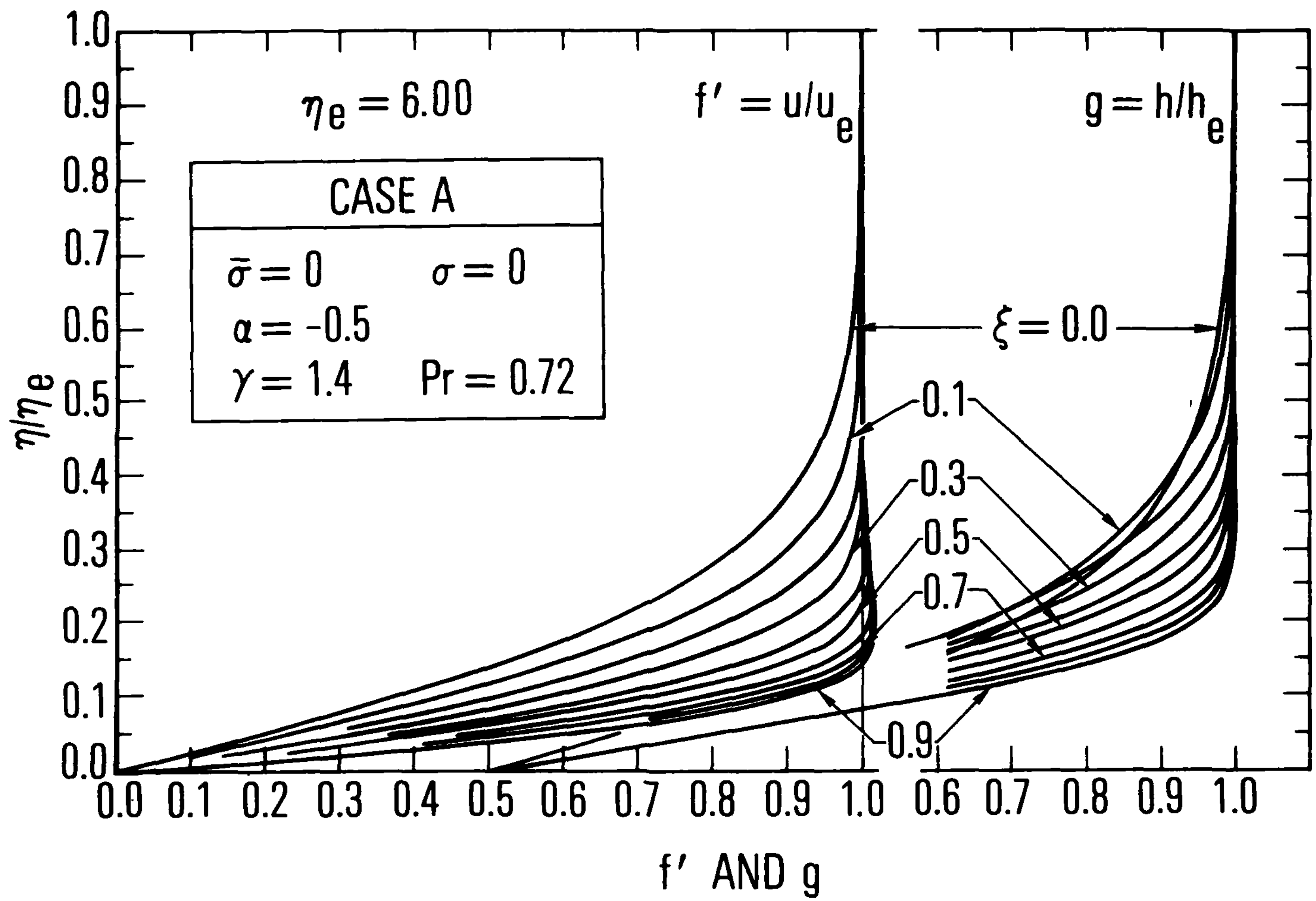

Fig. 8. Composite profile summary, Case A

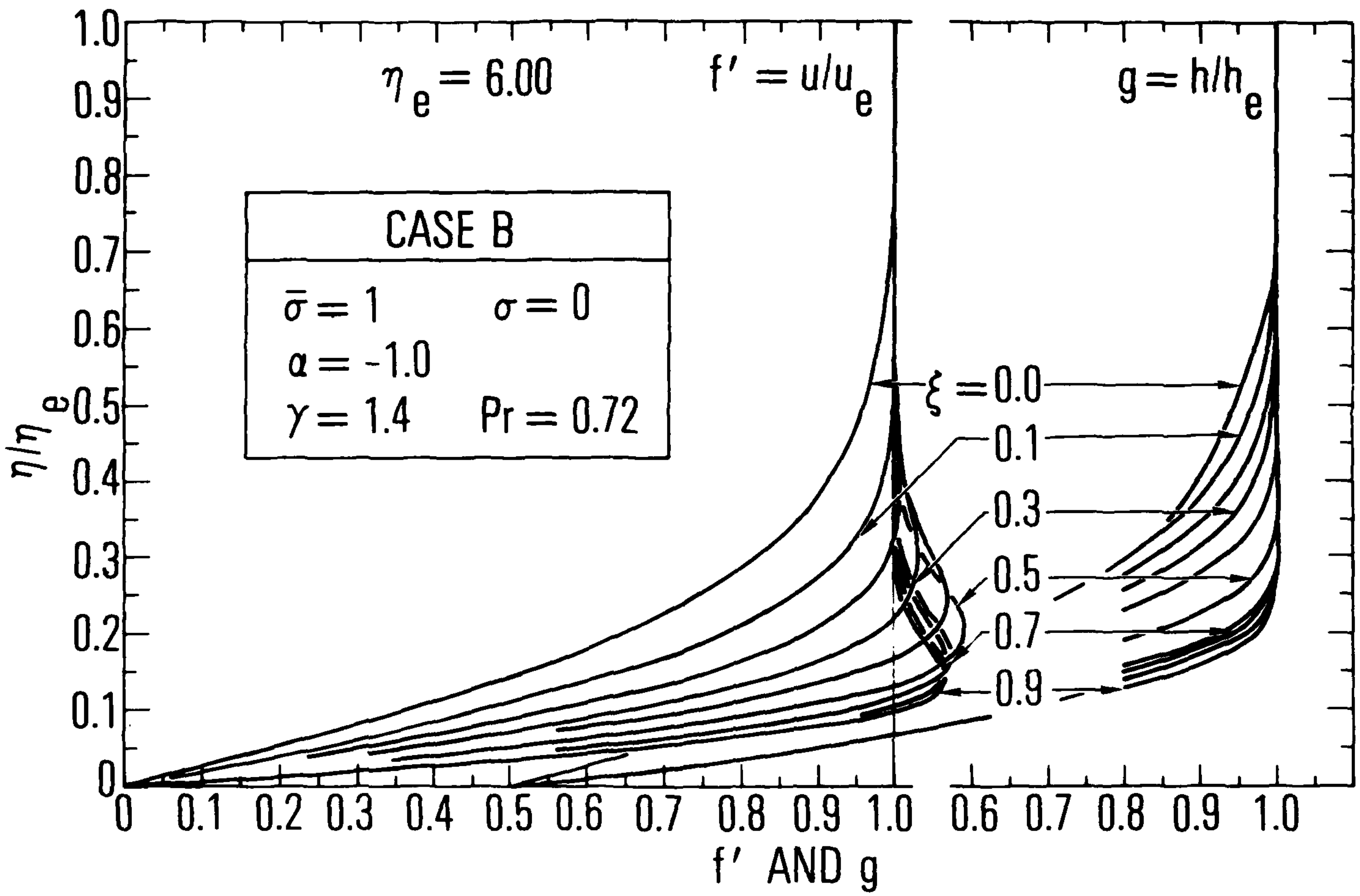

Fig. 8. Composite profile summary, Case B

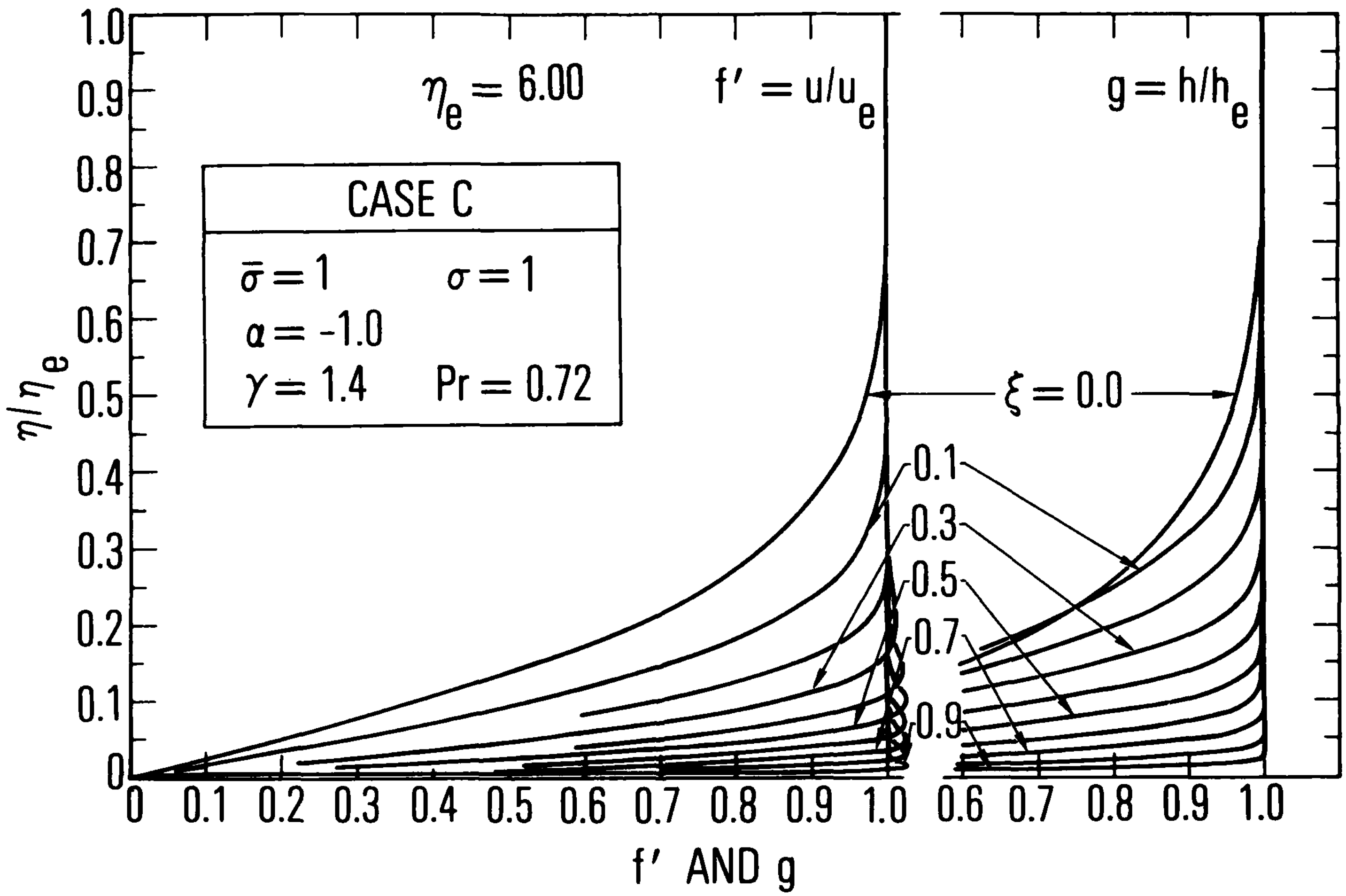

Fig. 8. Composite profile summary, Case C

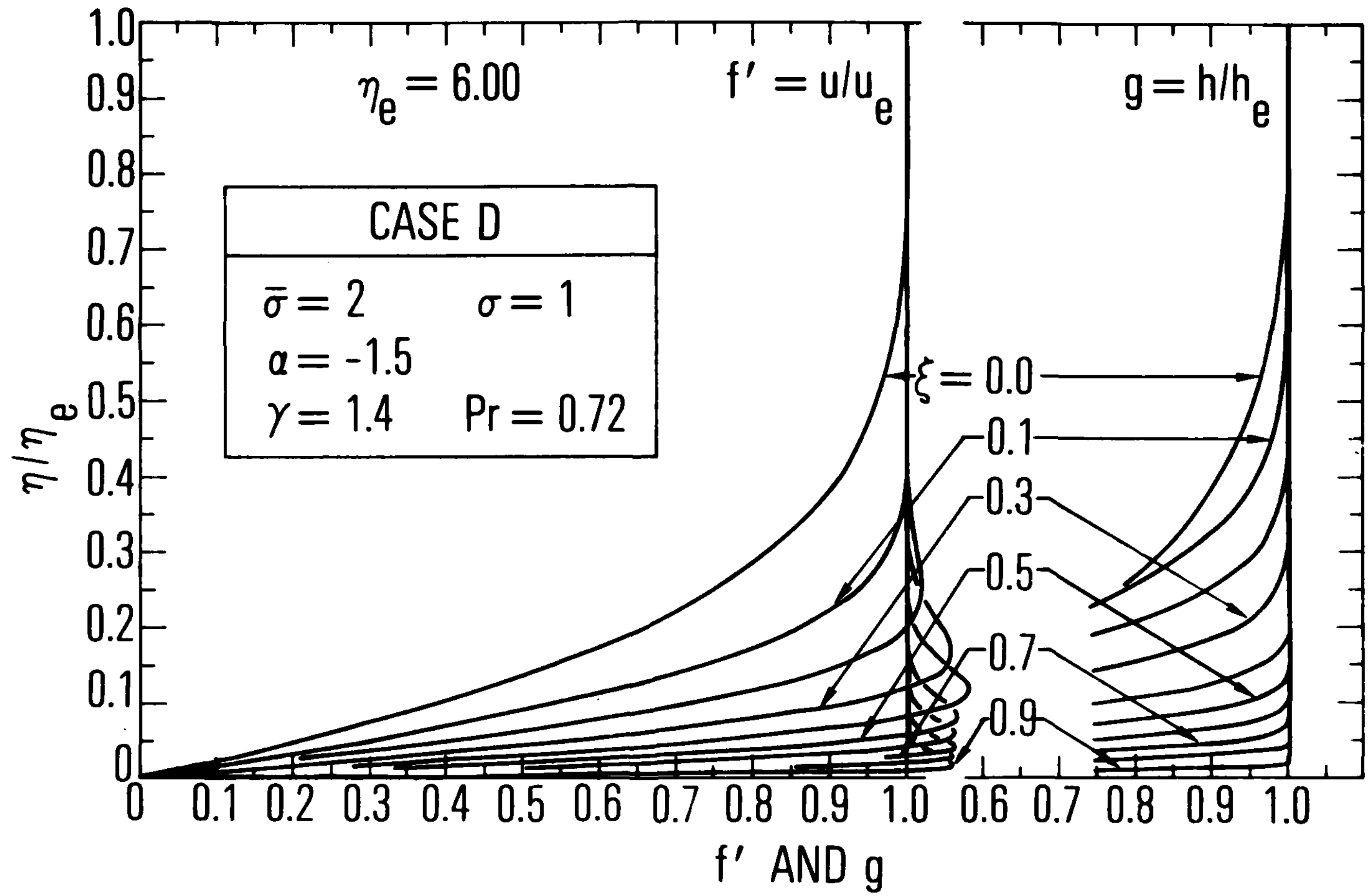

Fig. 8. Composite profile summary, Case D

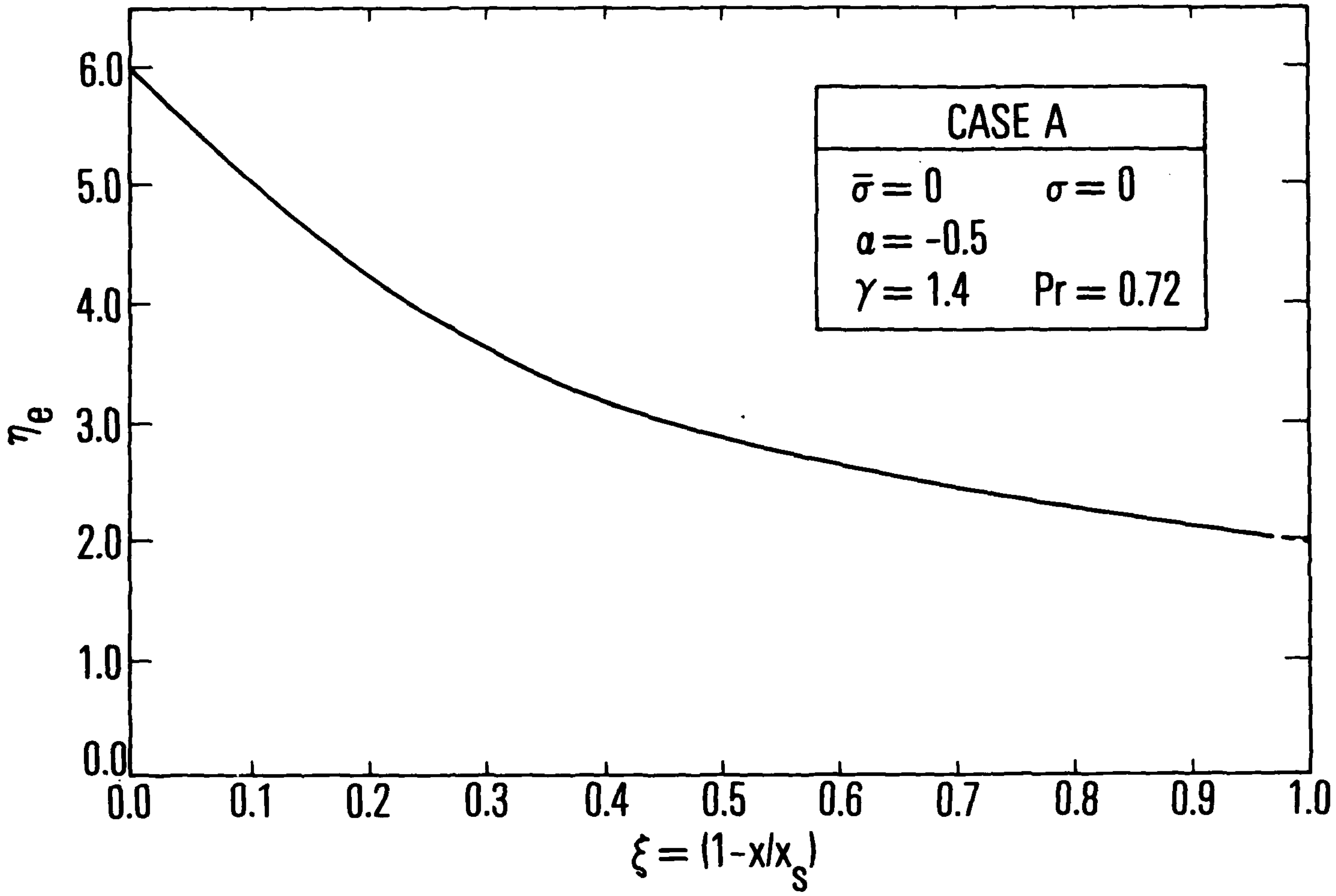

Fig. 9. Approximate η_e distribution, Case A

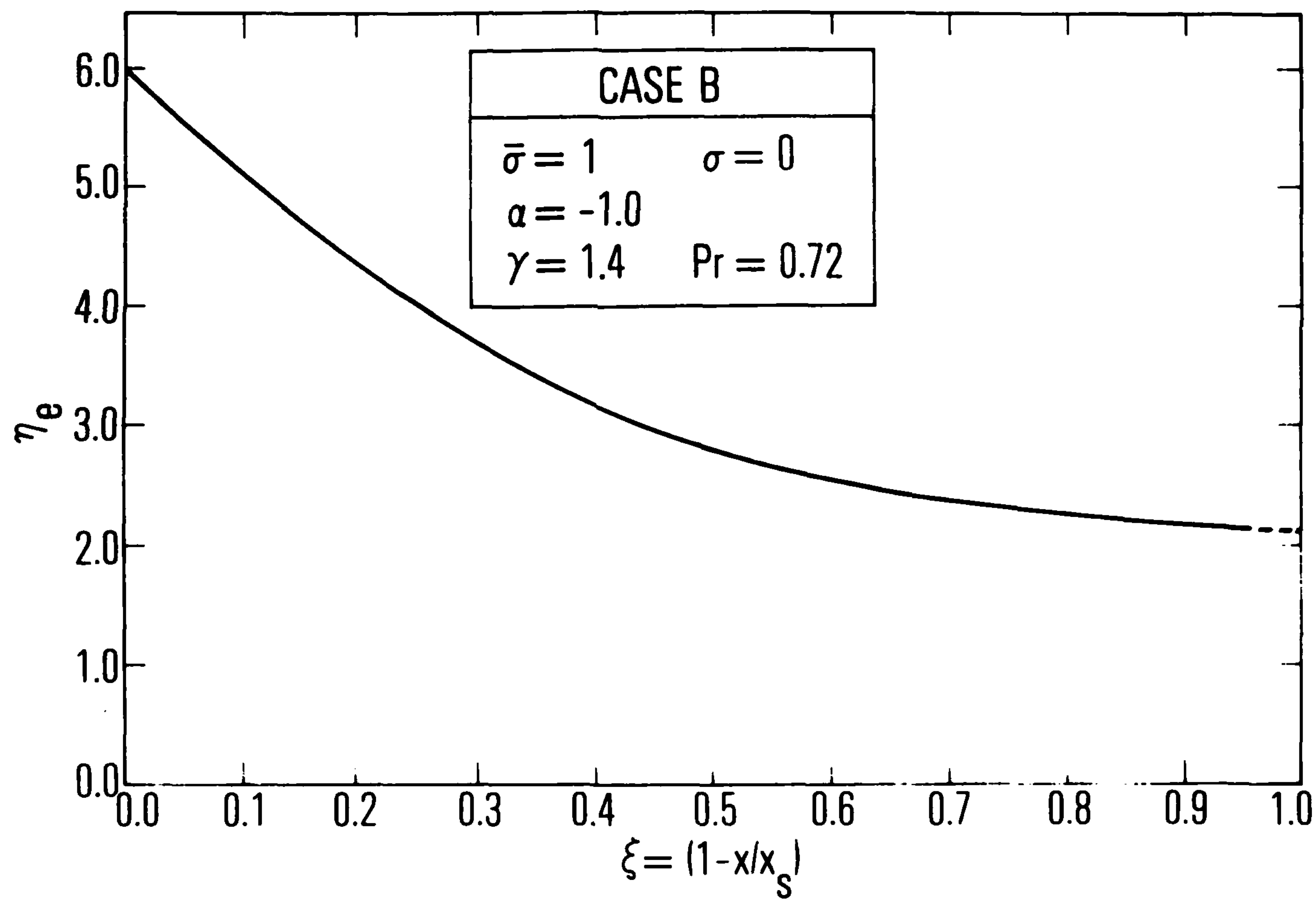

Fig. 9. Approximate η_e distribution, Case B

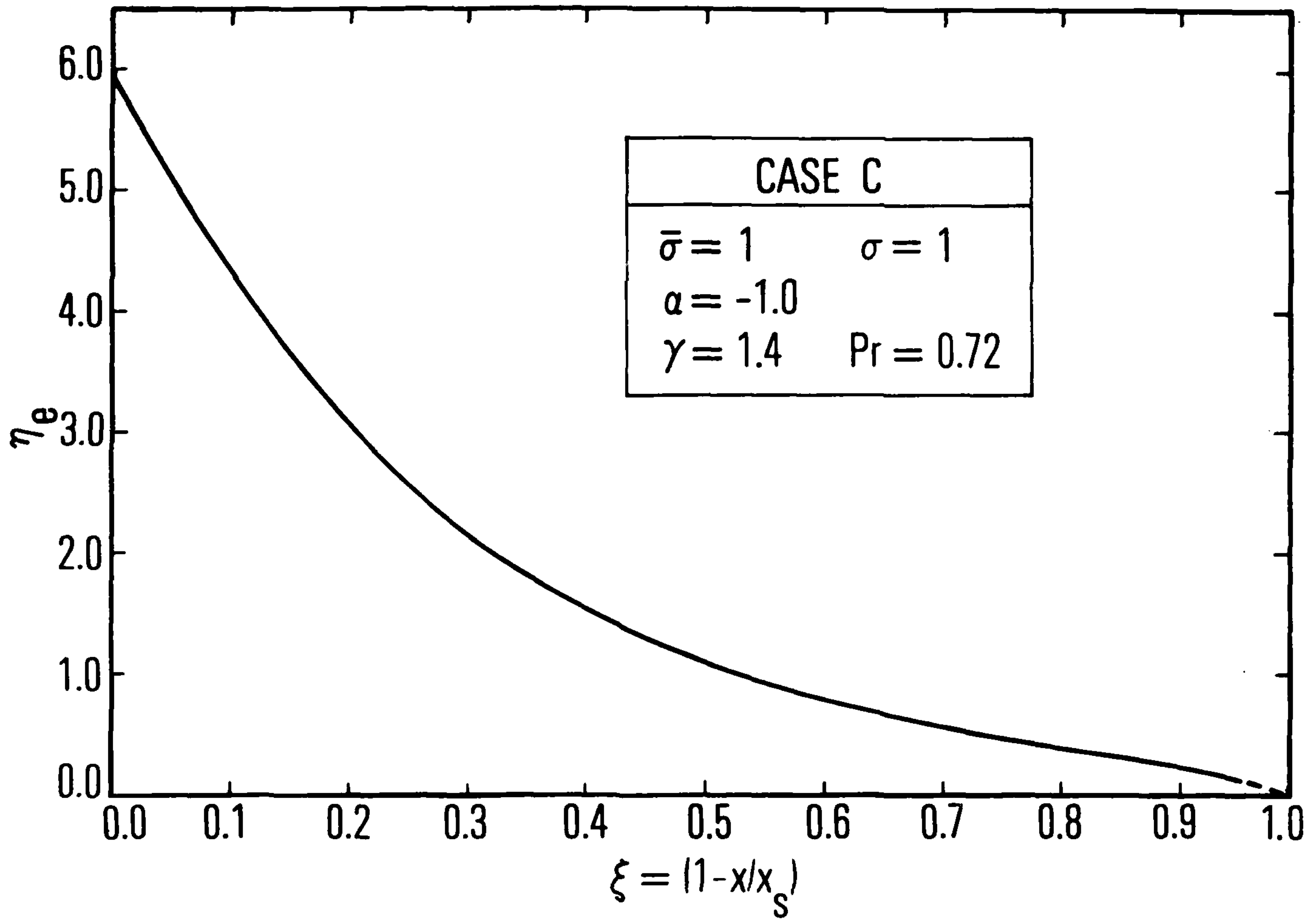

Fig. 9. Approximate η_e distribution, Case C

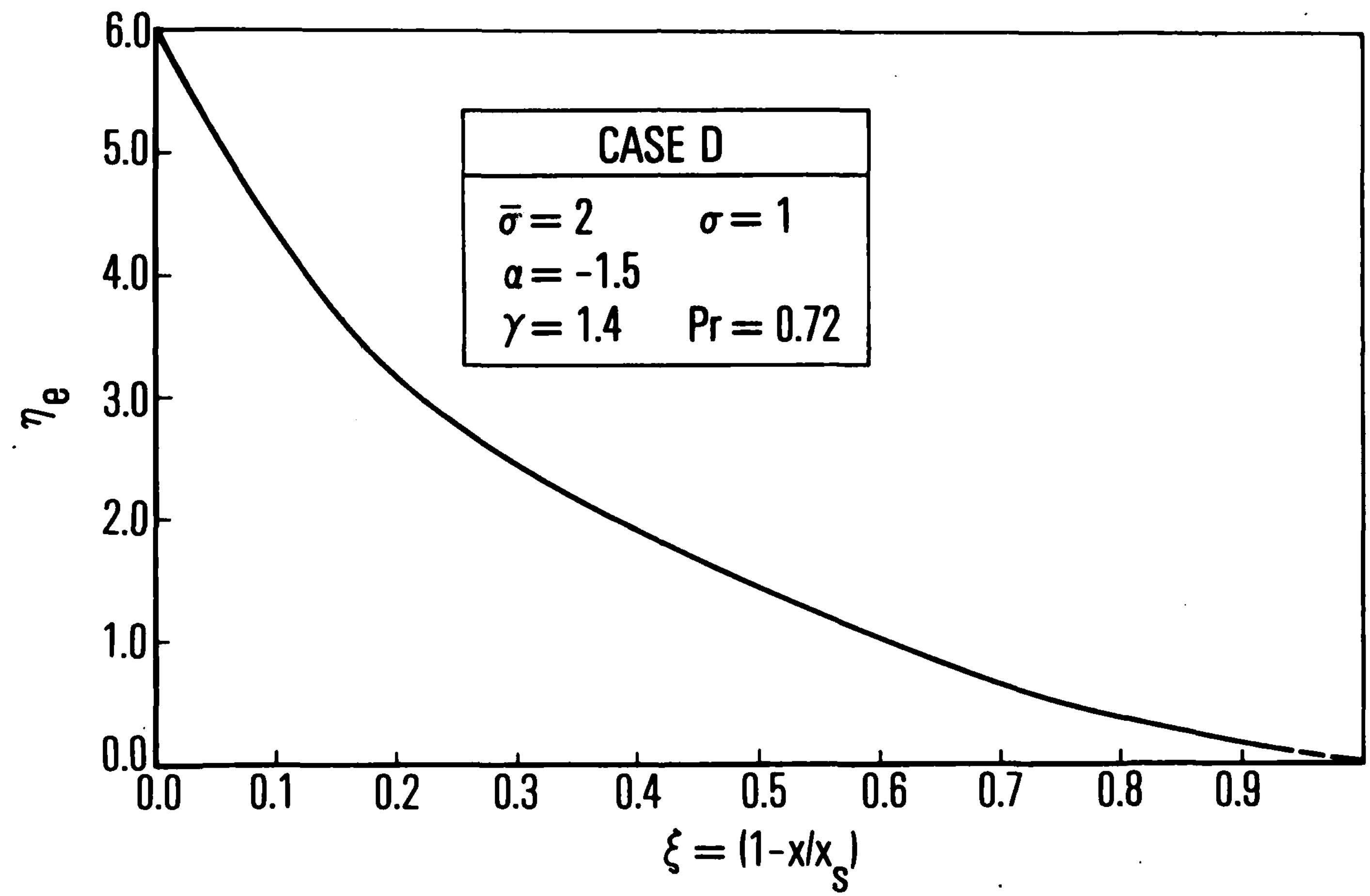

Fig. 9. Approximate η_e distribution, Case D

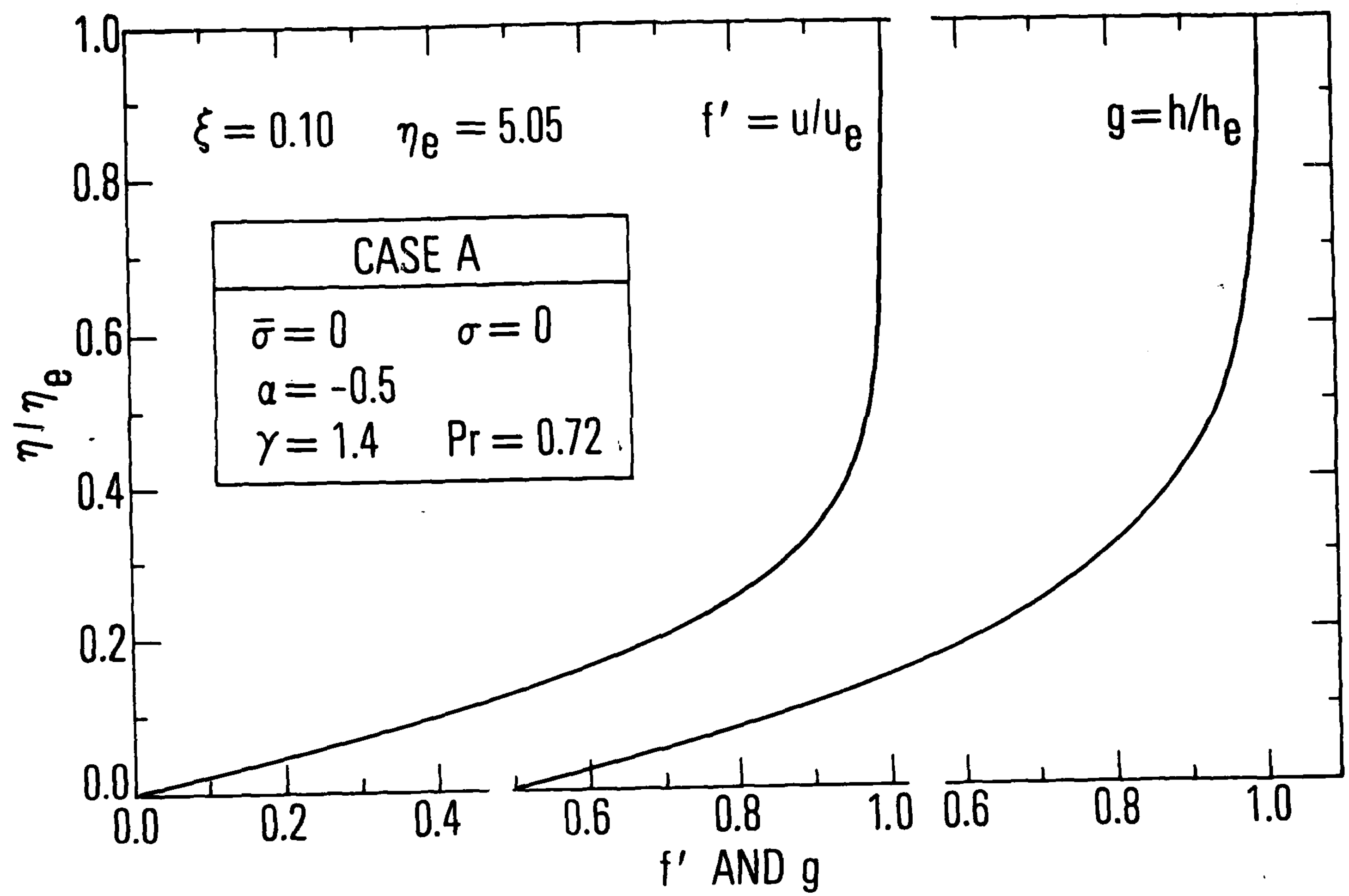

Fig. 10A-1. Detailed boundary-layer profiles, $\zeta = 0.10$, Case A

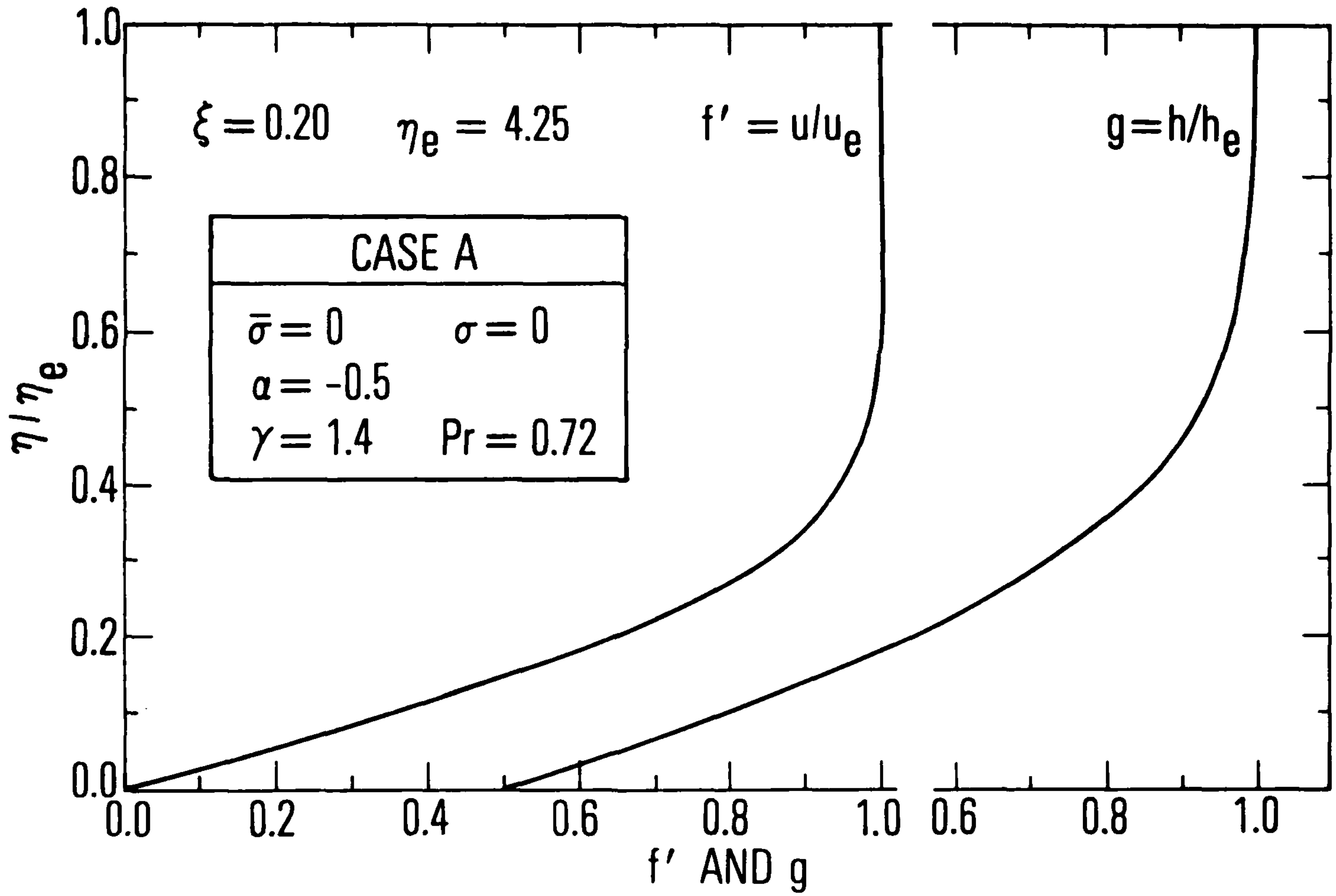

Fig. 10A-2. Detailed boundary-layer profiles, $\zeta = 0.20$, Case A

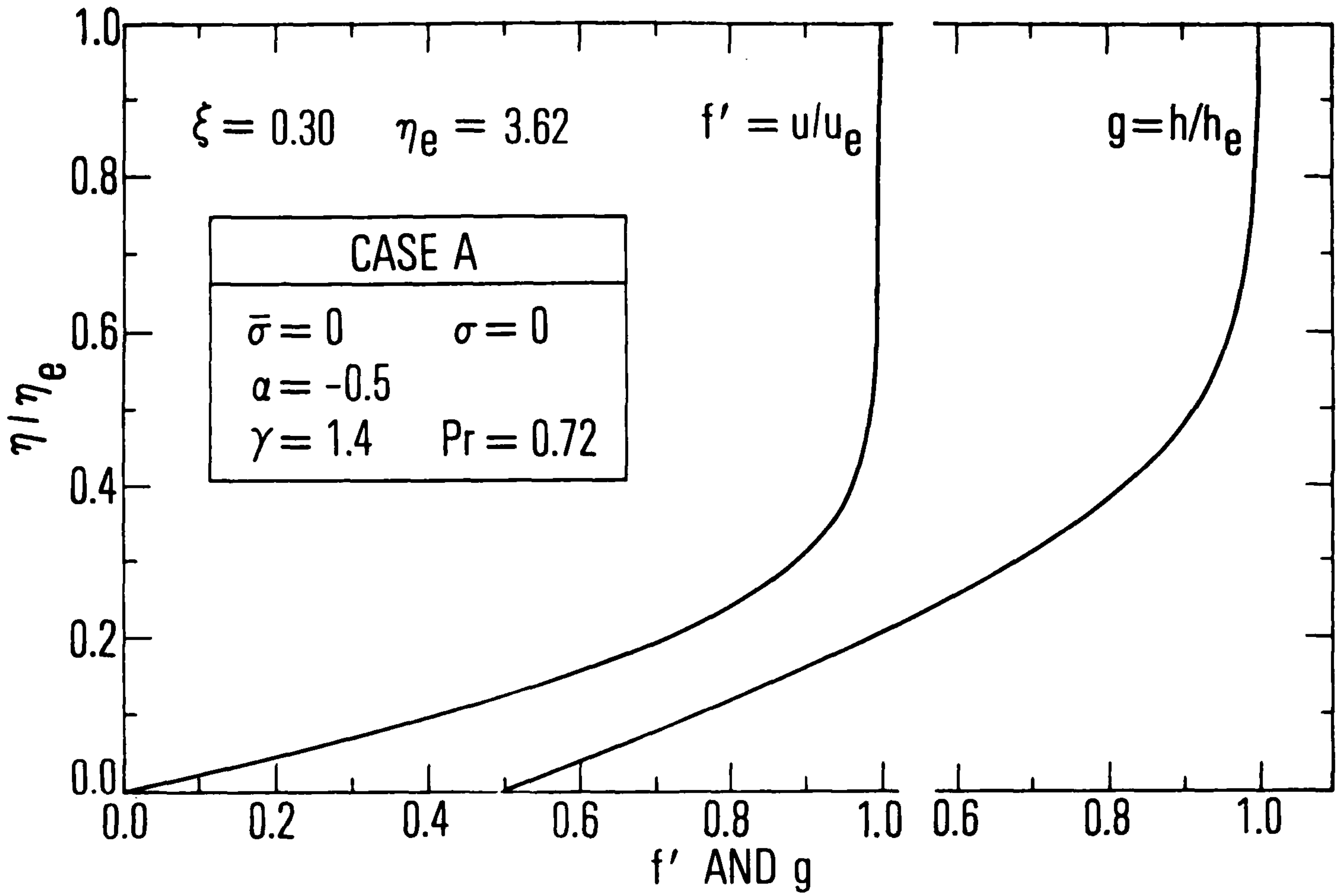

Fig. 10A-3. Detailed boundary-layer profiles, $\zeta = 0.30$, Case A

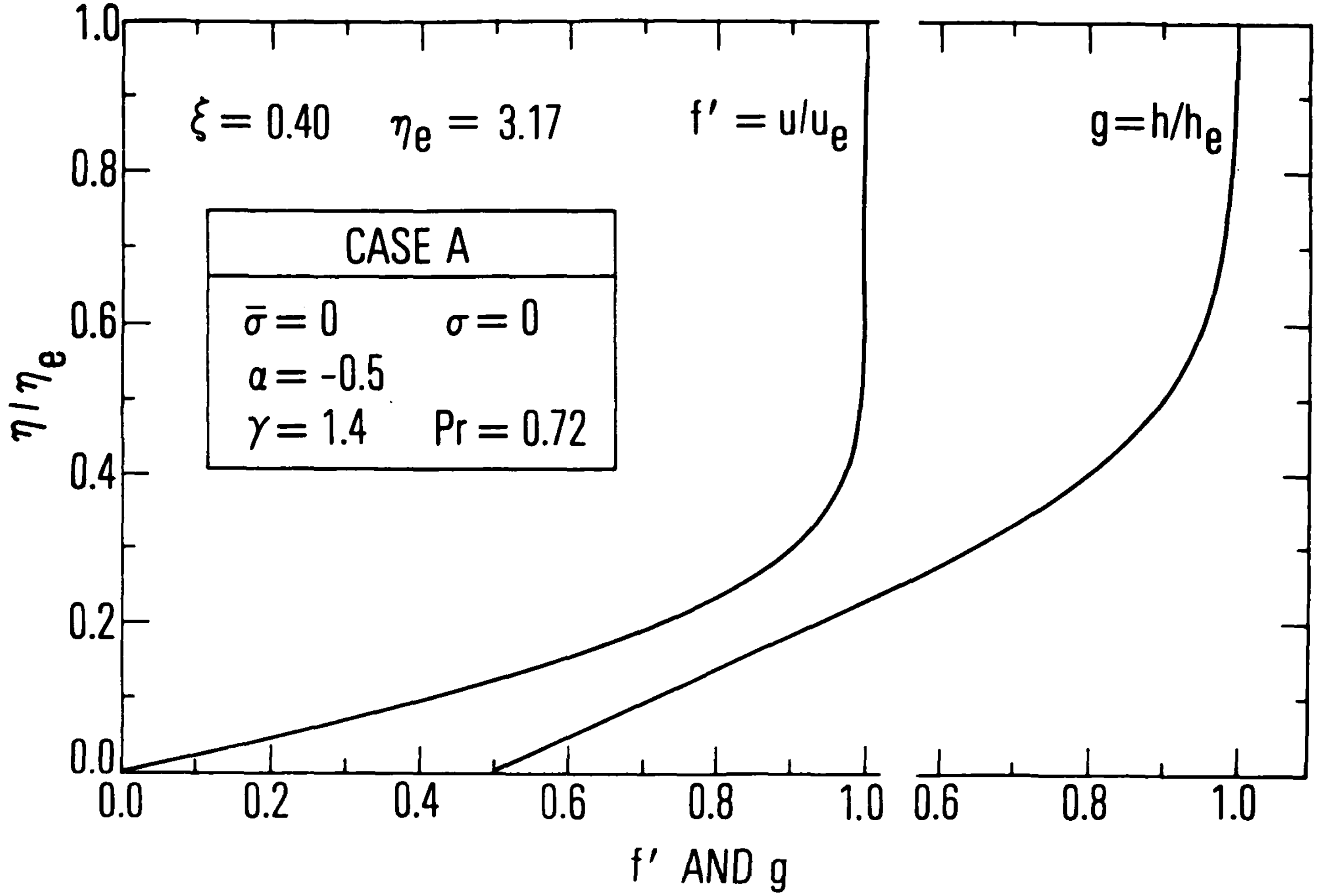

Fig. 10A-4. Detailed boundary-layer profiles, $\zeta = 0.40$, Case A

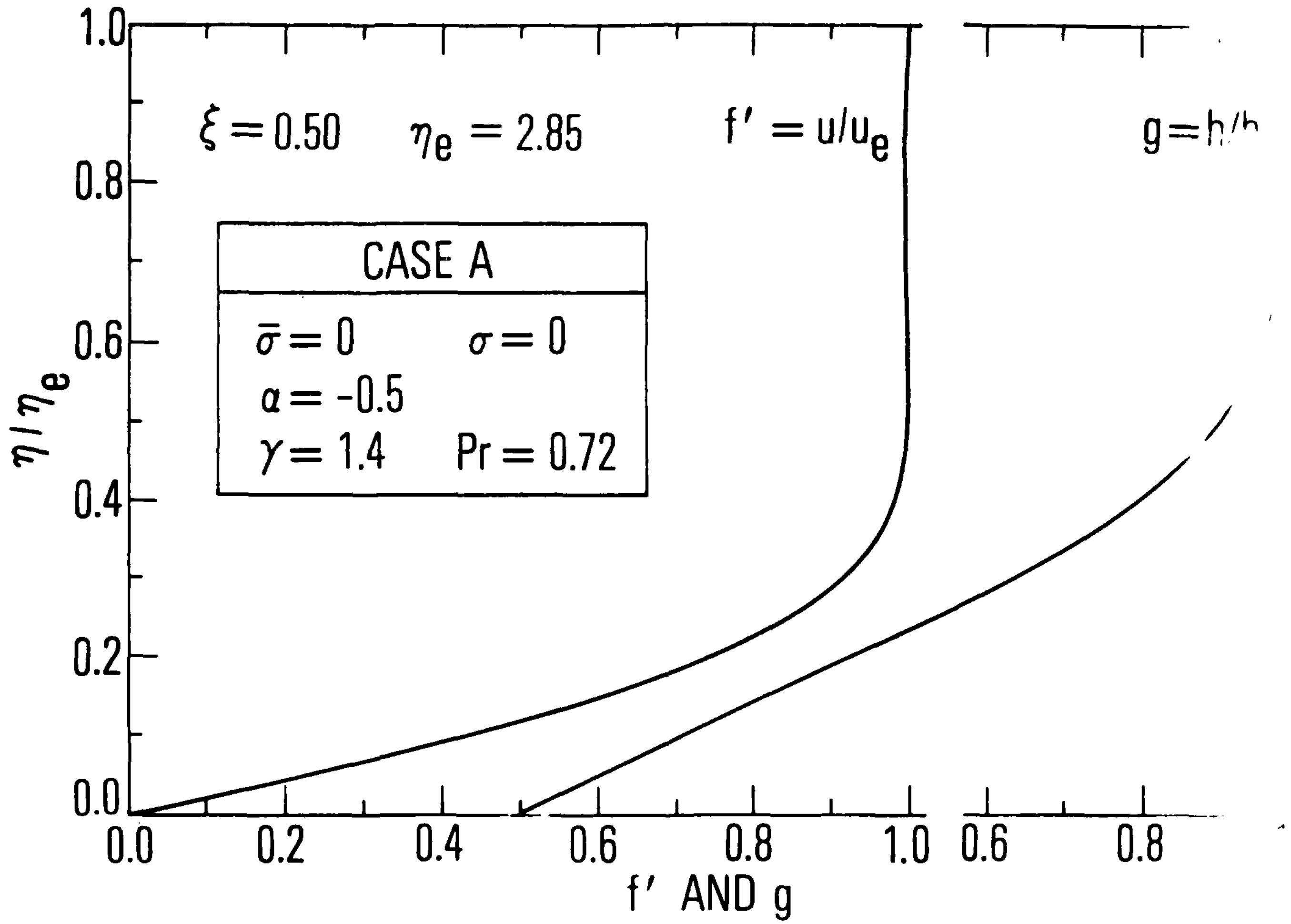

Fig. 10A-5. Detailed boundary-layer profiles, $\zeta = 0.50$, Case A

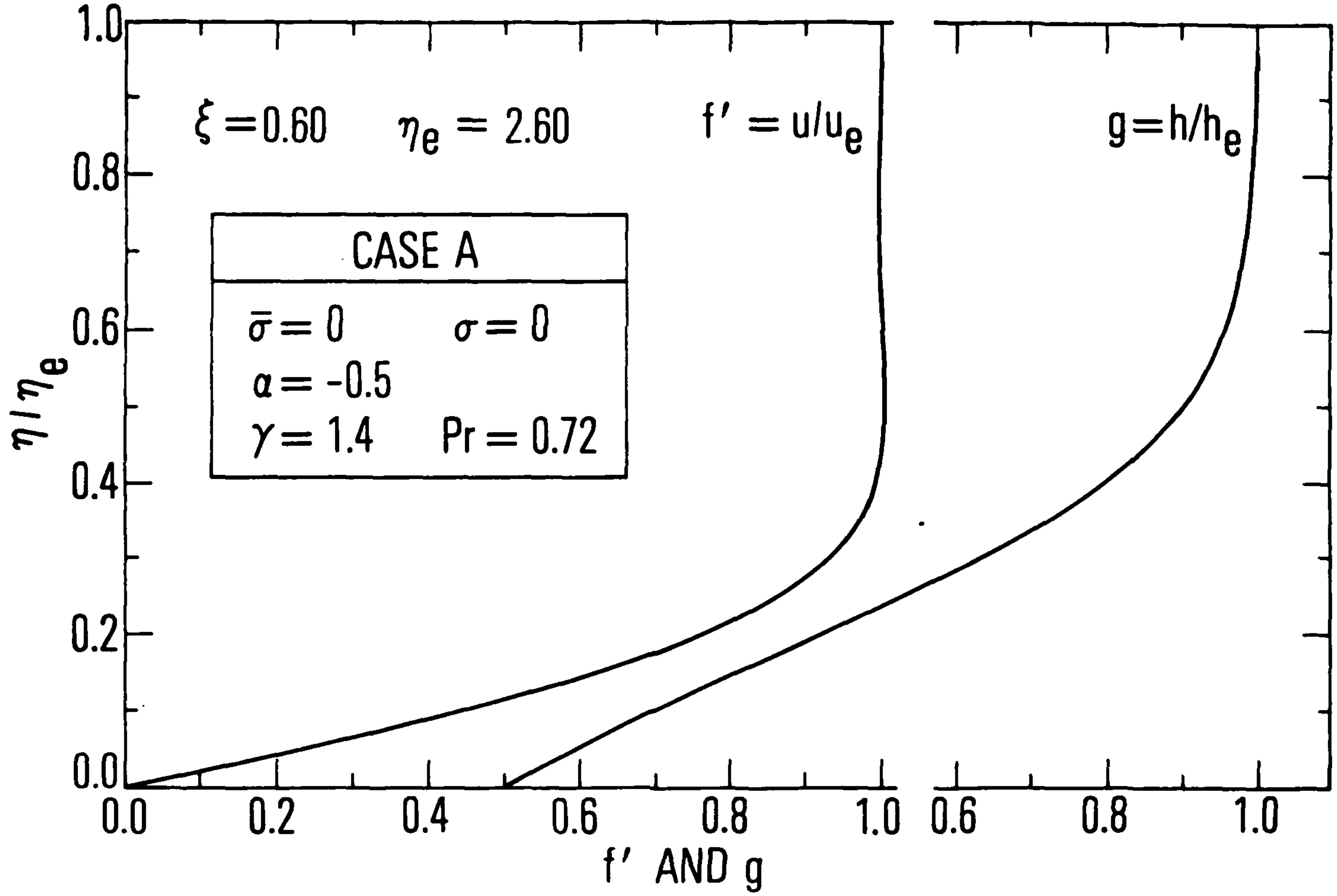

Fig. 10A-6. Detailed boundary-layer profiles, $\zeta = 0.60$, Case A

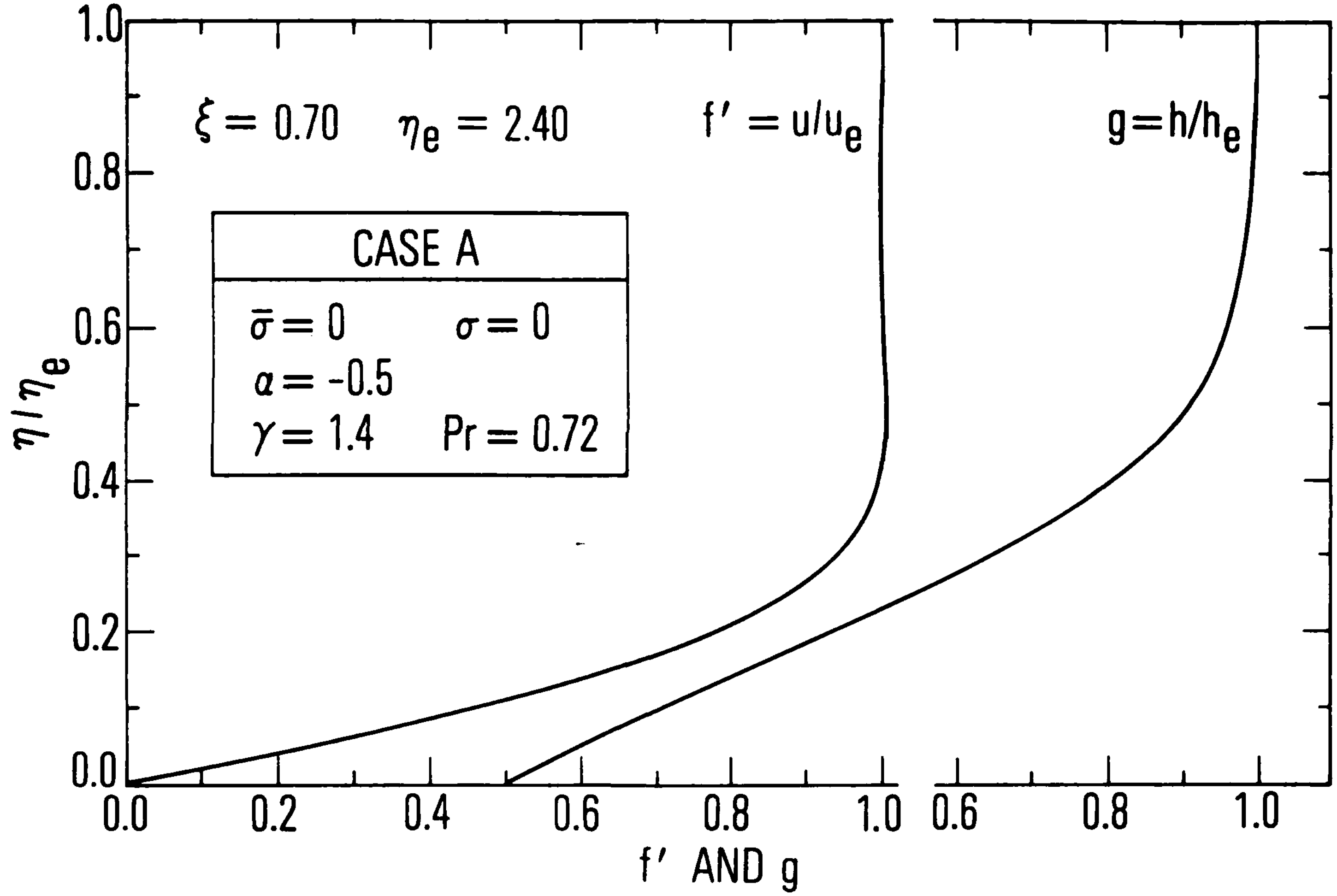

Fig. 10A-7. Detailed boundary-layer profiles, $\zeta = 0.70$, Case A

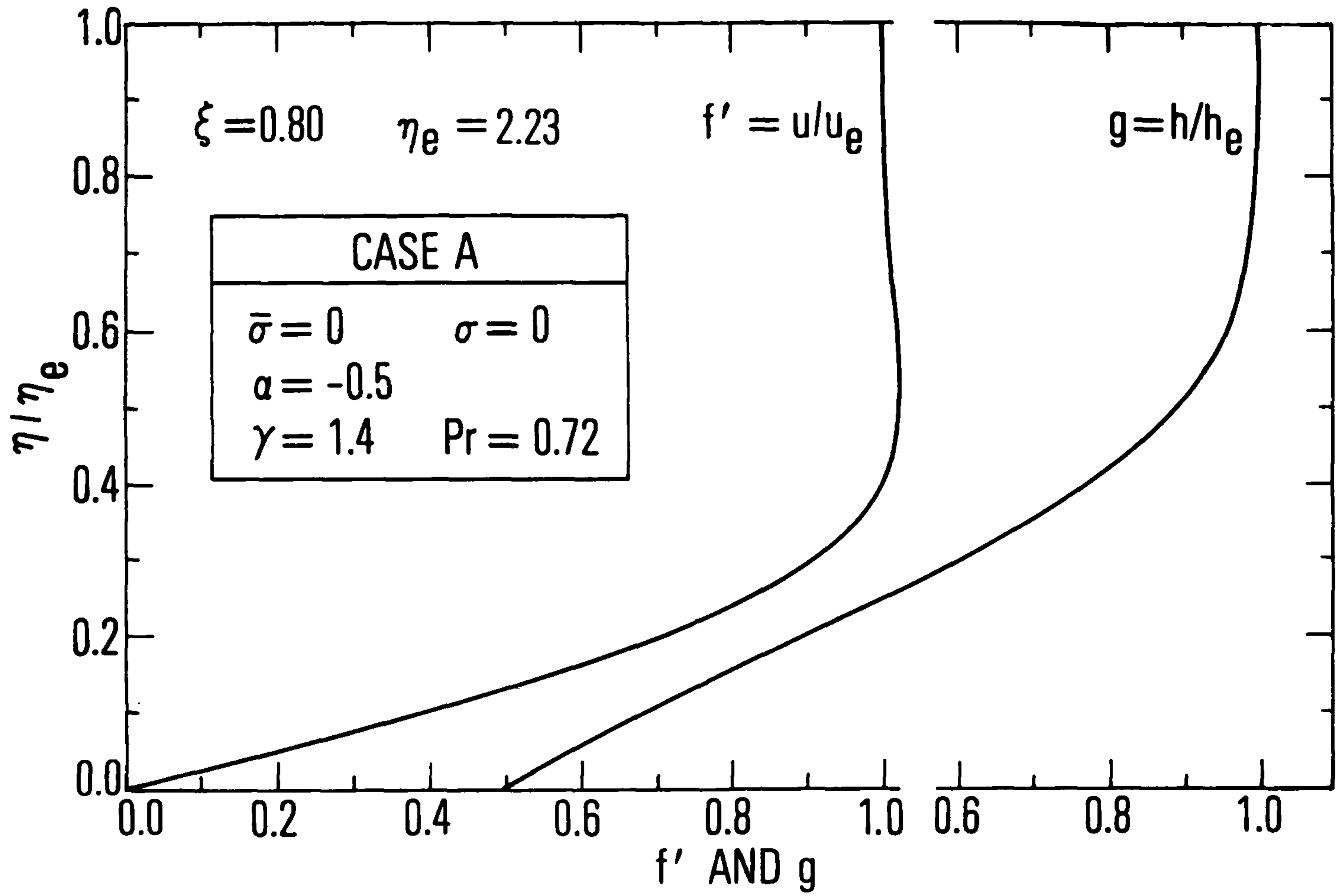

Fig. 10A-8. Detailed boundary-layer profiles, ζ = 0.80, Case A

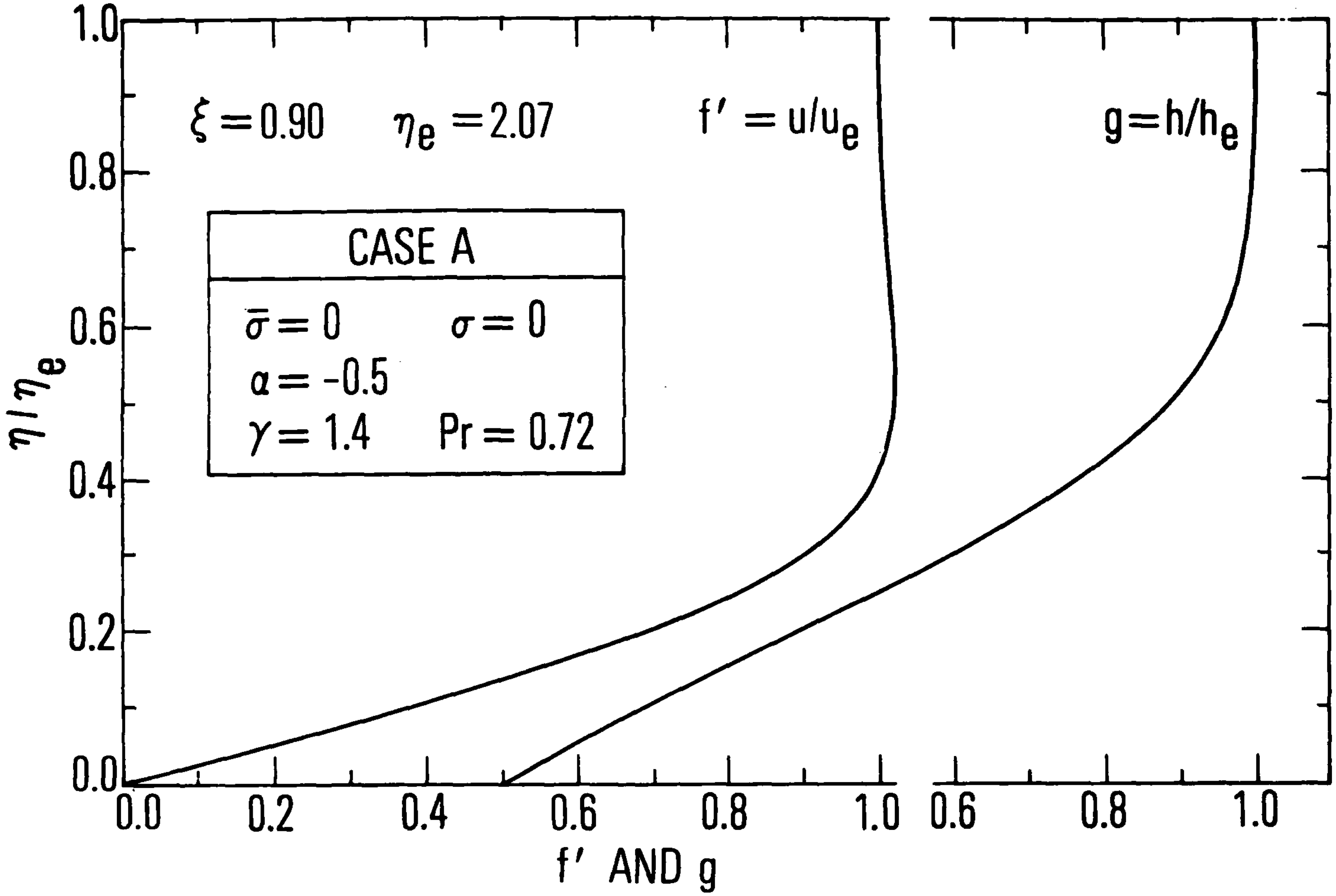

Fig. 10A-9. Detailed boundary-layer profiles, $\zeta = 0.90$, Case A

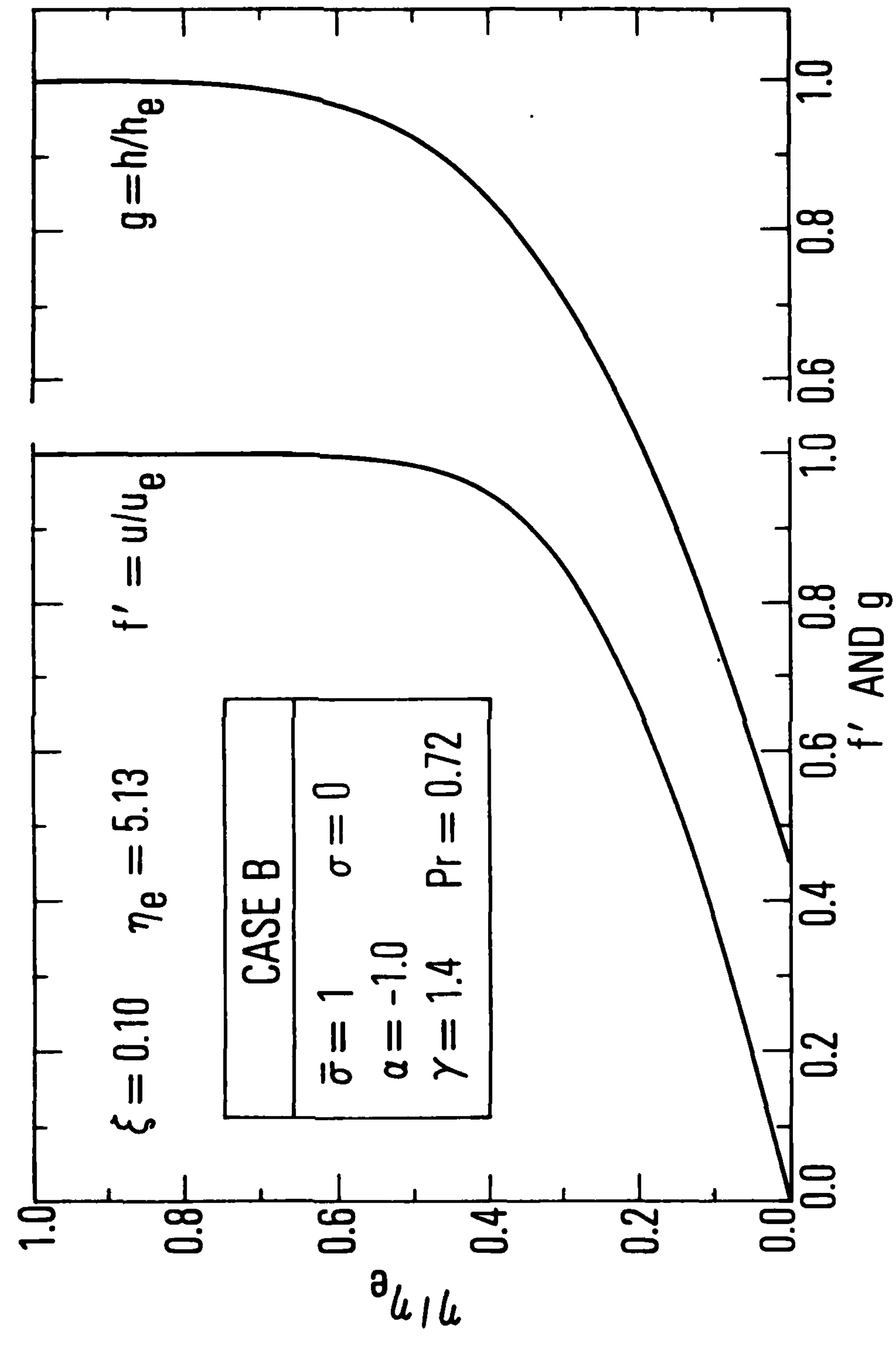

Fig. 10B-1. Detailed boundary-layer profiles, $\xi = 0.10$, Case B

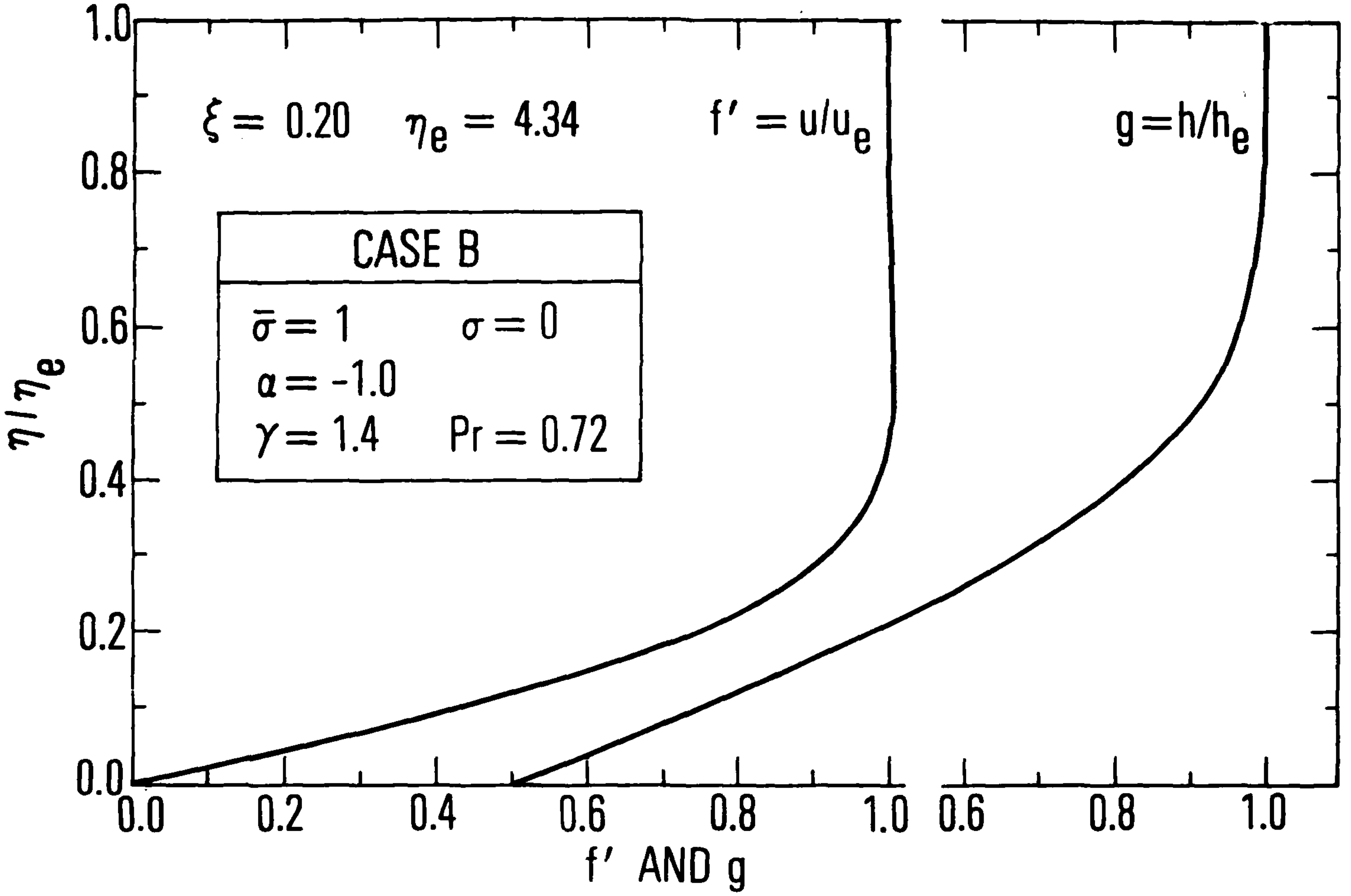

Fig. 10B-2. Detailed boundary-layer profiles, $\zeta = 0.20$, Case B

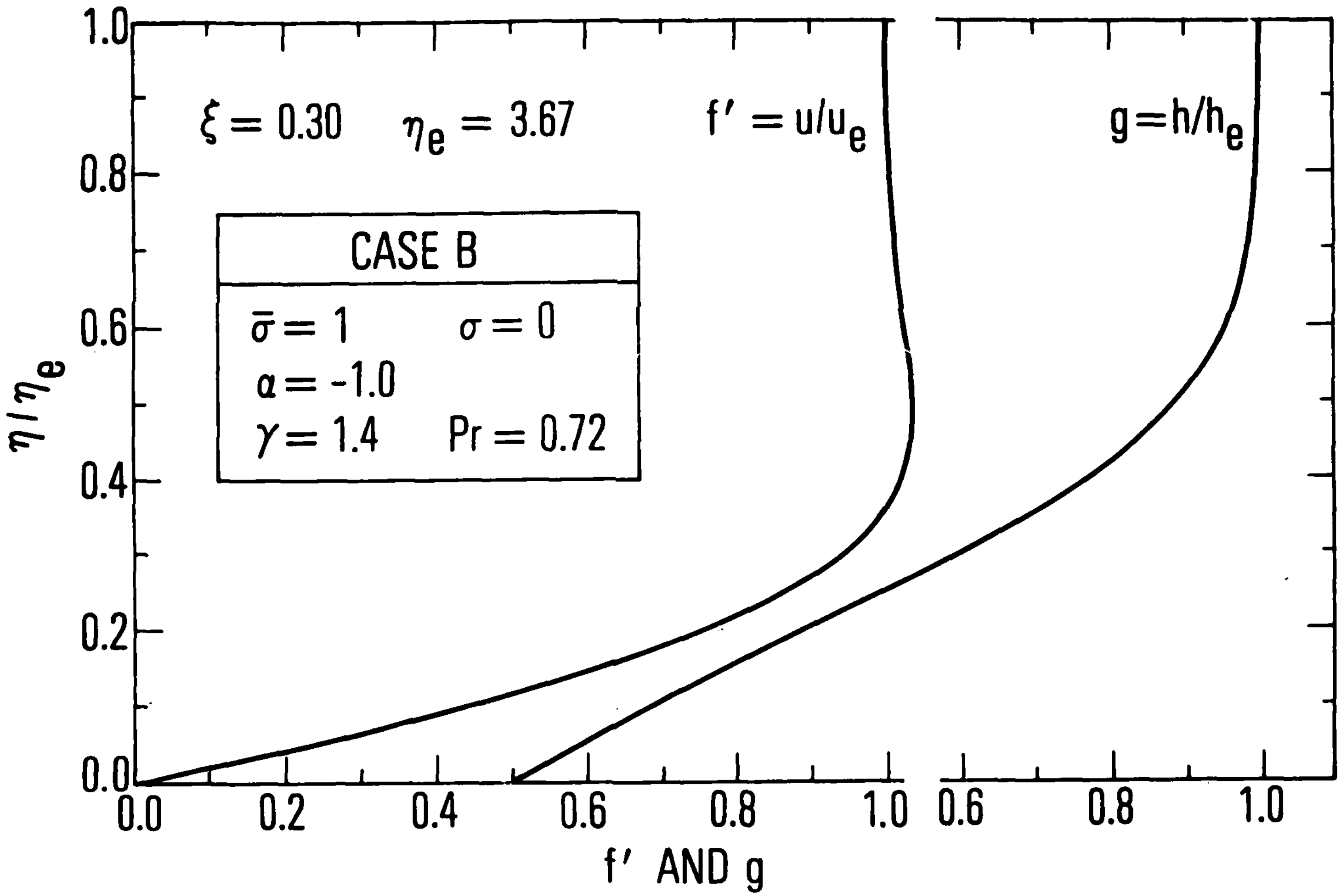

Fig. 10B-3. Detailed boundary-layer profiles, $\zeta = 0.30$, Case B

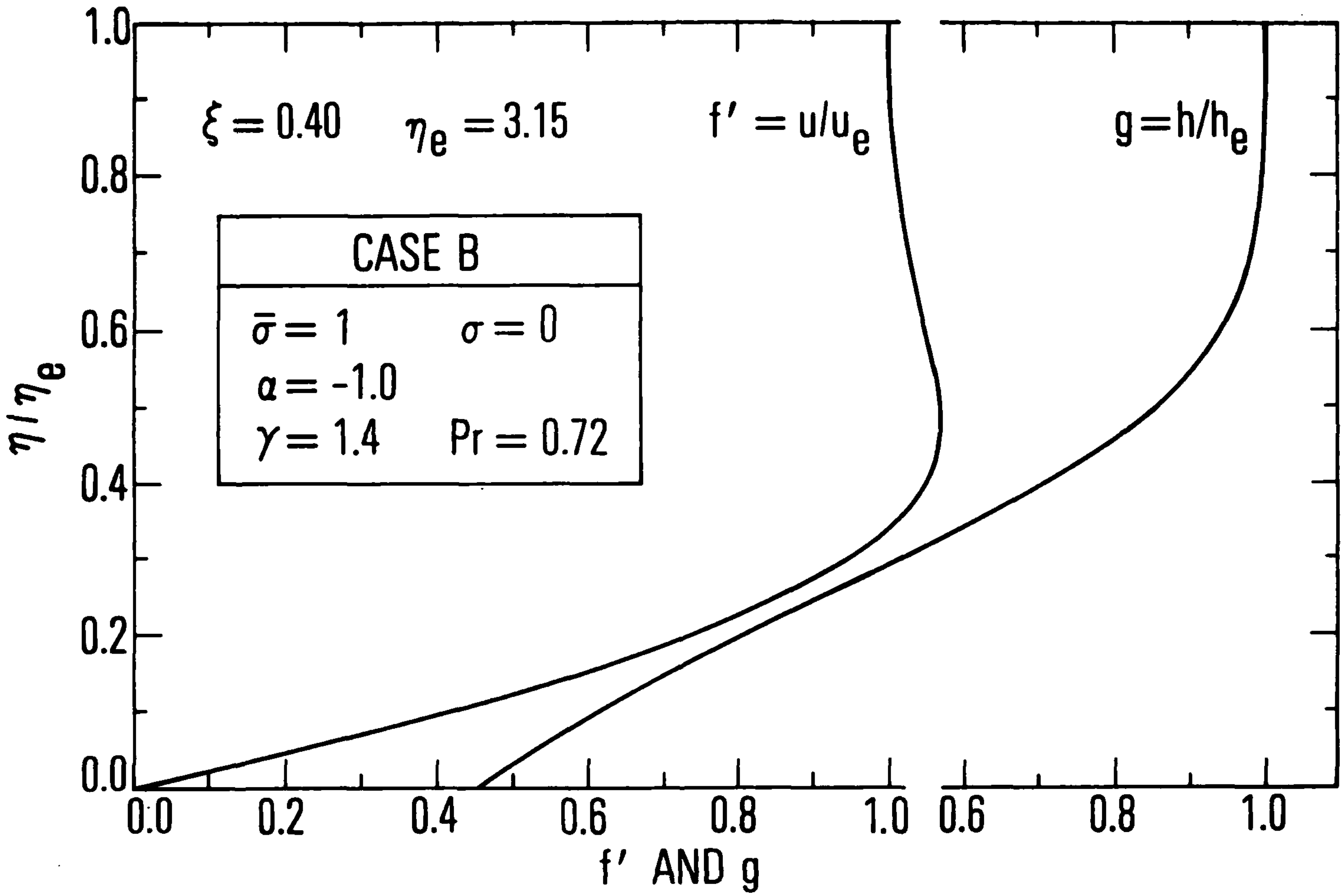

Fig. 10B-4. Detailed boundary-layer profiles, $\zeta = 0.40$, Case B

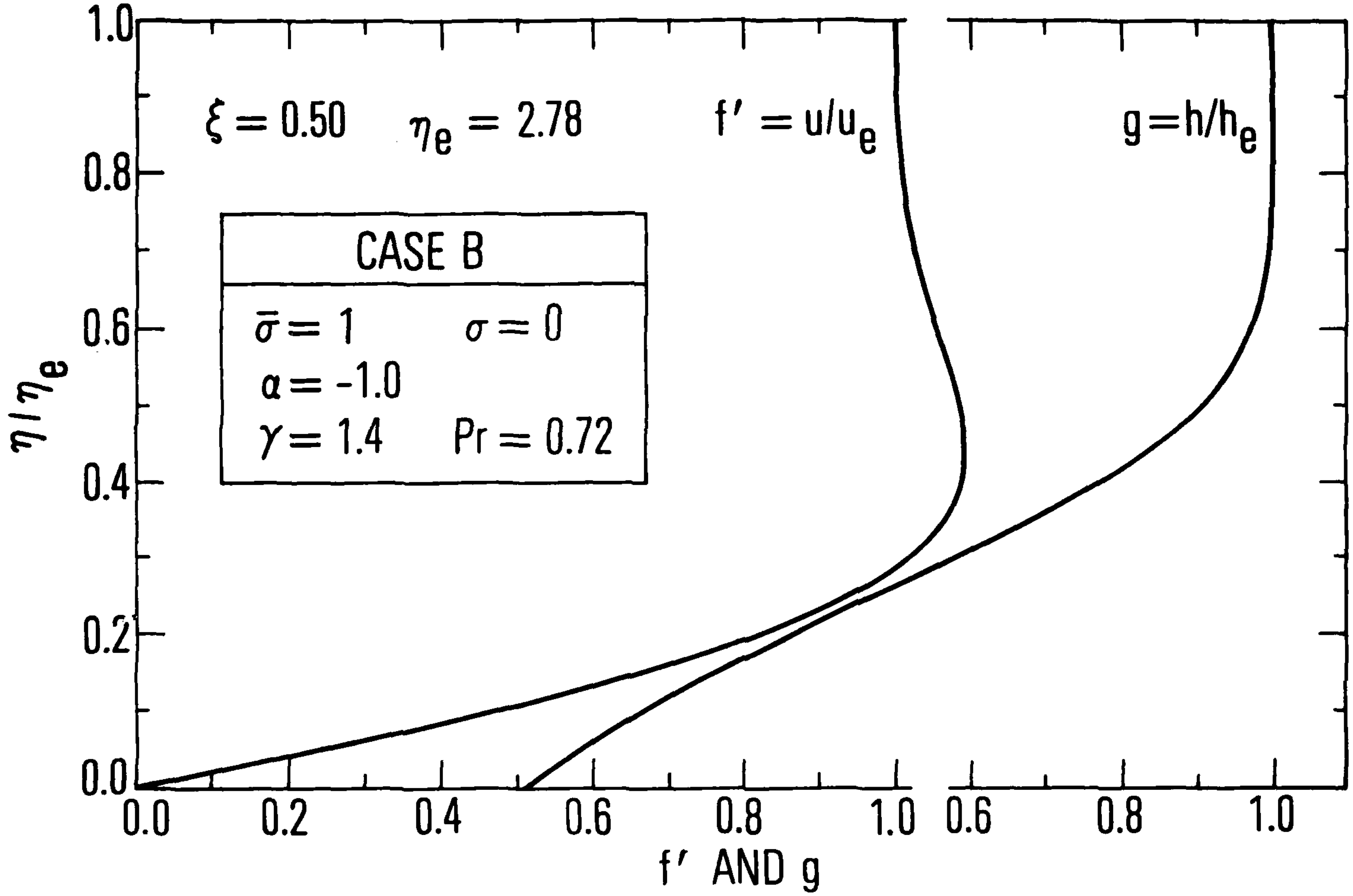

Fig. 10B-5. Detailed boundary-layer profiles, $\zeta = 0.50$, Case B

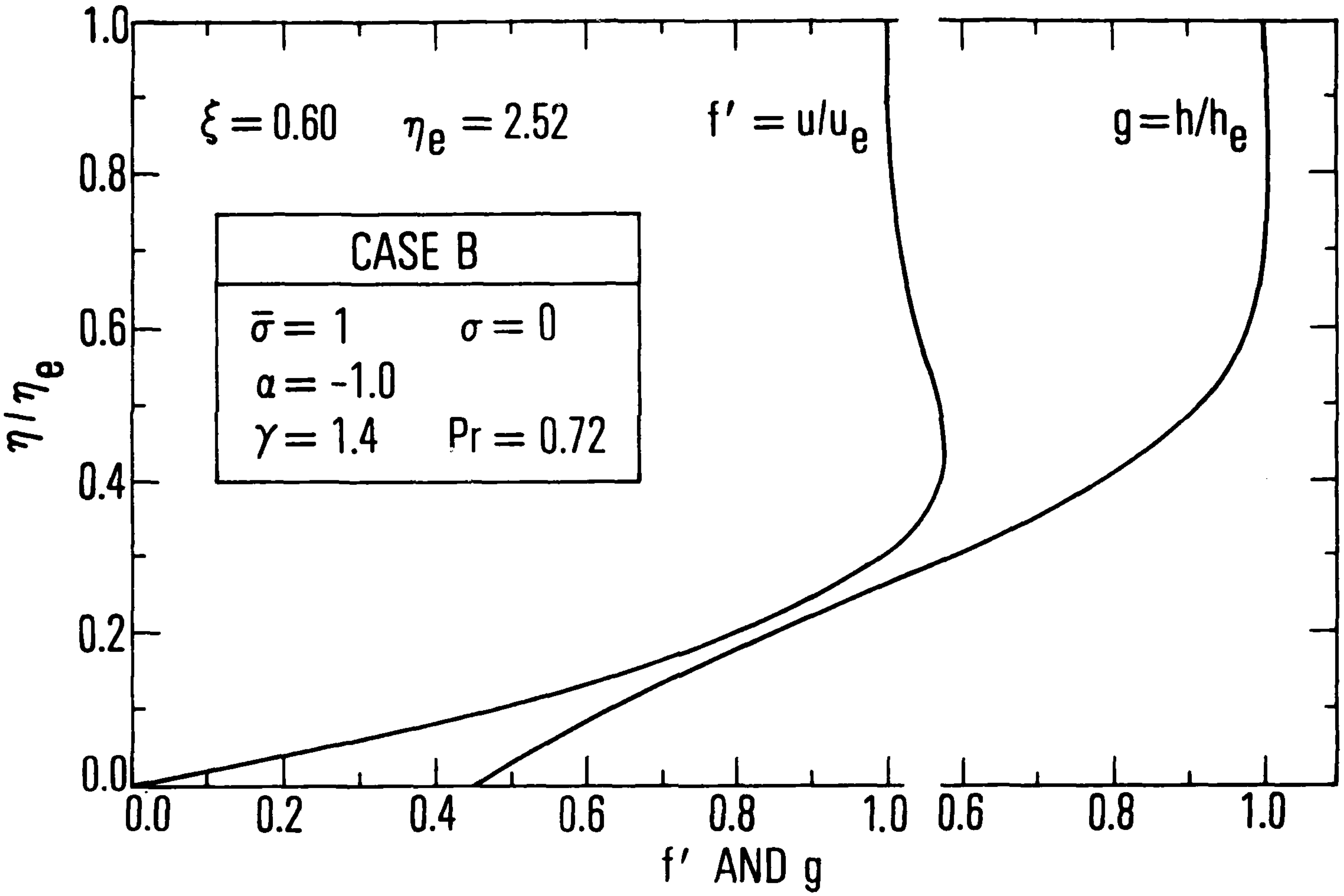

Fig. 10B-6. Detailed boundary-layer profiles, $\zeta = 0.60$, Case B

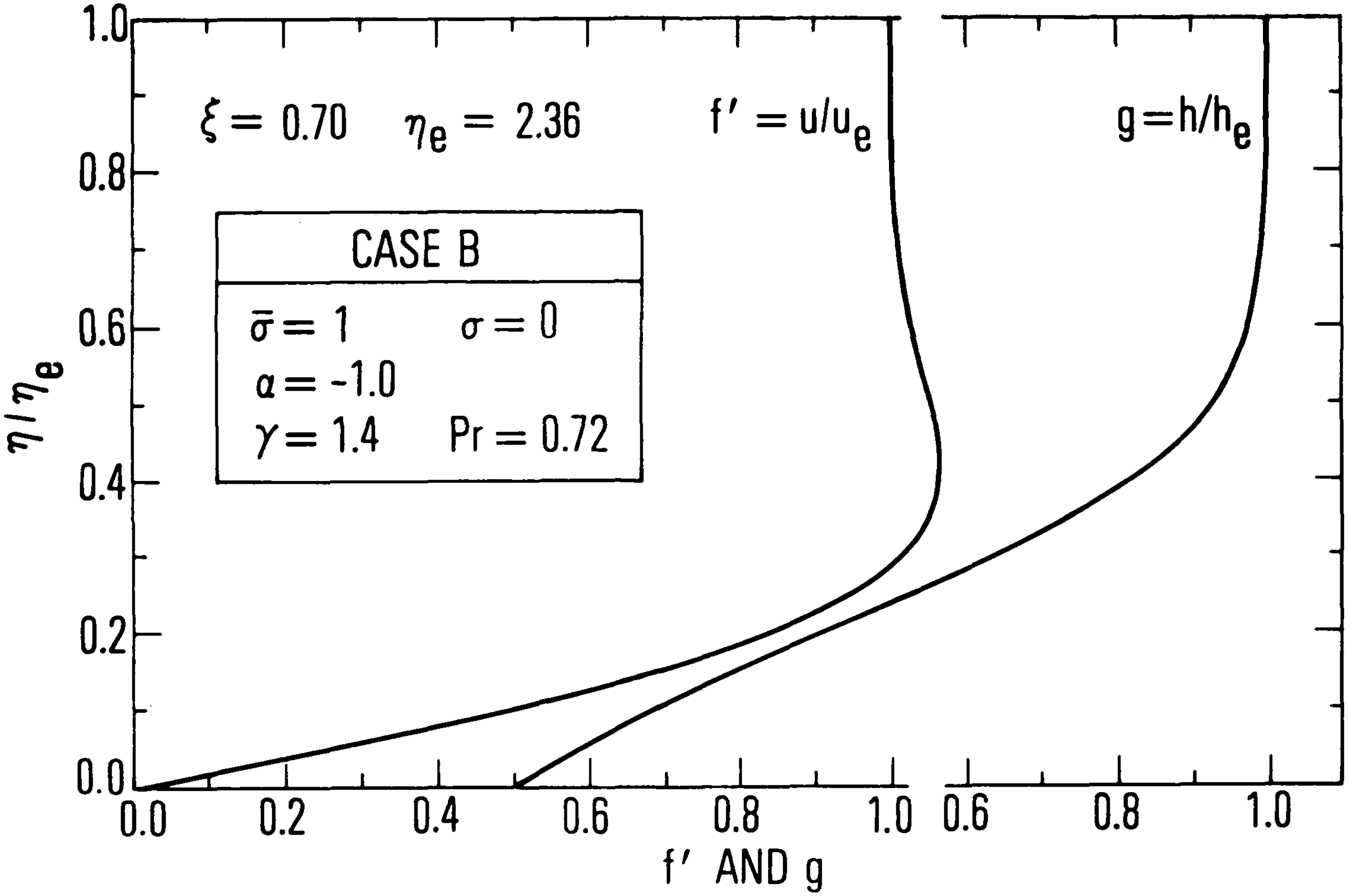

Fig. 10B-7. Detailed boundary-layer profiles, $\zeta = 0.70$, Case B

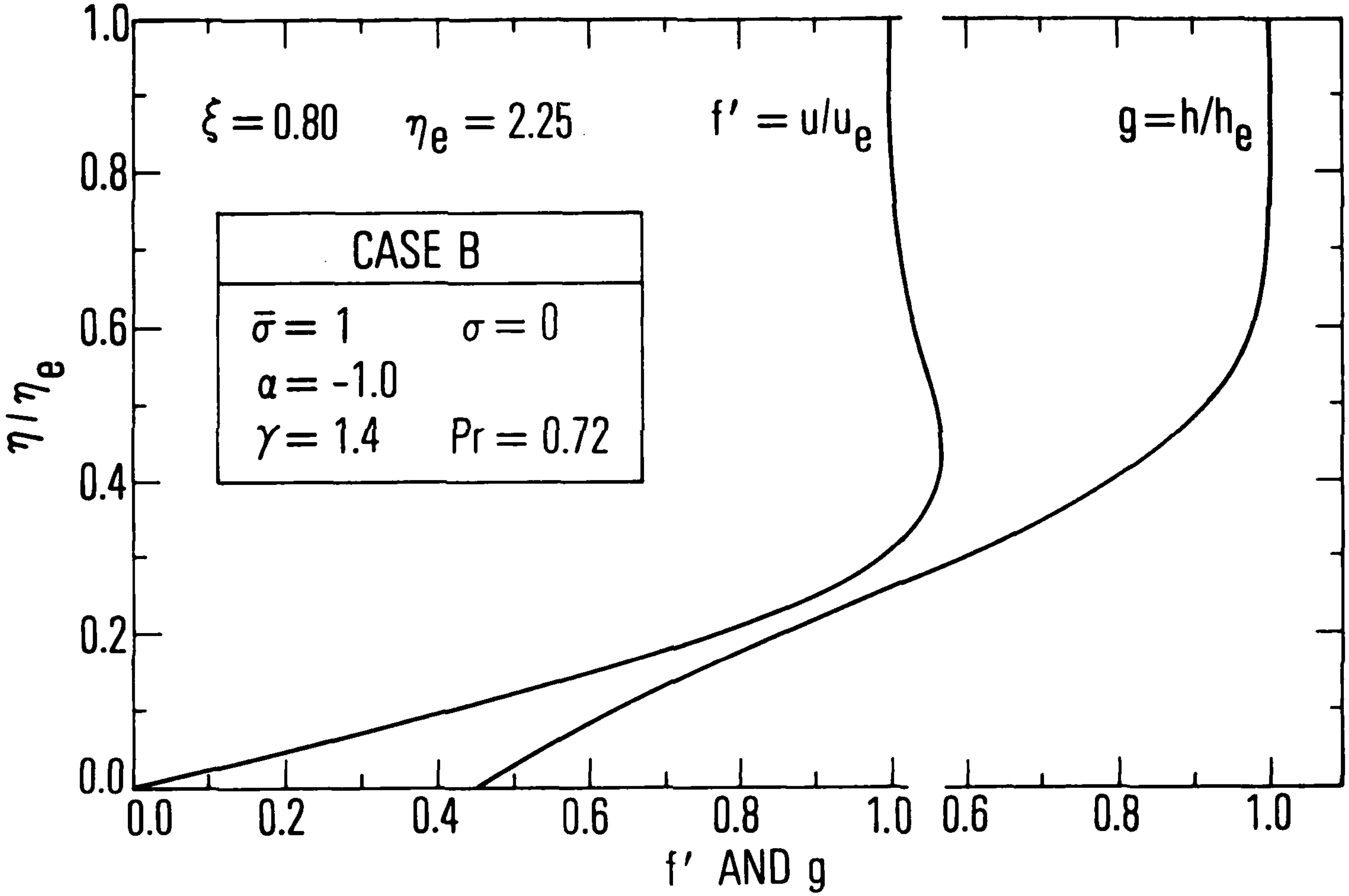

Fig. 10B-8. Detailed boundary-layer profiles, $\zeta = 0.80$, Case B

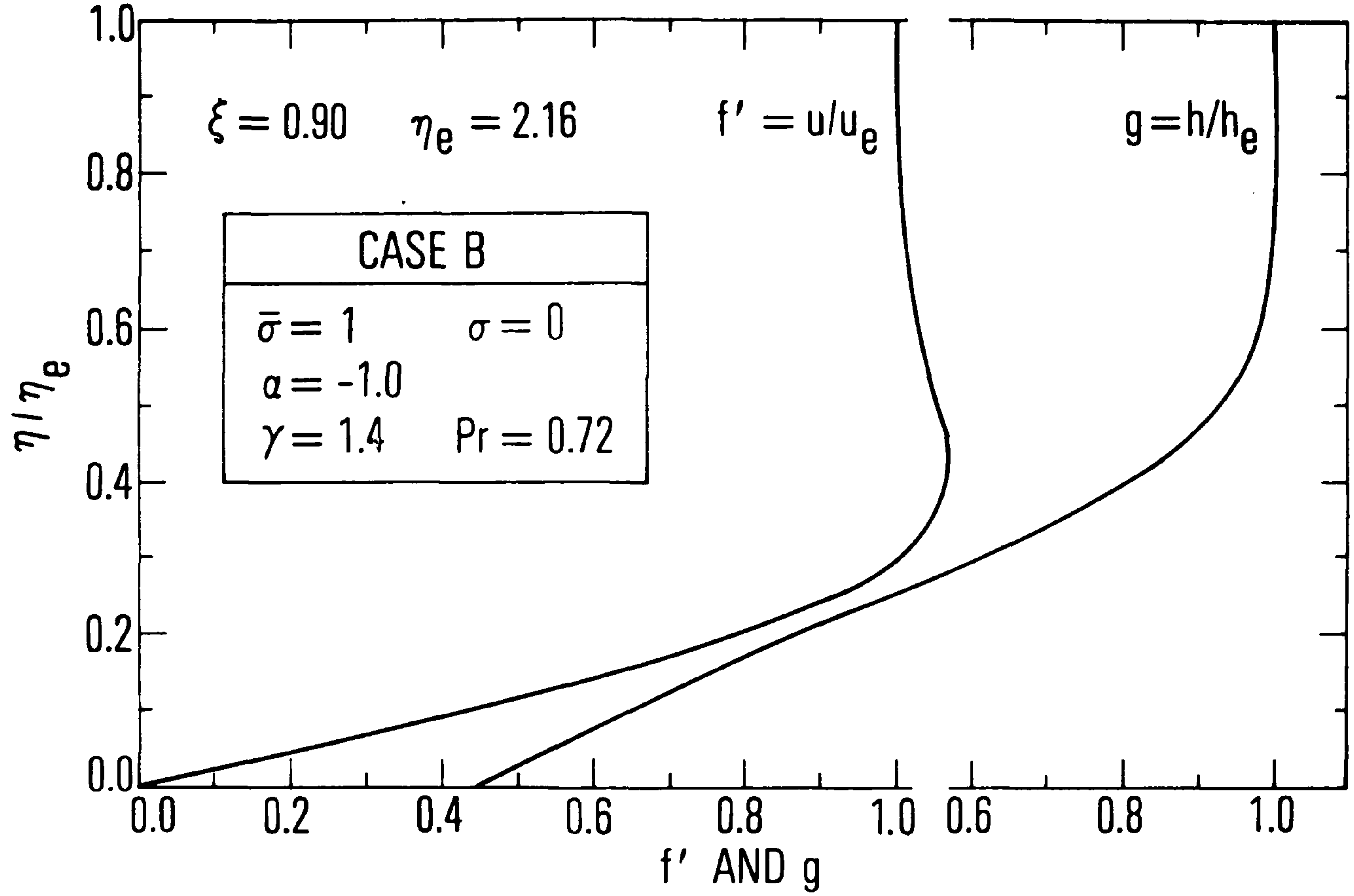

Fig. 10B-9. Detailed boundary-layer profiles, ζ = 0.90, Case B

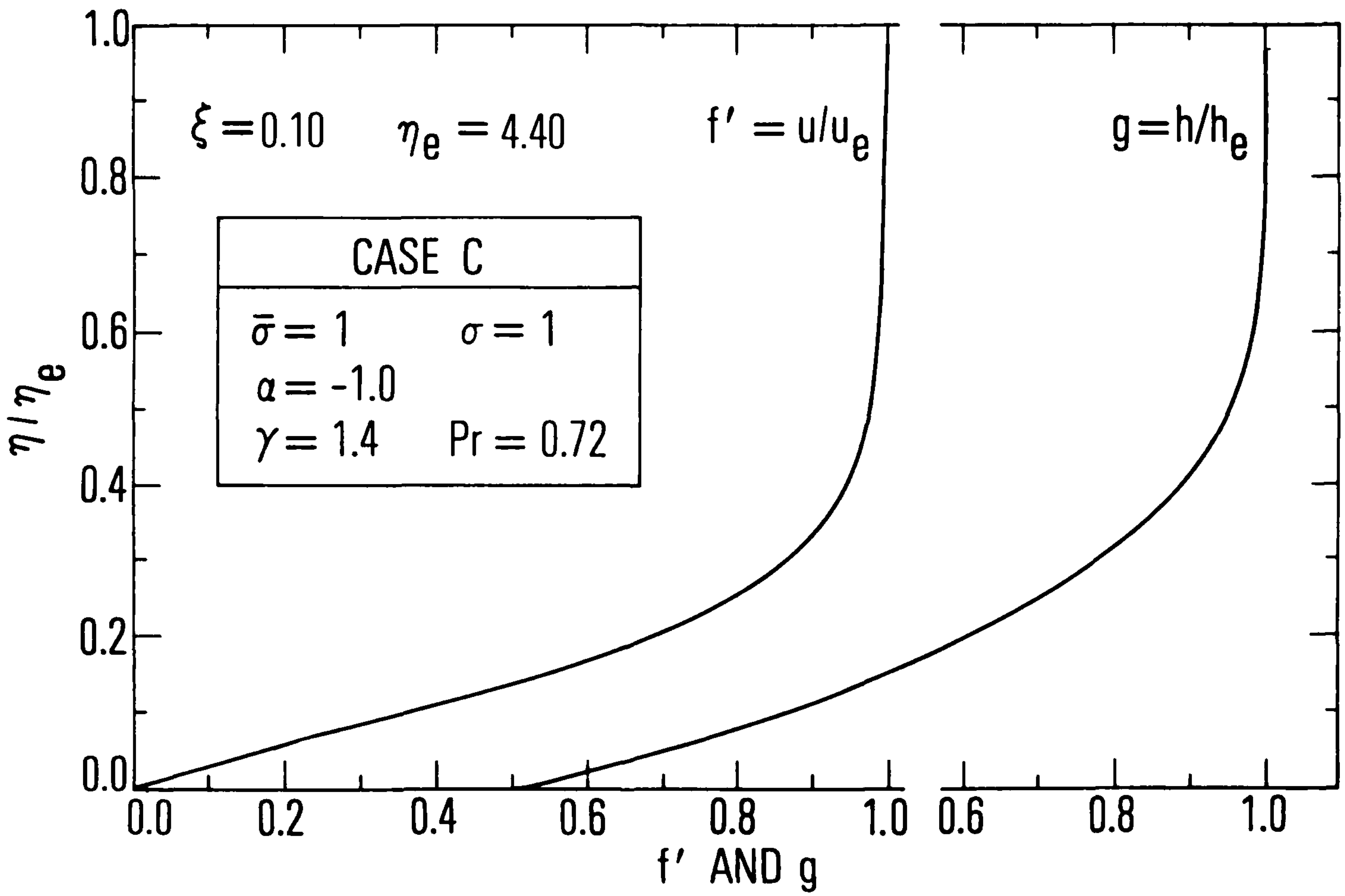

Fig. 10C-1. Detailed boundary-layer profiles, $\zeta = 0.10$, Case C

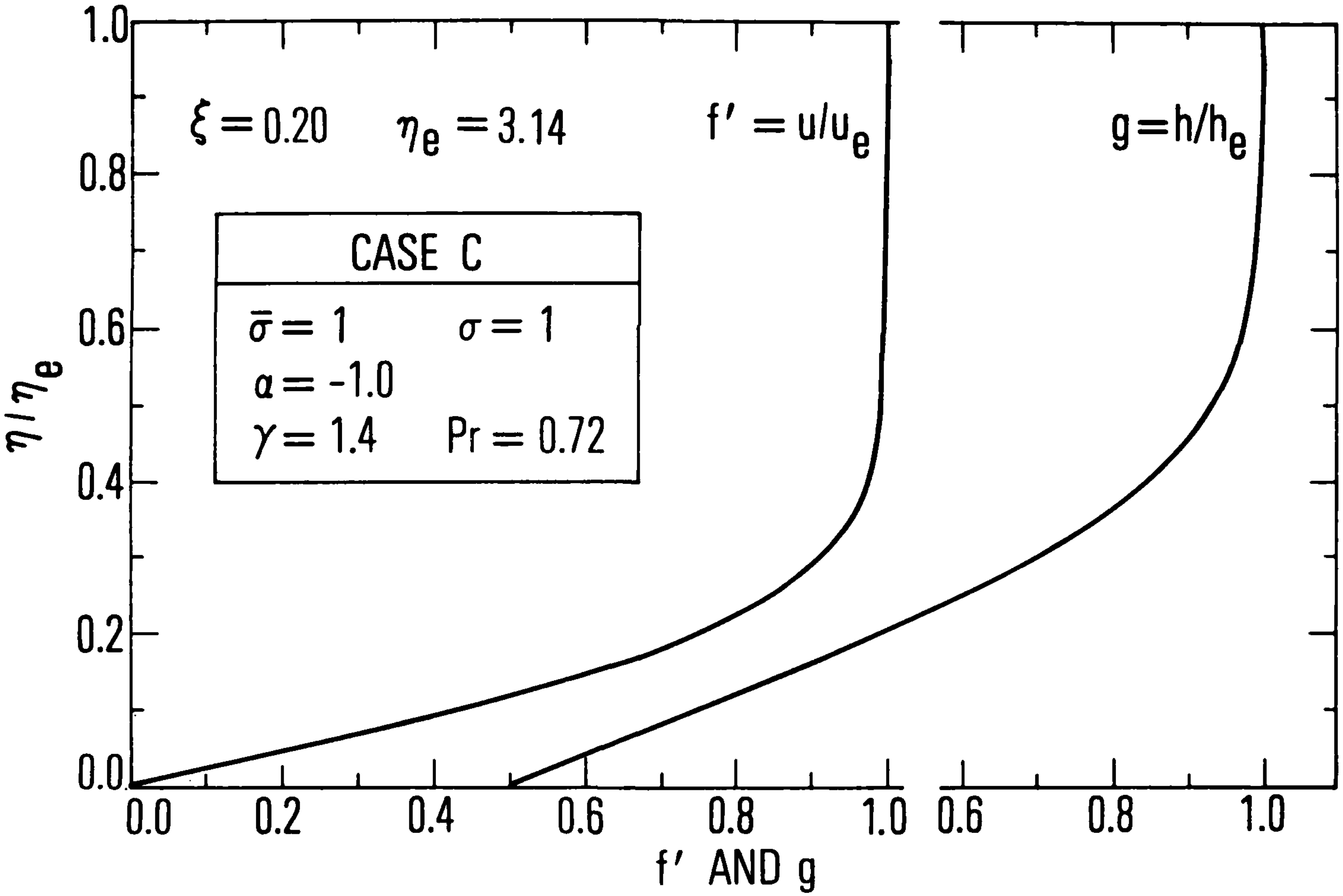

Fig. 10C-2. Detailed boundary-layer profiles, $\zeta = 0.20$, Case C

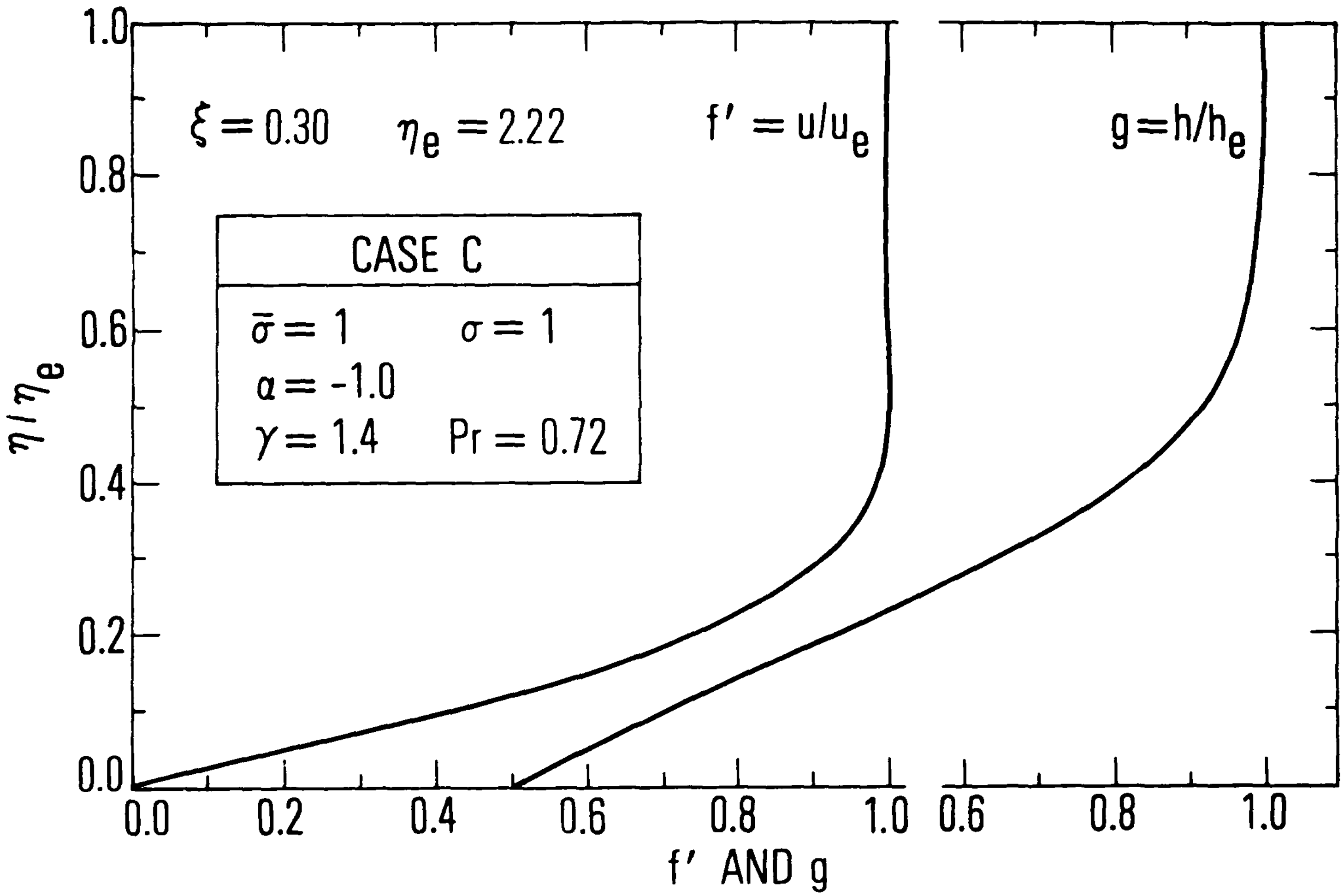

Fig. 10C-3. Detailed boundary-layer profiles, $\zeta = 0.30$, Case C

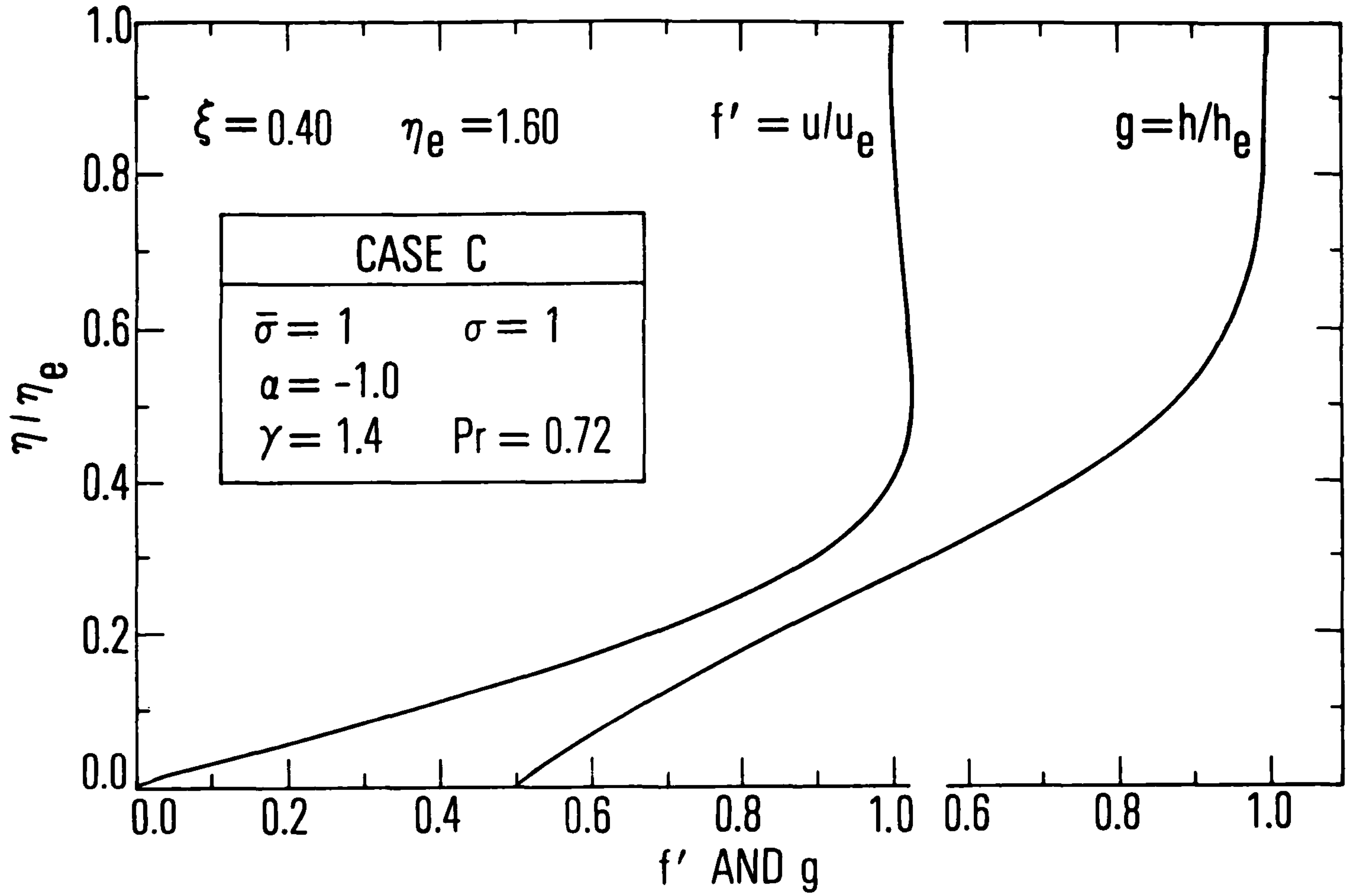

Fig. 10C-4. Detailed boundary-layer profiles, $\zeta = 0.40$, Case C

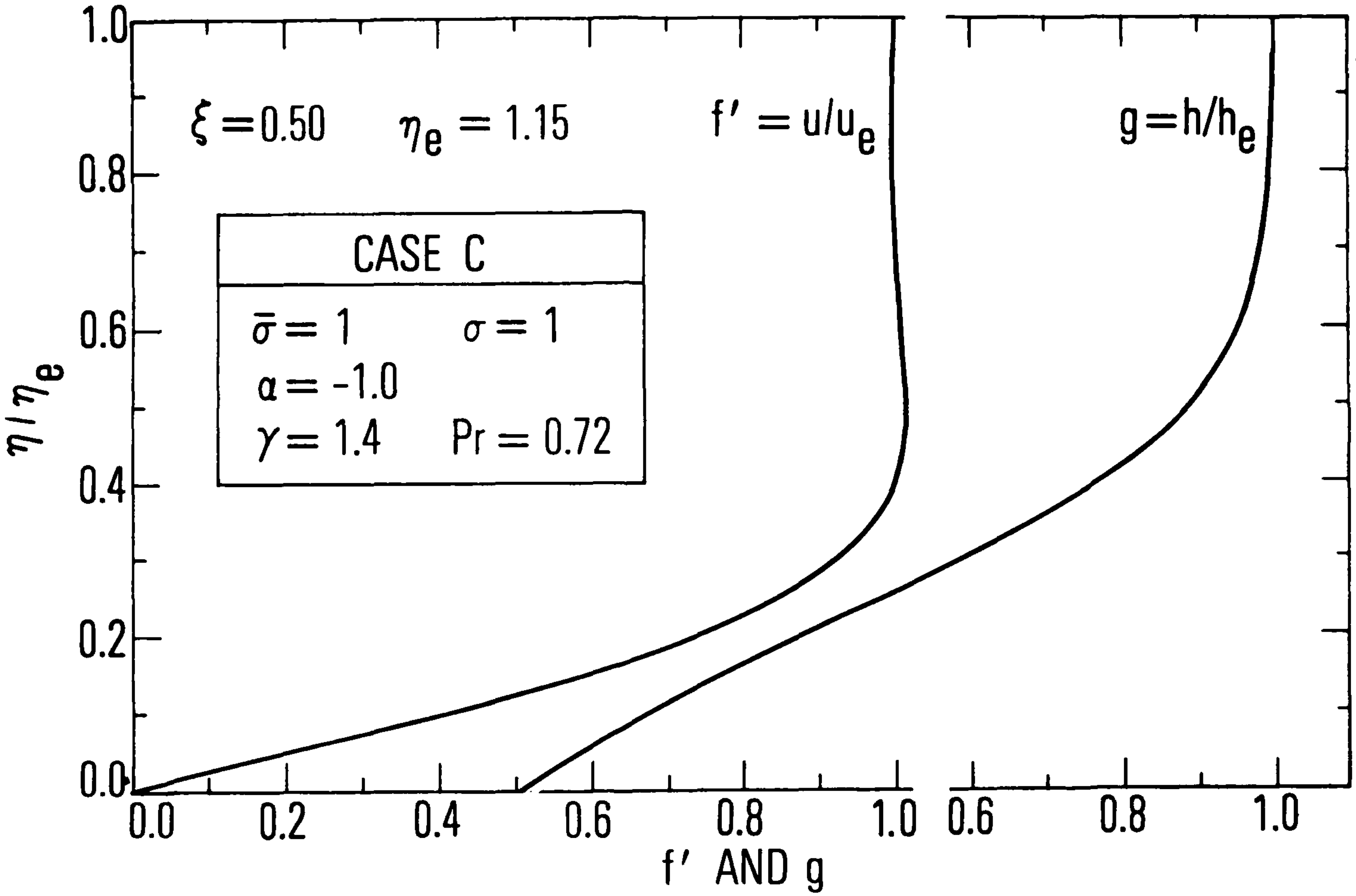

Fig. 10C-5. Detailed boundary-layer profiles, $\zeta = 0.50$, Case C

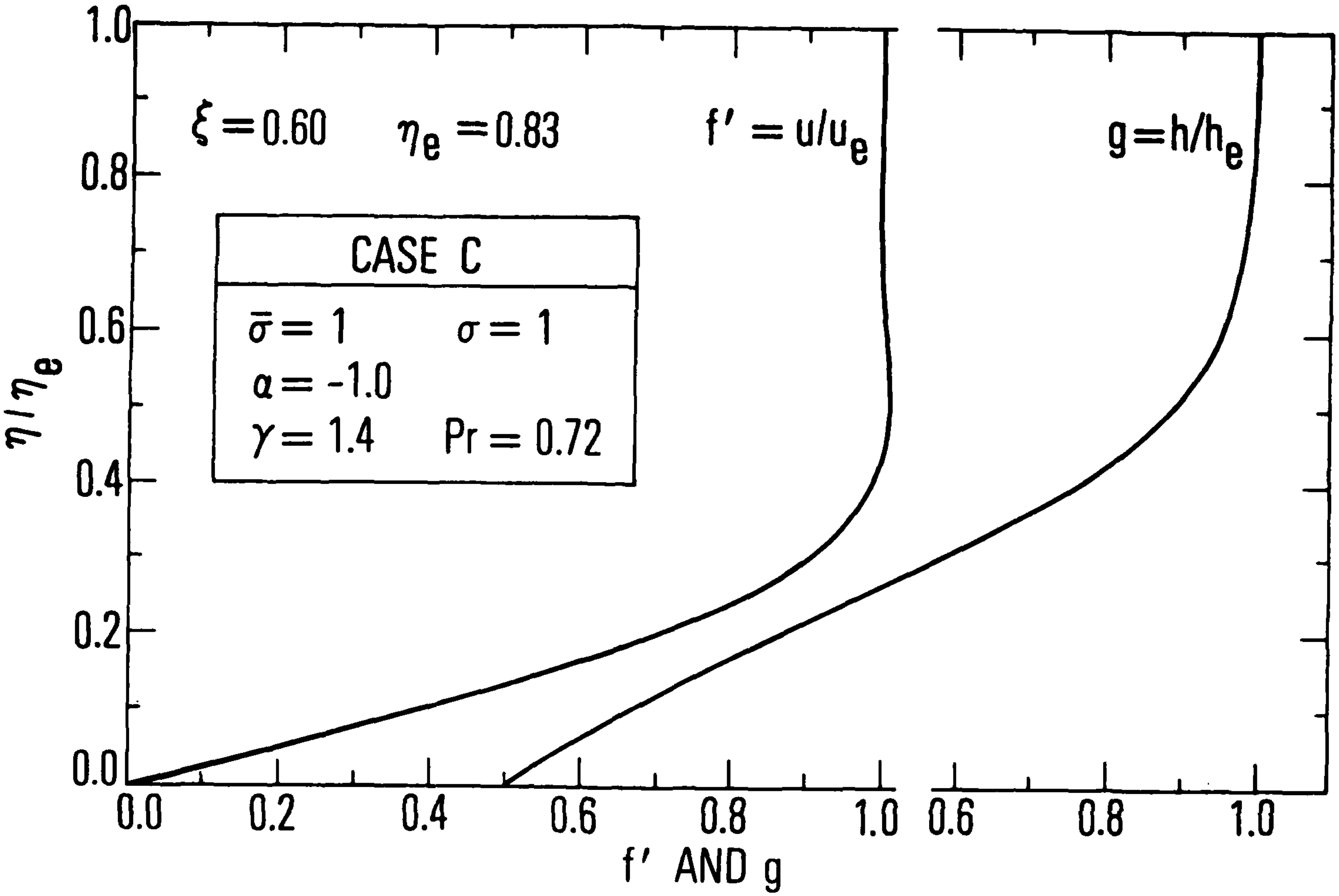

Fig. 10C-6. Detailed boundary-layer profiles, $\zeta = 0.60$, Case C

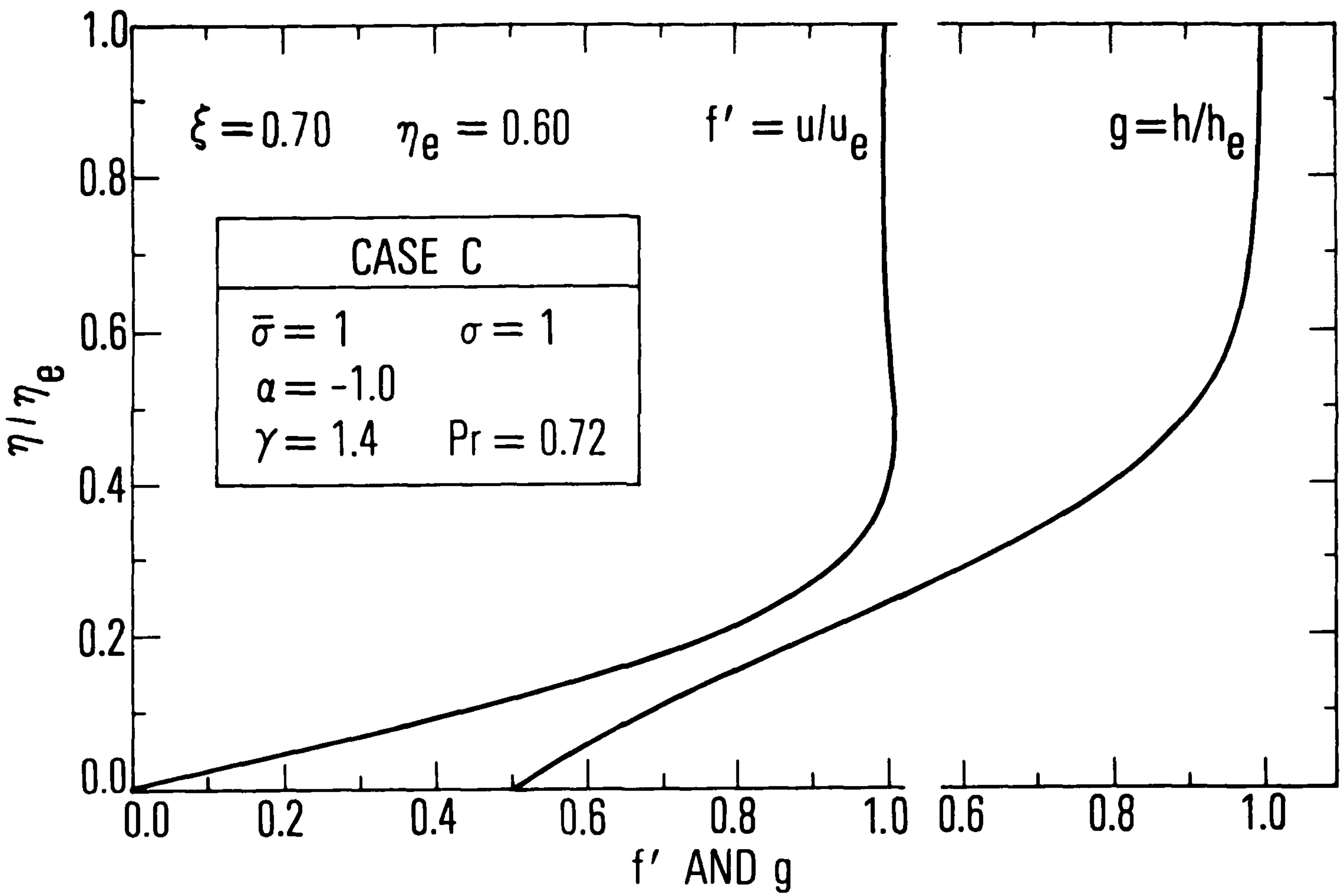

Fig. 10C-7. Detailed boundary-layer profiles, $\zeta = 0.70$, Case C

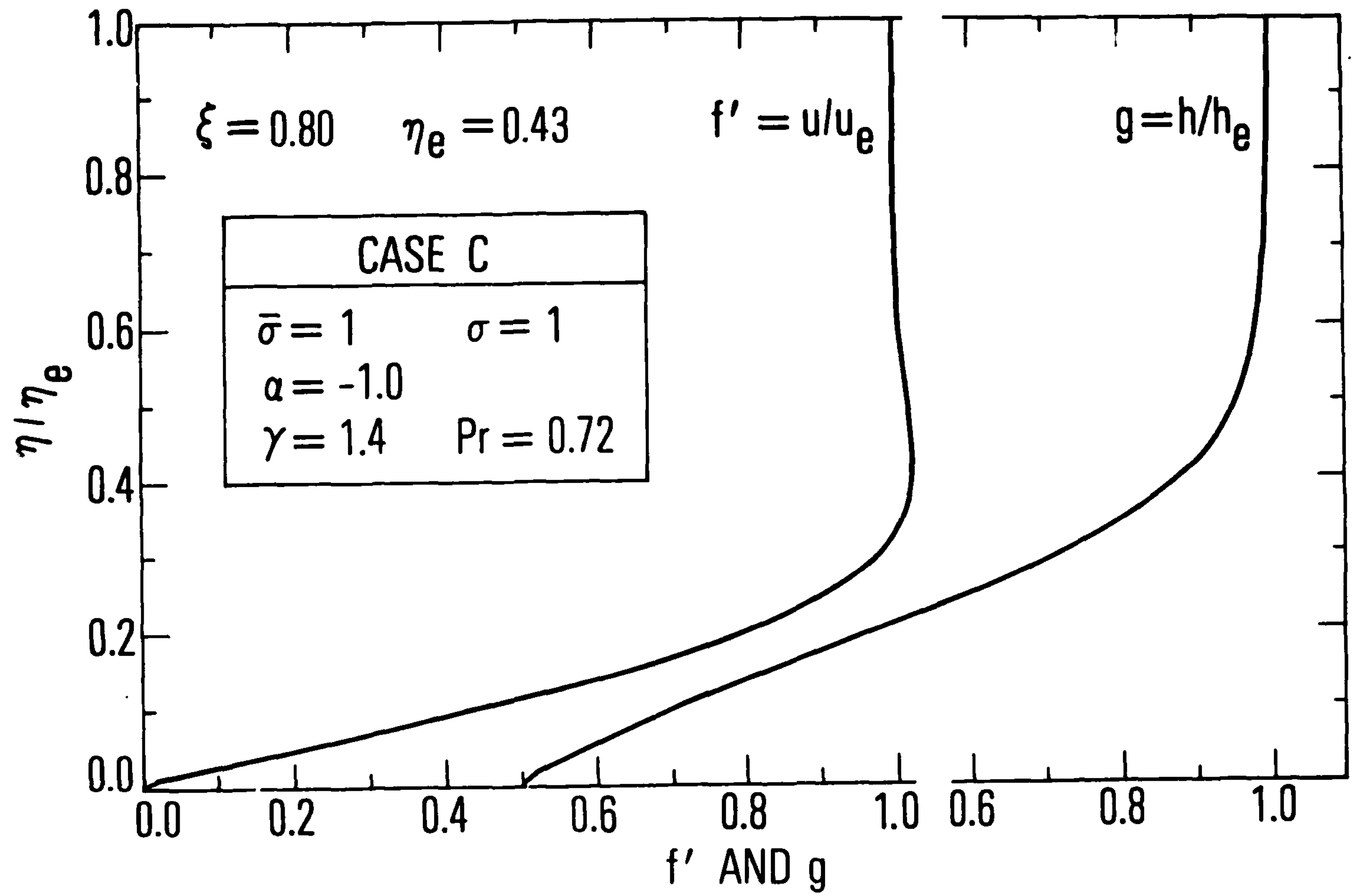

Fig. 10C-8. Detailed boundary-layer profiles, $\zeta = 0.80$, Case C

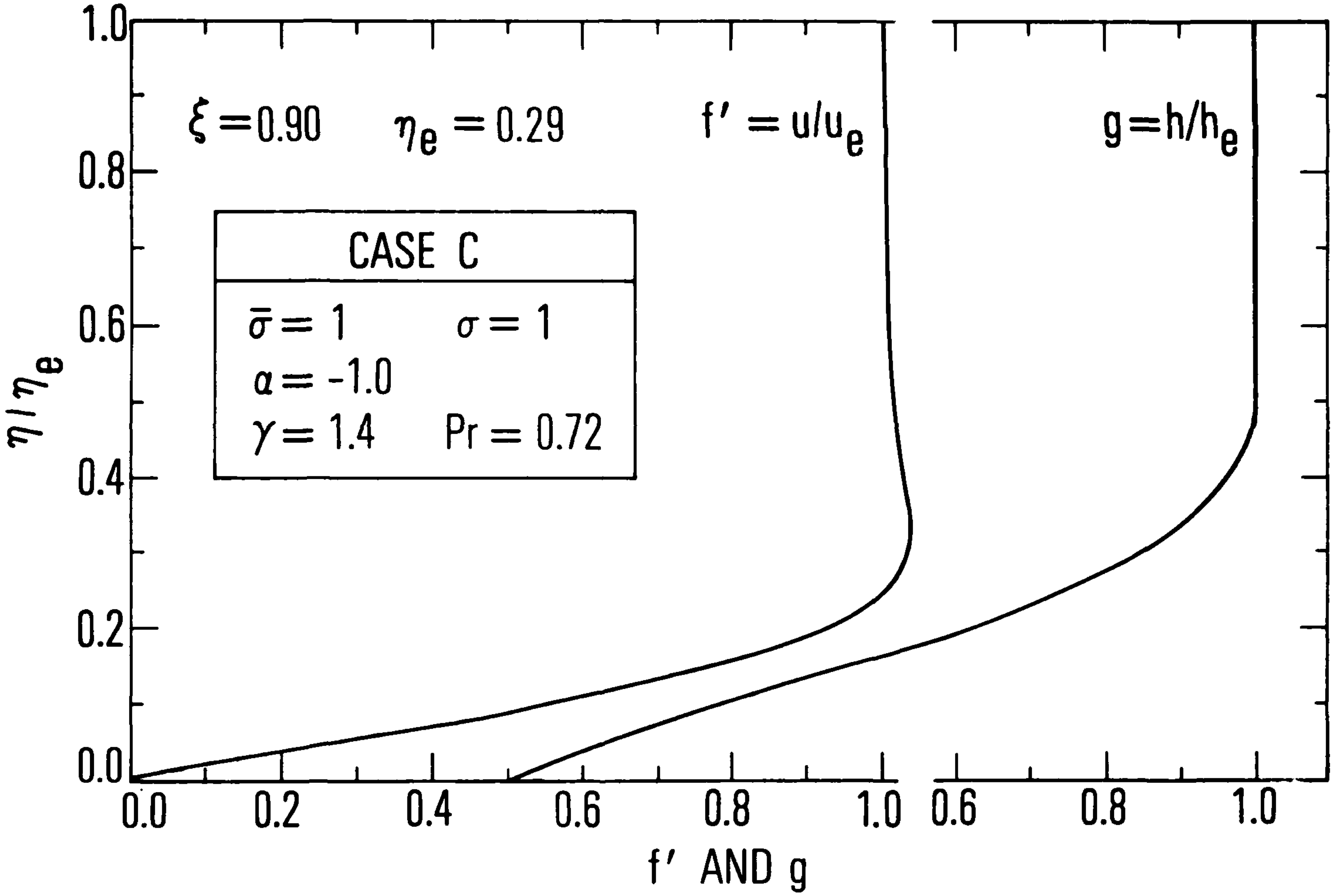

Fig. 10C-9. Detailed boundary-layer profiles, $\zeta = 0.90$, Case C

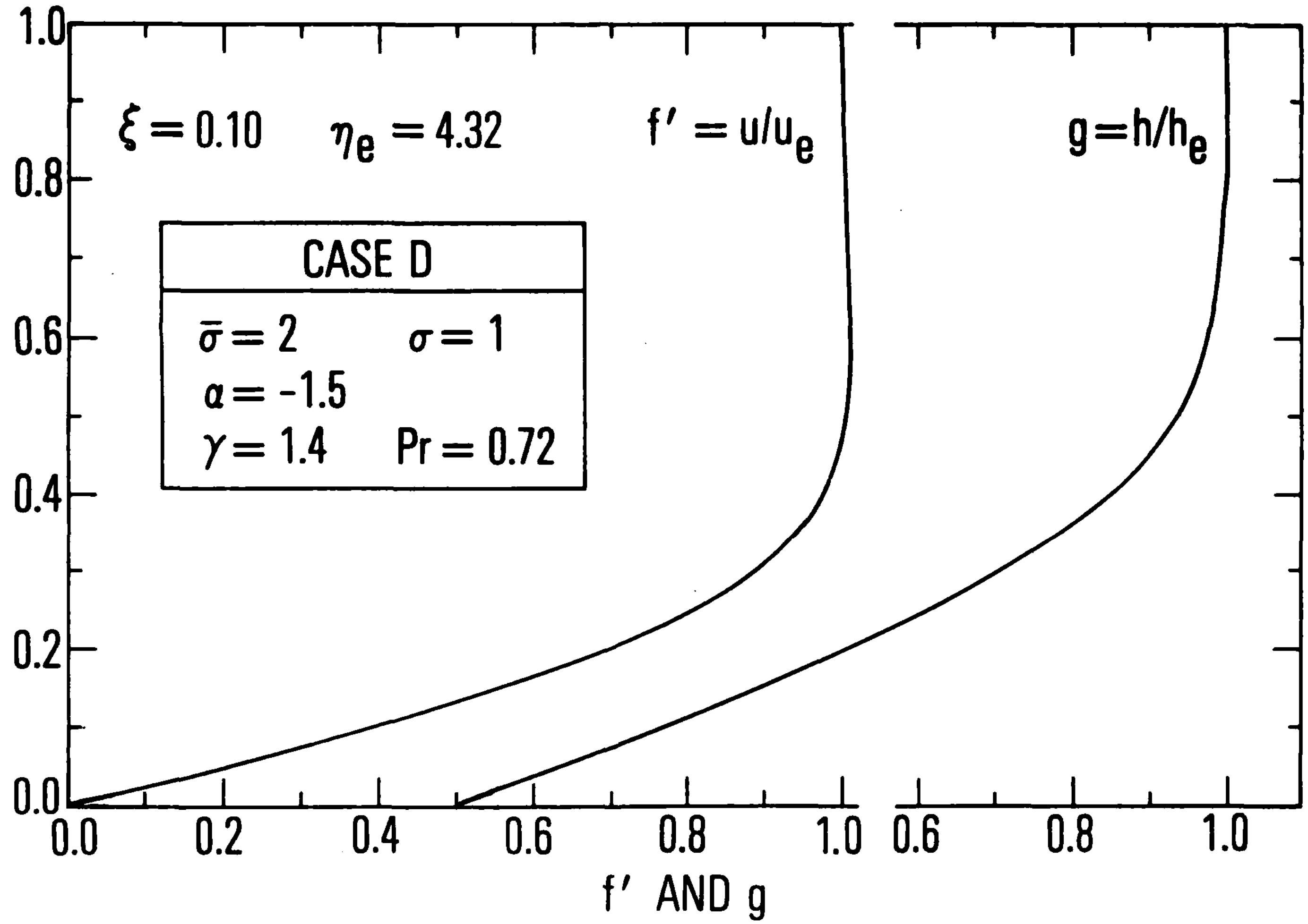

Fig. 10D-1. Detailed boundary-layer profiles, $\zeta = 0.10$, Case D

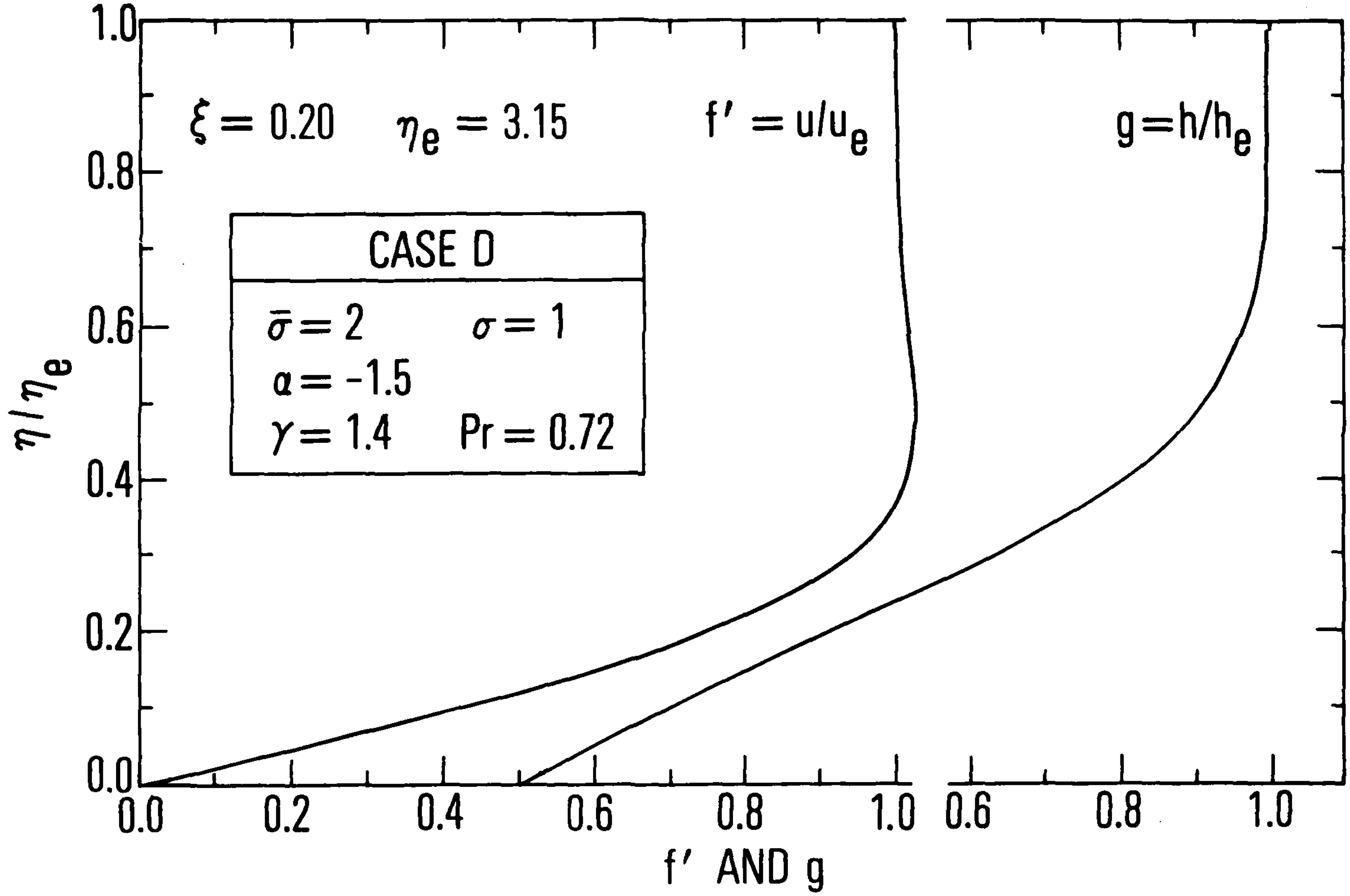

Fig. 10D-2. Detailed boundary-layer profiles, $\zeta = 0.20$, Case D

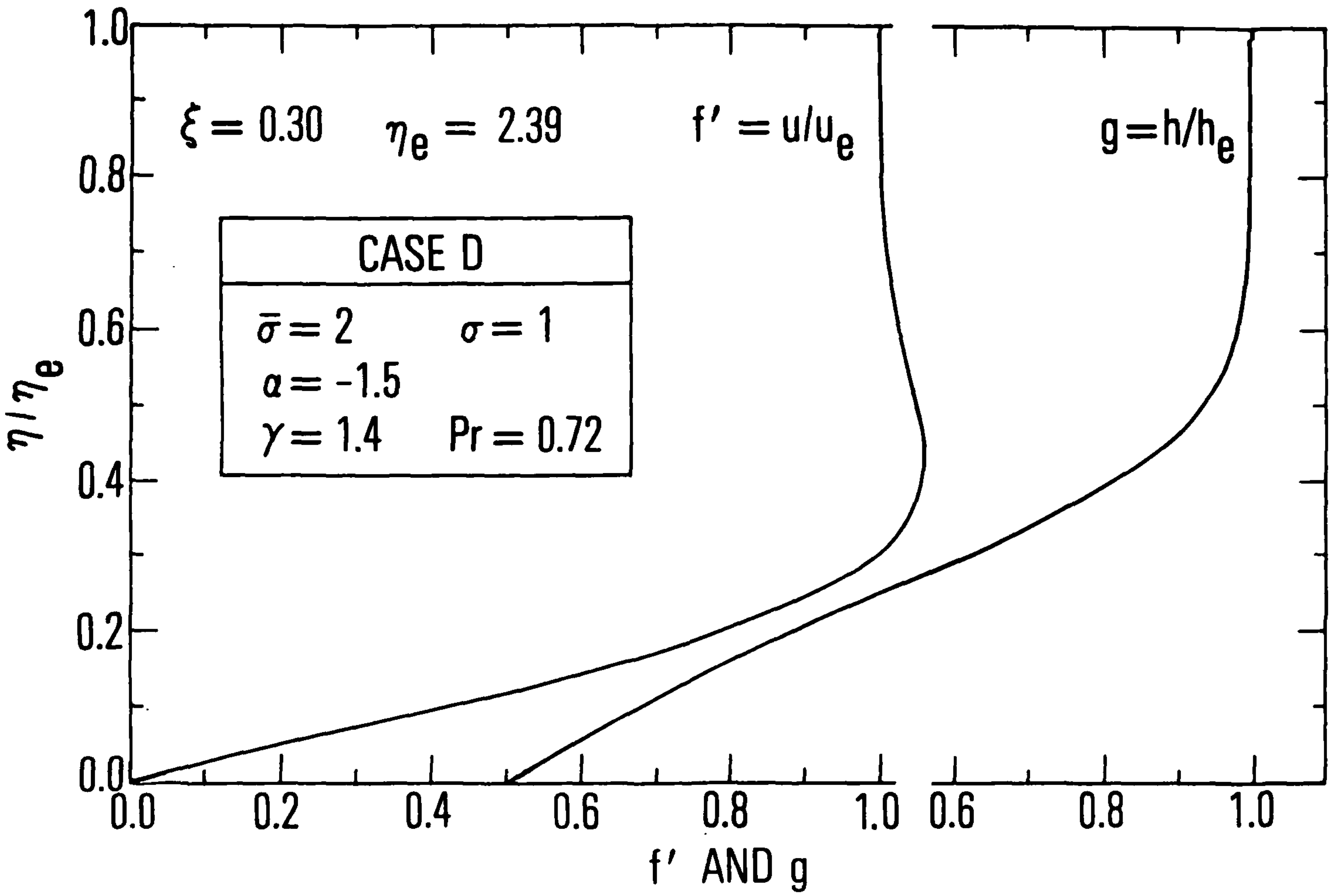

Fig. 10D-3. Detailed boundary-layer profiles, $\zeta = 0.30$, Case D

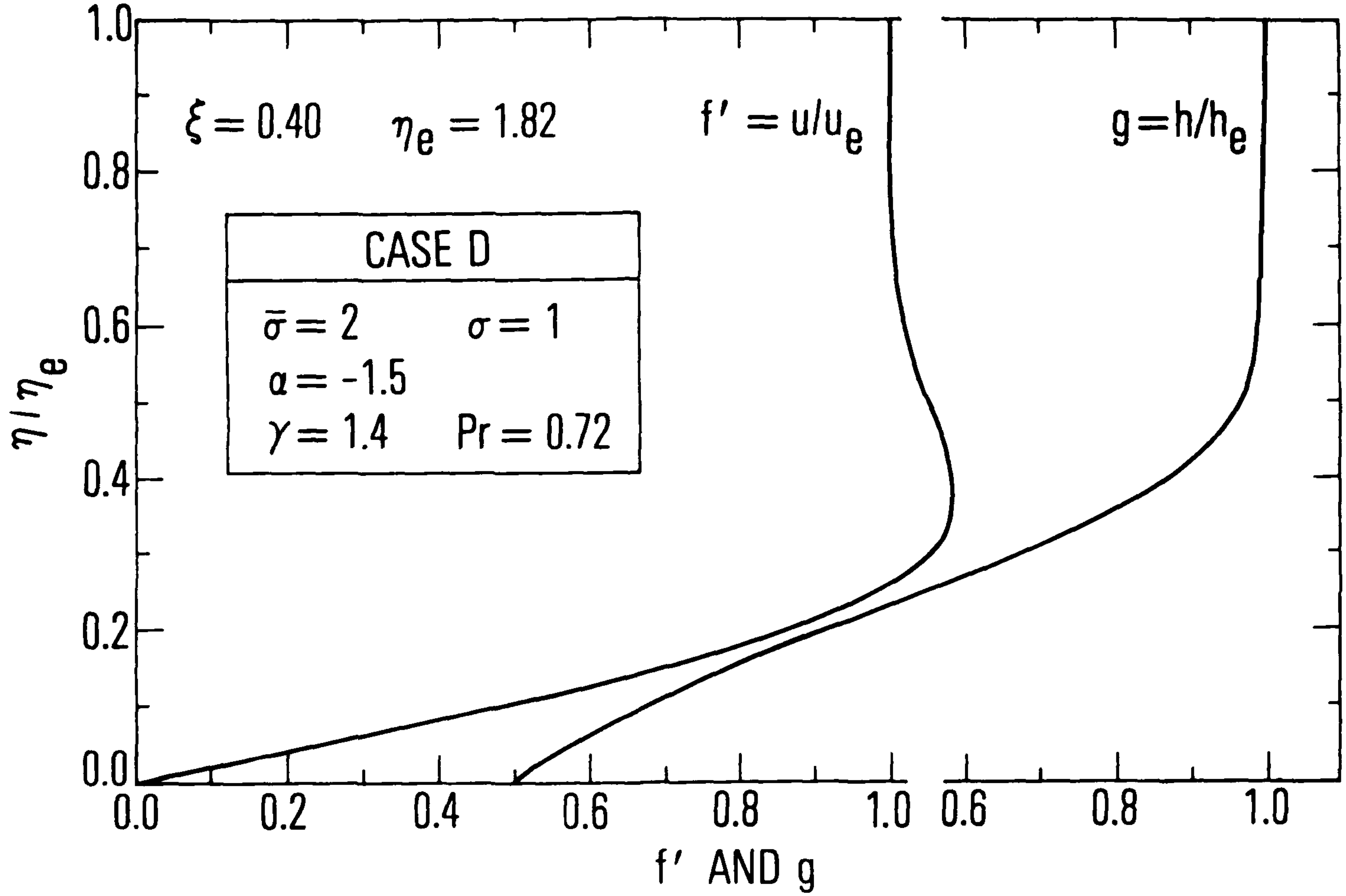

Fig. 10D-4. Detailed boundary-layer profiles, $\zeta = 0.40$, Case D

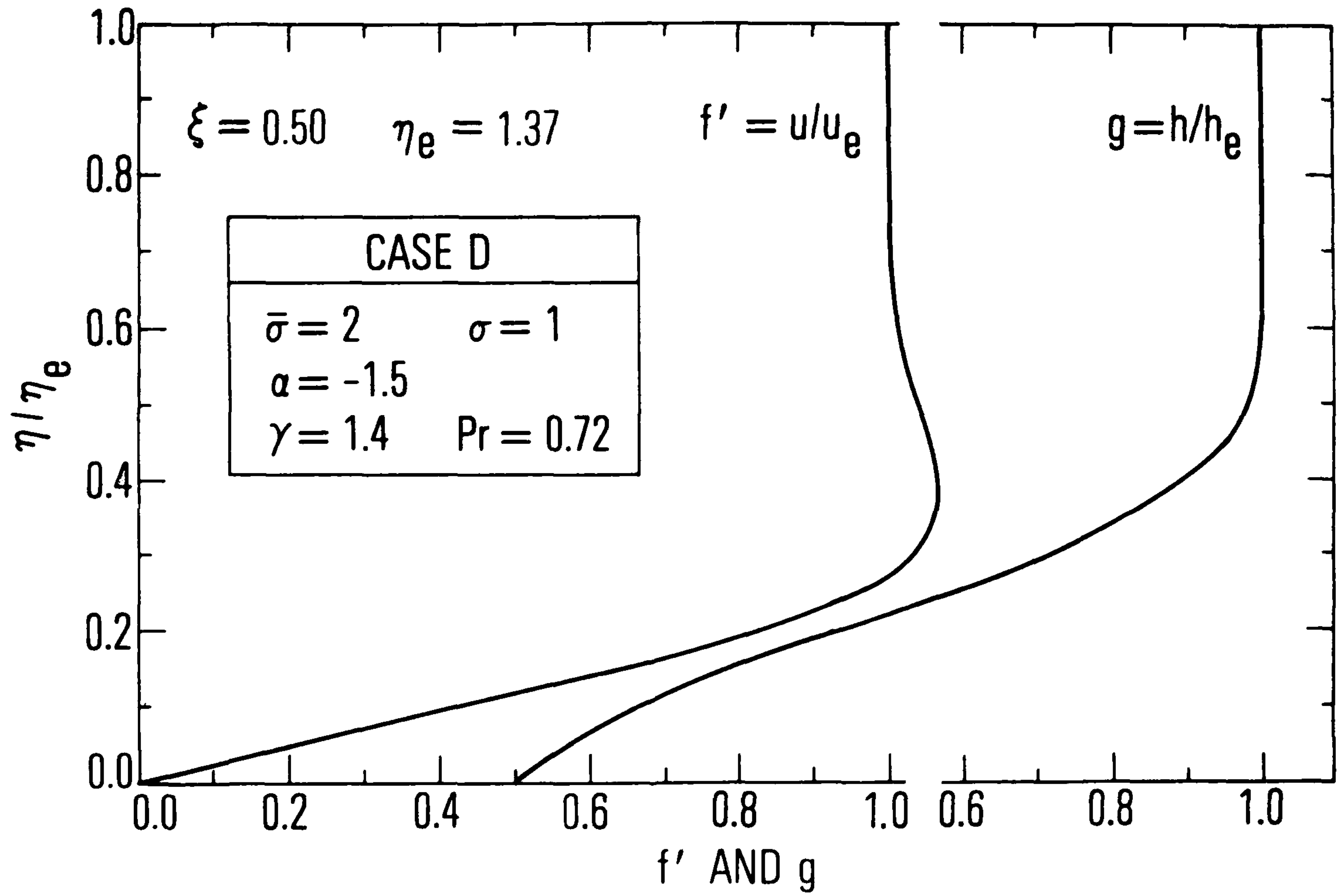

Fig. 10D-5. Detailed boundary-layer profiles, $\zeta = 0.50$, Case D

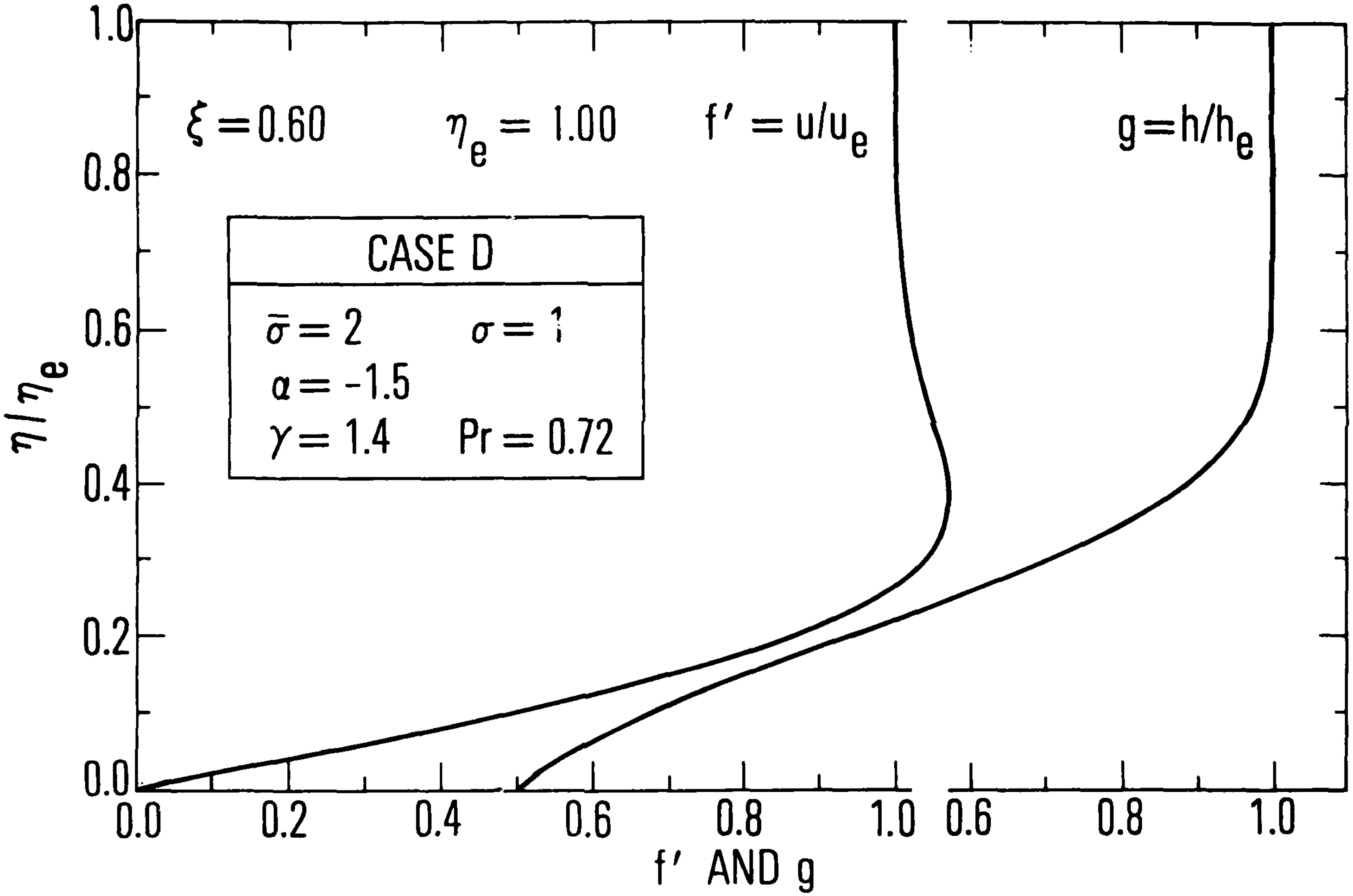

Fig. 10D-6. Detailed boundary-layer profiles, $\zeta = 0.60$, Case D

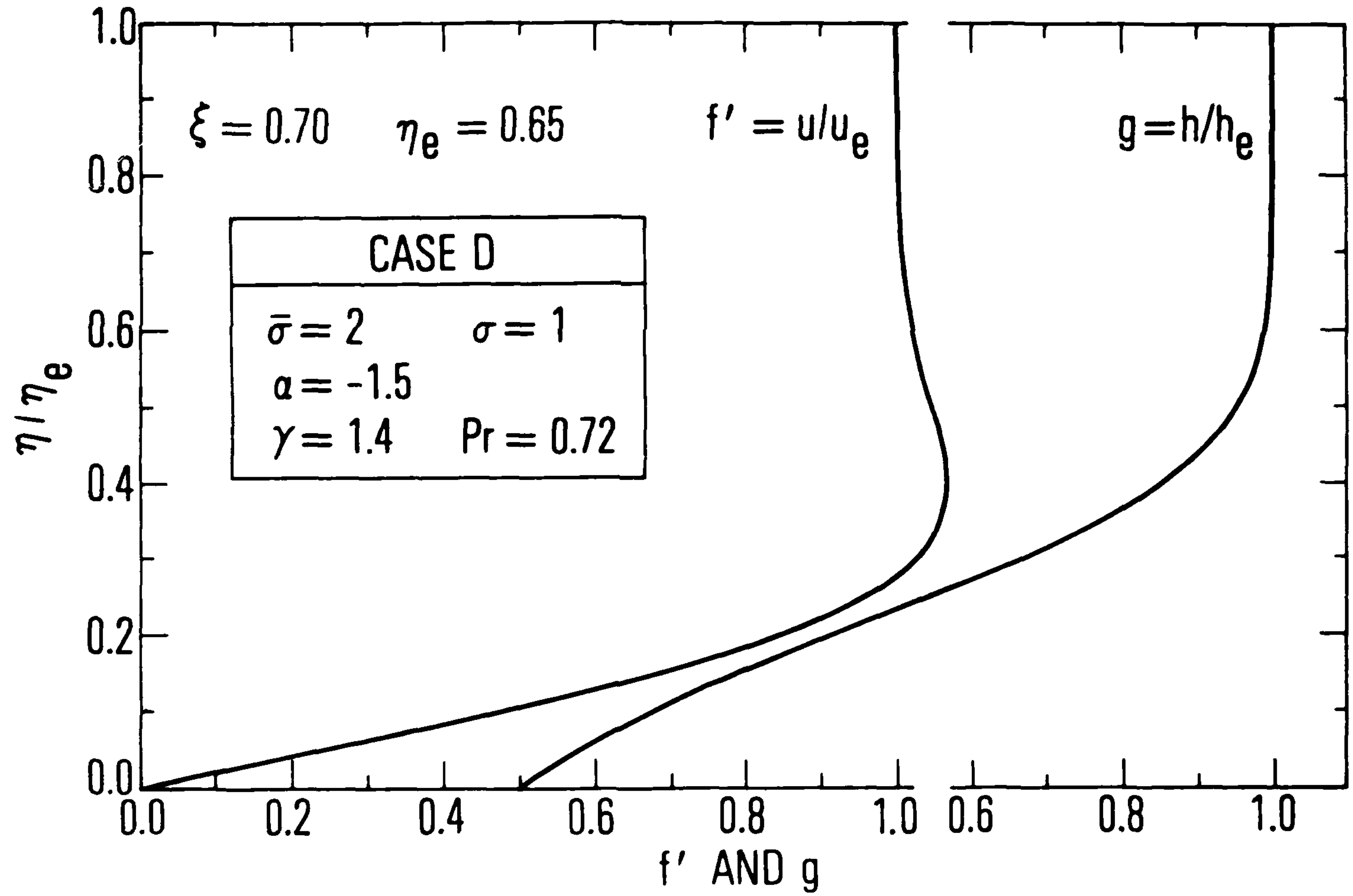

Fig. 10D-7. Detailed boundary-layer profiles, $\zeta = 0.70$, Case D

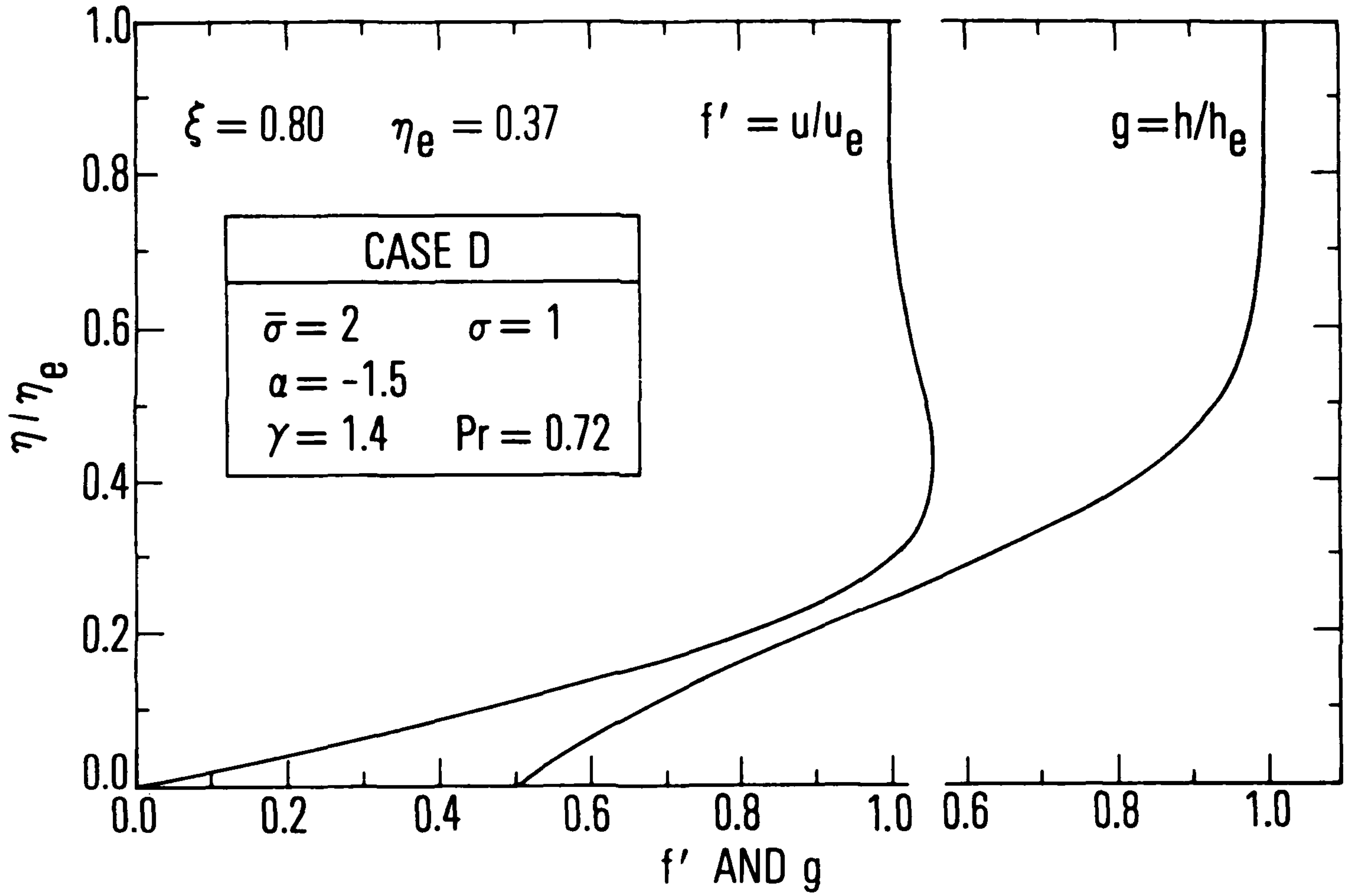

Fig. 10D-8. Detailed boundary-layer profiles, ζ = 0.80, Case D

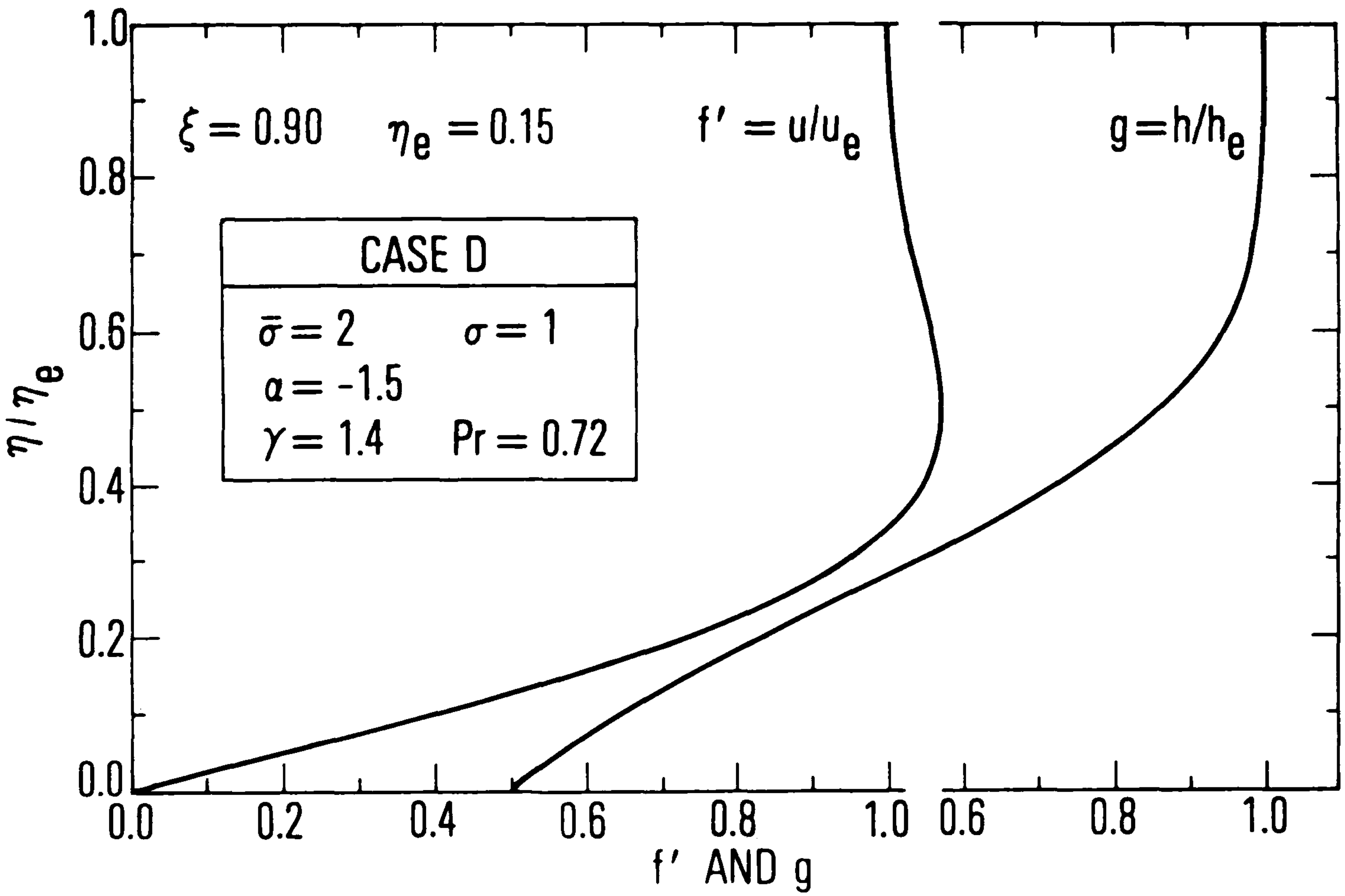

Fig. 10D-9. Detailed boundary-layer profiles, ξ = 0.90, Case D

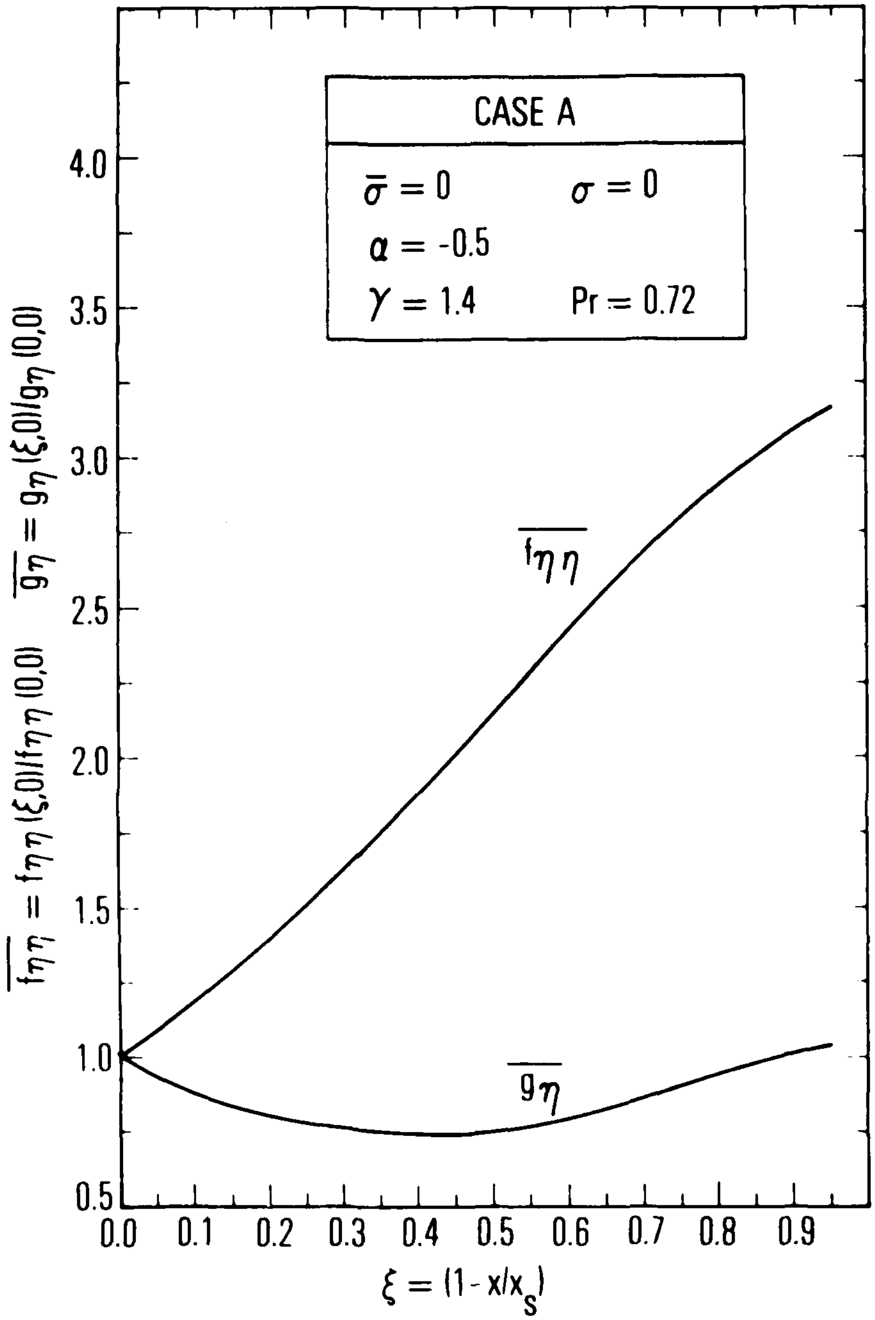

Fig. 11. Wall gradient of f' and g, Case A

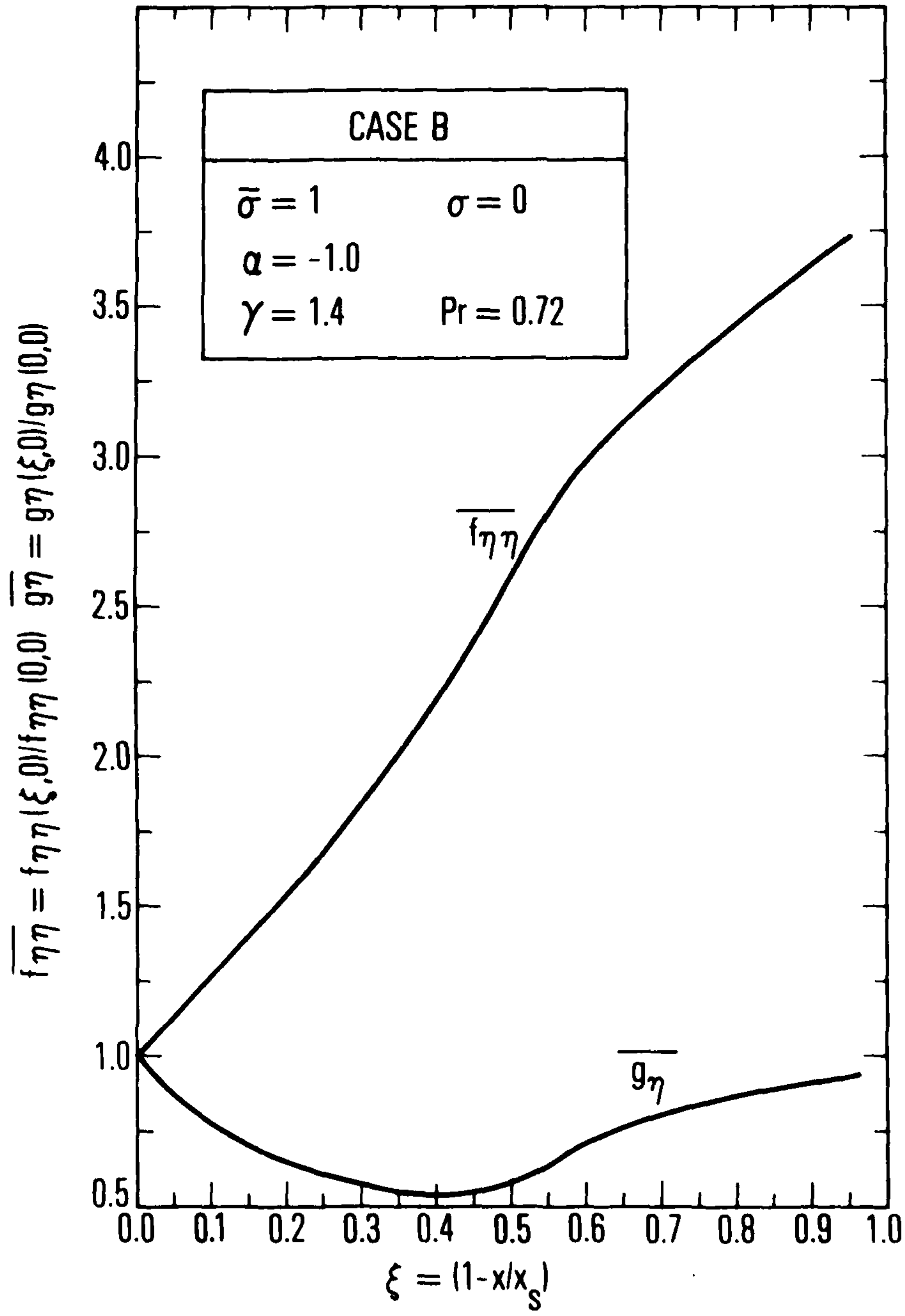

Fig. 11. Wall gradient of f' and g, Case B

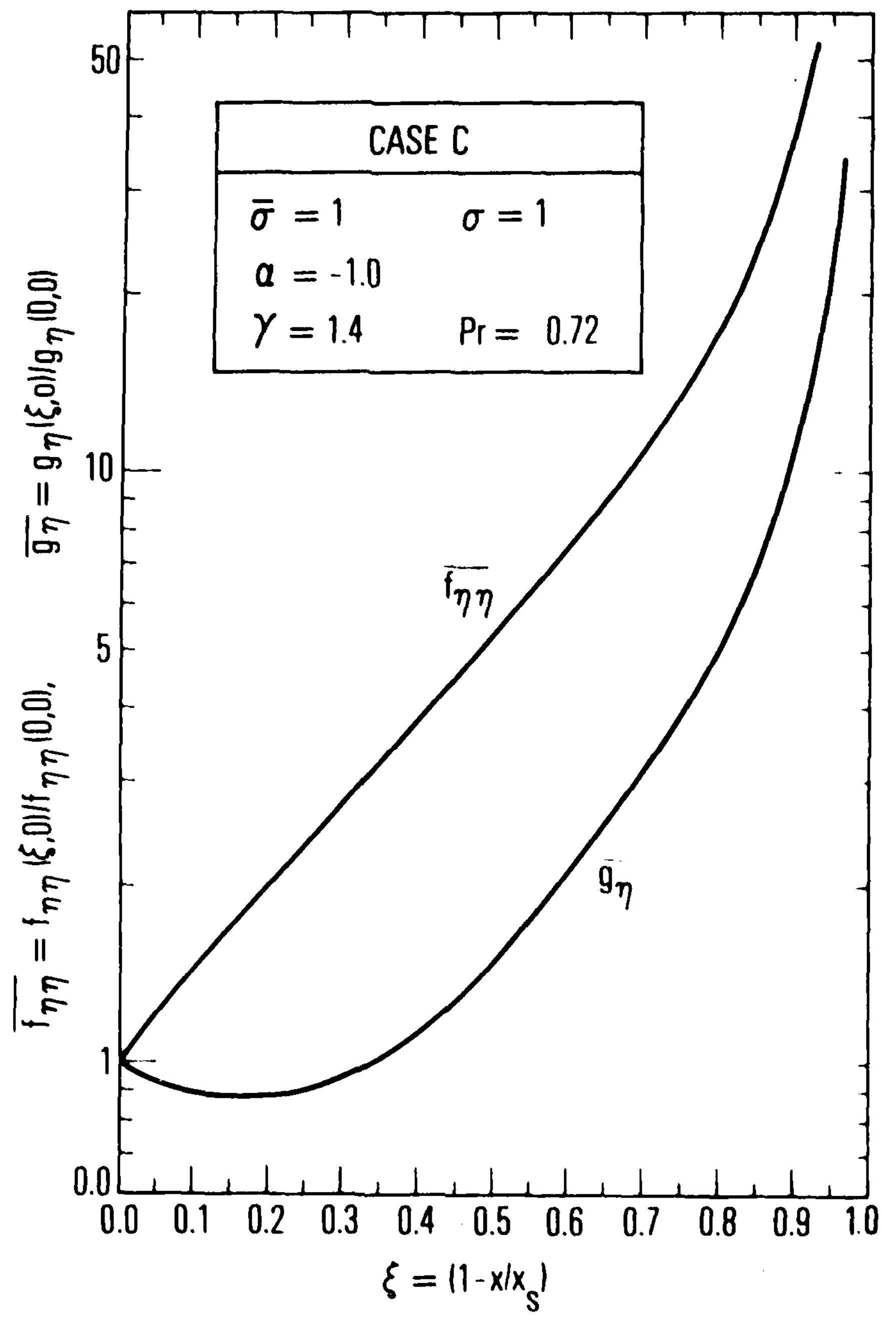

Fig. 11. Wall gradient of f′ and g, Case C

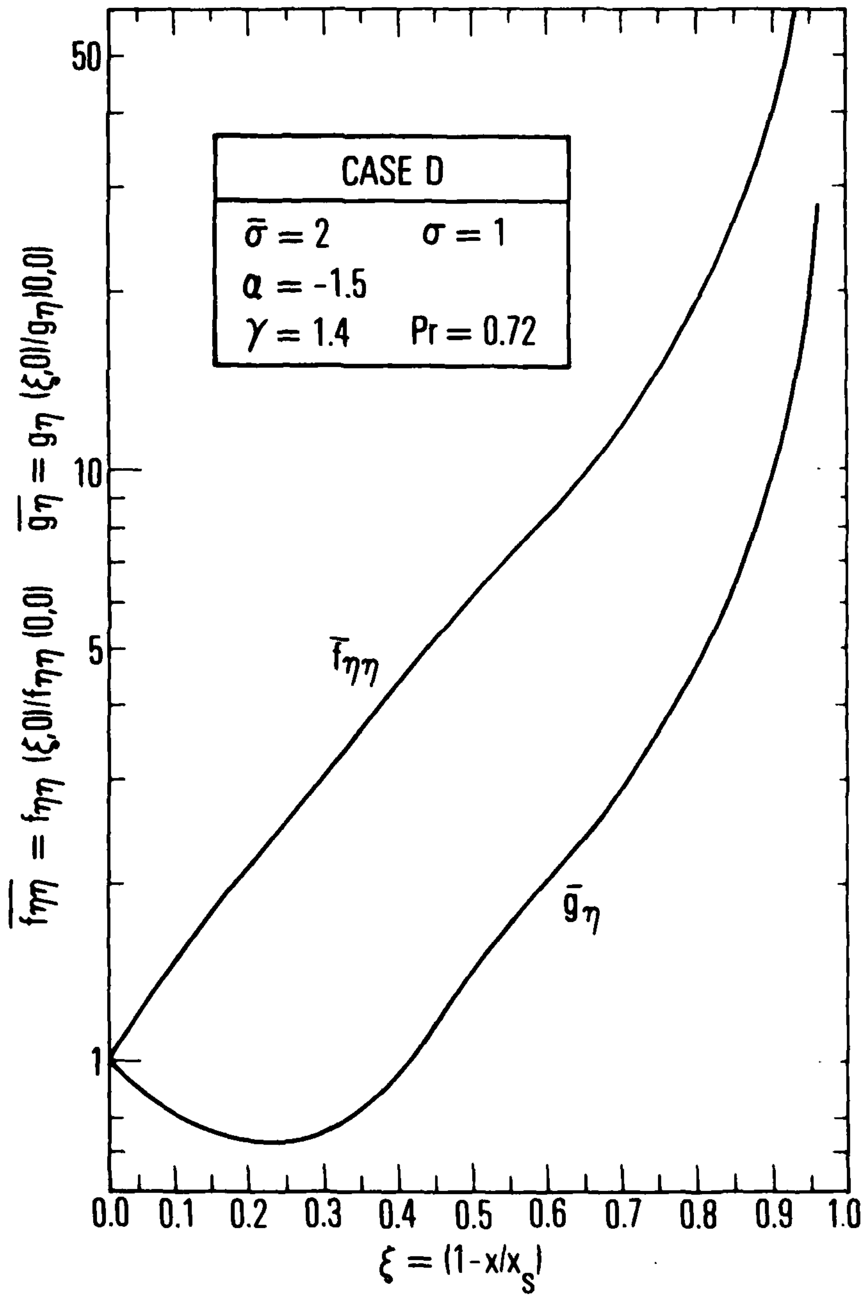

Fig. 11. Wall gradient of f′ and g, Case D

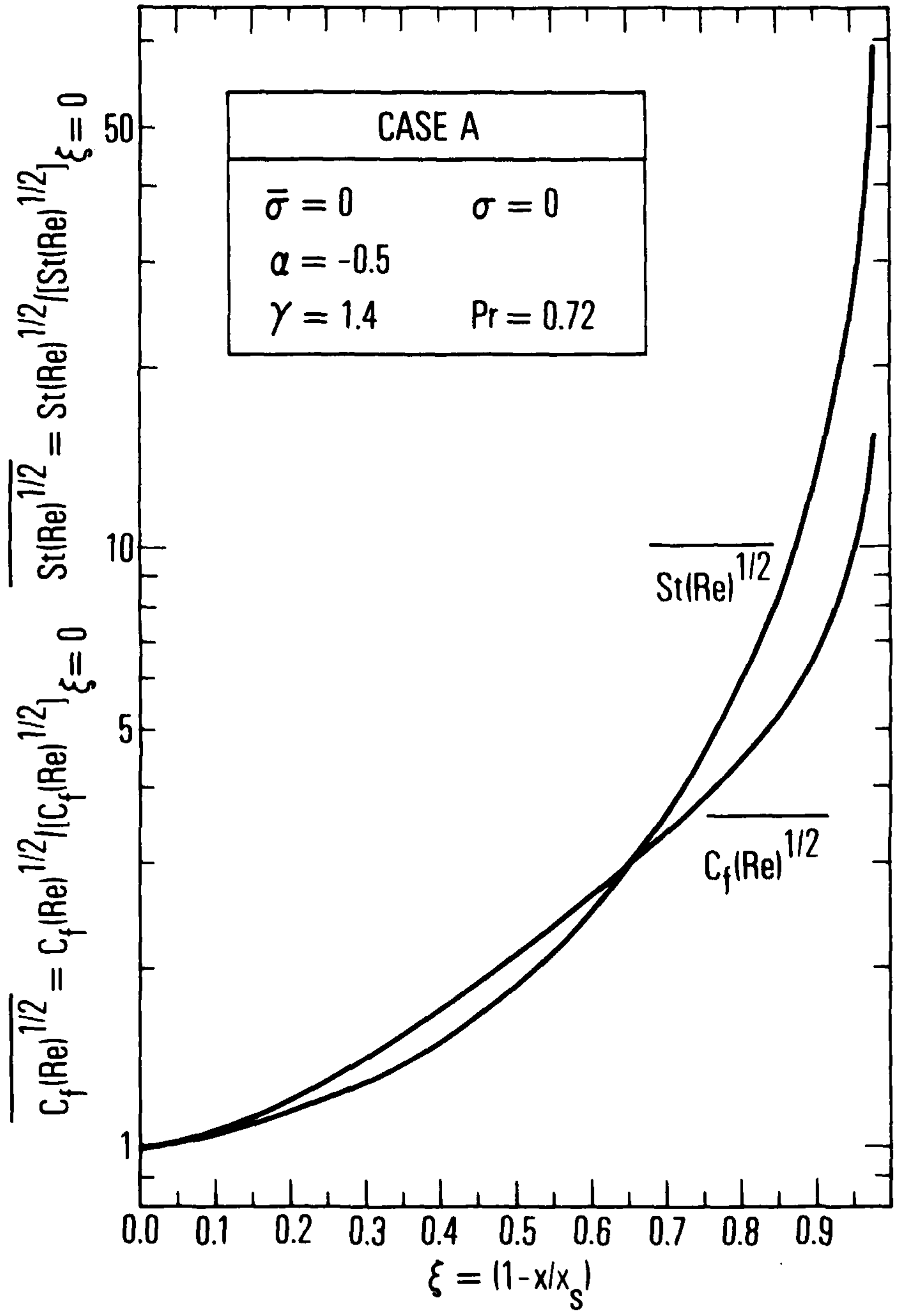

Fig. 12. Friction coefficient and Stanton number, Case A

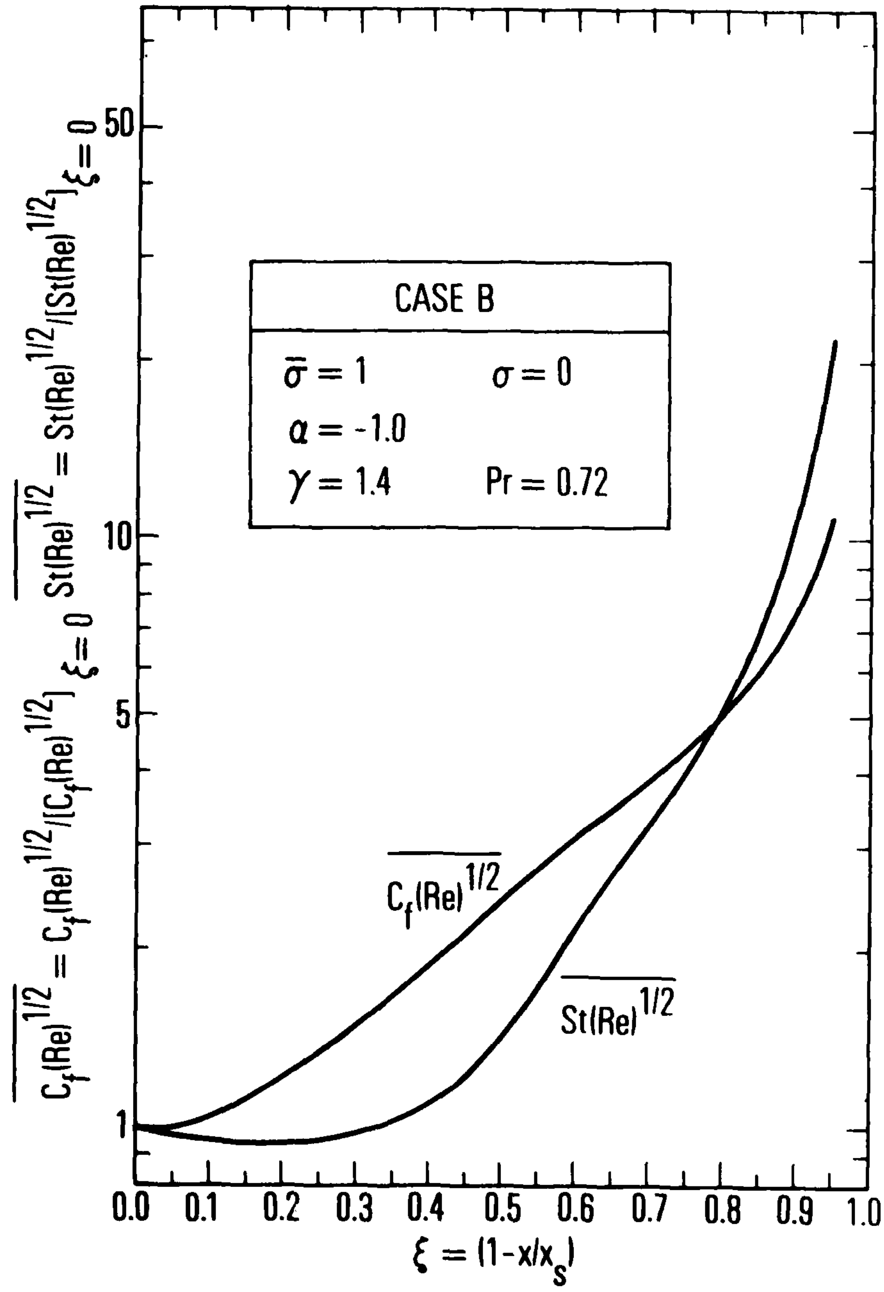

Fig. 12. Friction coefficient and Stanton number, Case B

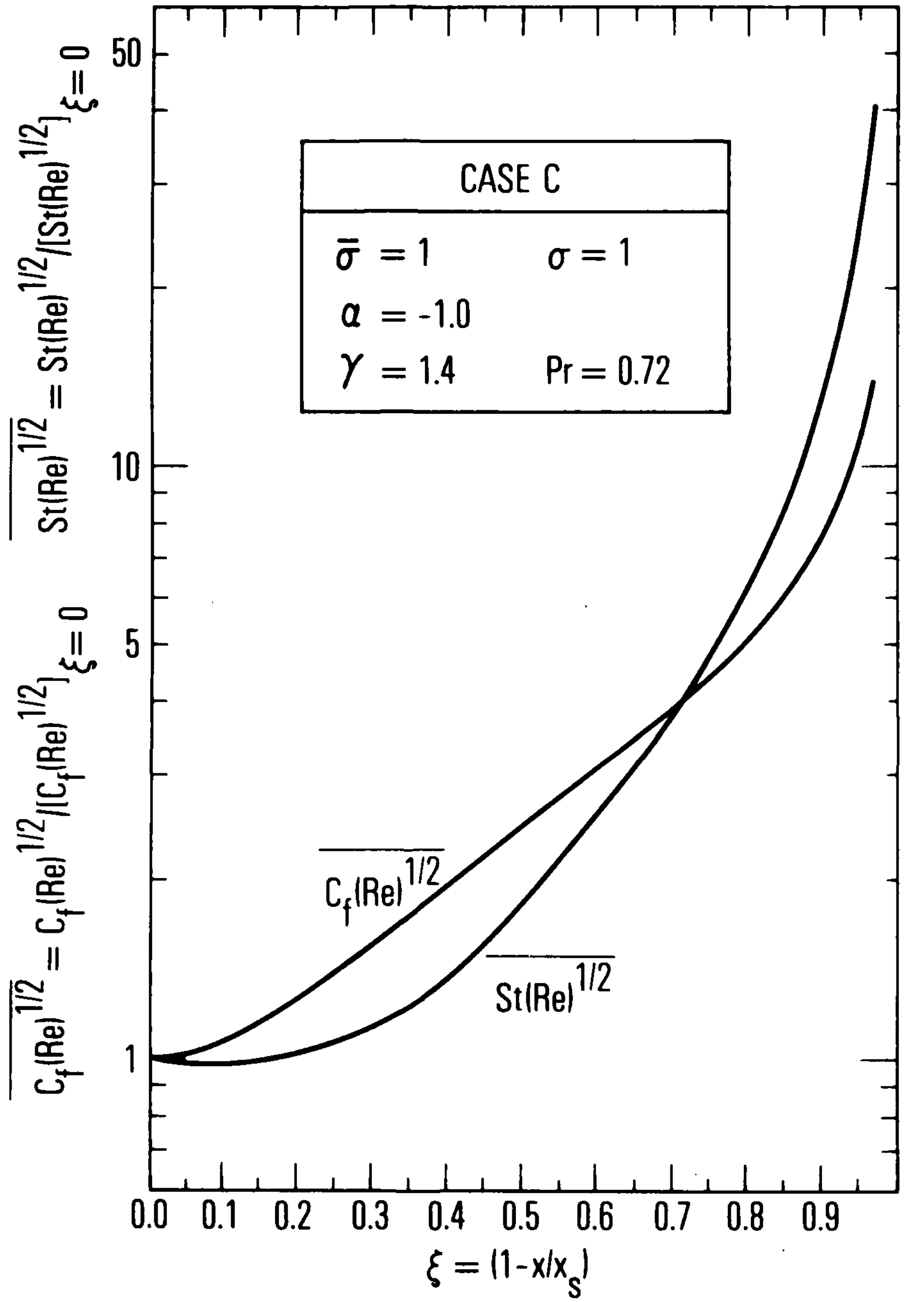

Fig. 12. Friction coefficient and Stanton number, Case C

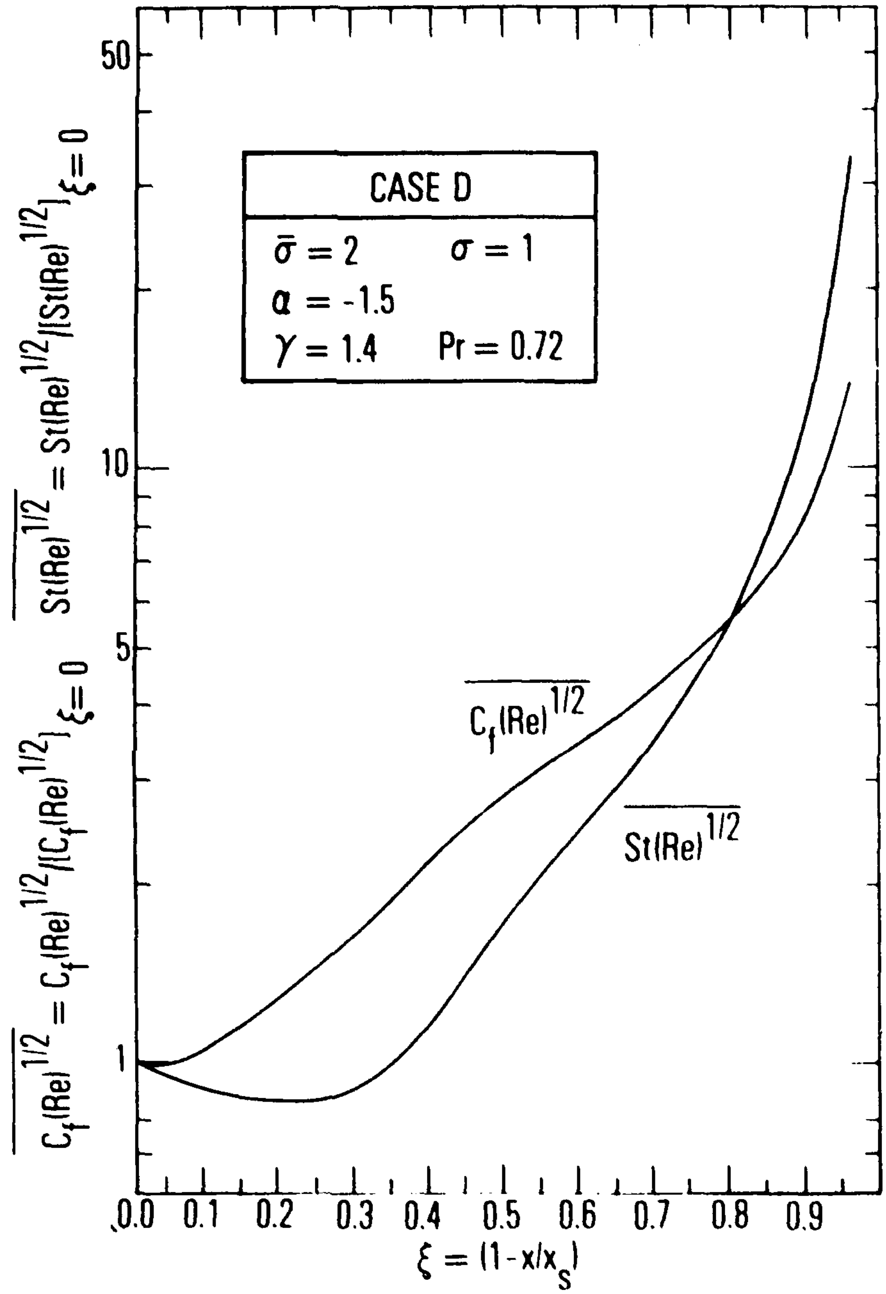

Fig. 12. Friction coefficient and Stanton number, Case D

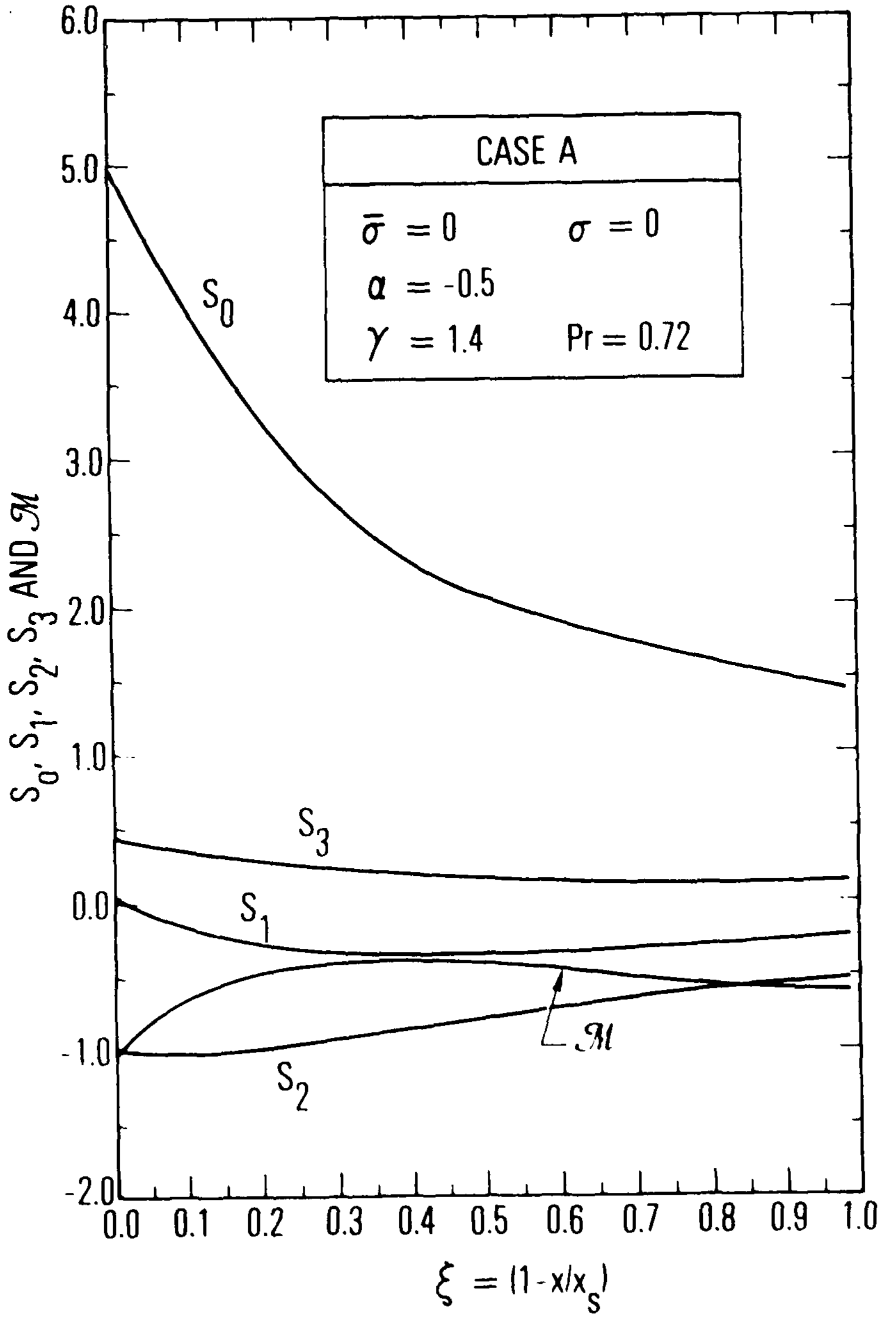

Fig. 13. Integral lengths and lateral mass flux, Case A

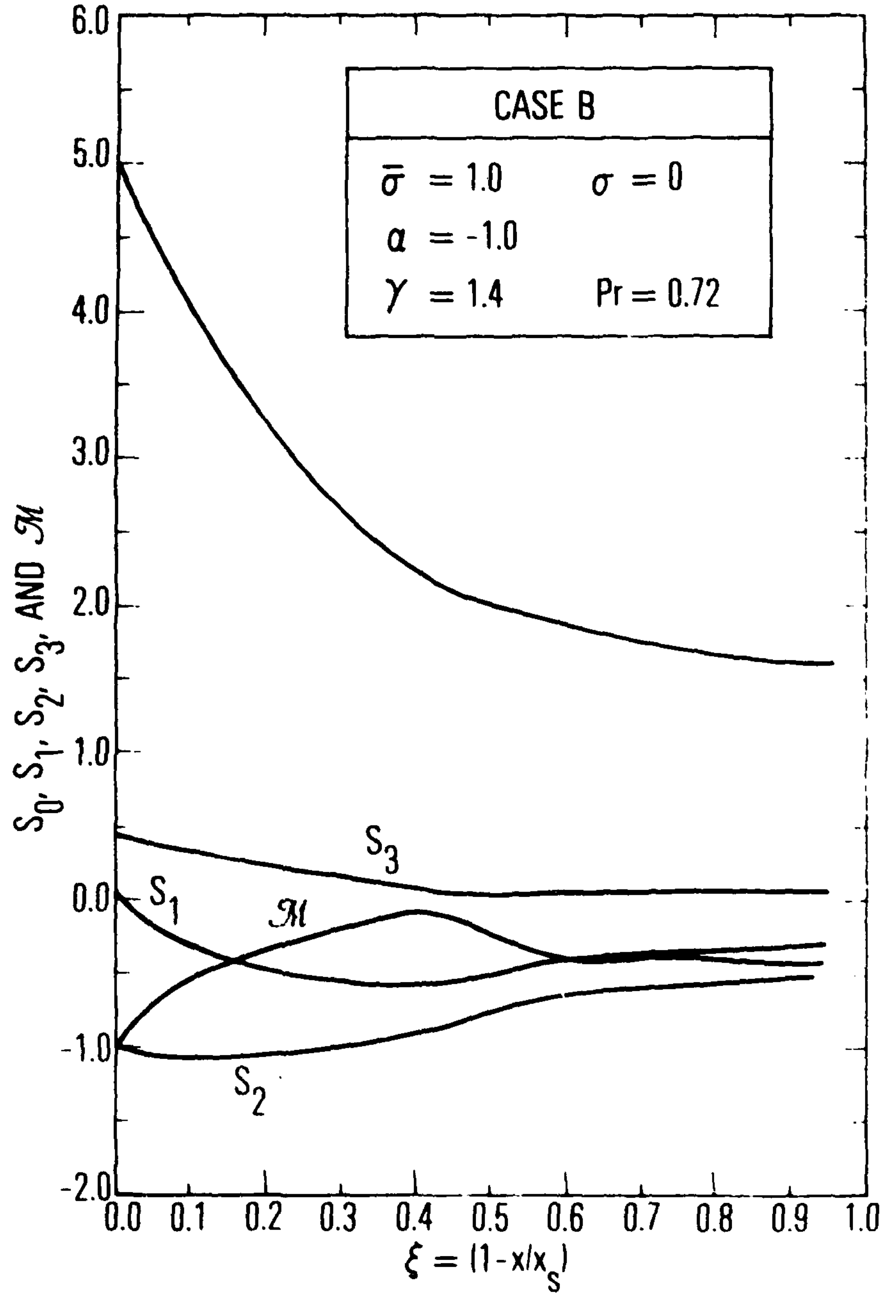

Fig. 13. Integral lengths and lateral mass flux, Case B

AD-A084 435 AEROSPACE CORP EL SEGUNDO CA AEROPHYSICS LAB F/G 20/4
NUMERICAL SOLUTIONS FOR LAMINAR BOUNDARY LAYER BEHIND BLAST WAV--ETC(U)
MAY 80 S W LIU, H MIRELS F04701-79-C-0080
UNCLASSIFIED TR-0080(5940-02)-2 SD -TR-80-23 NL

2 OF 2
AD
A084435

END
DATE
FILMED
7 80
DTIC

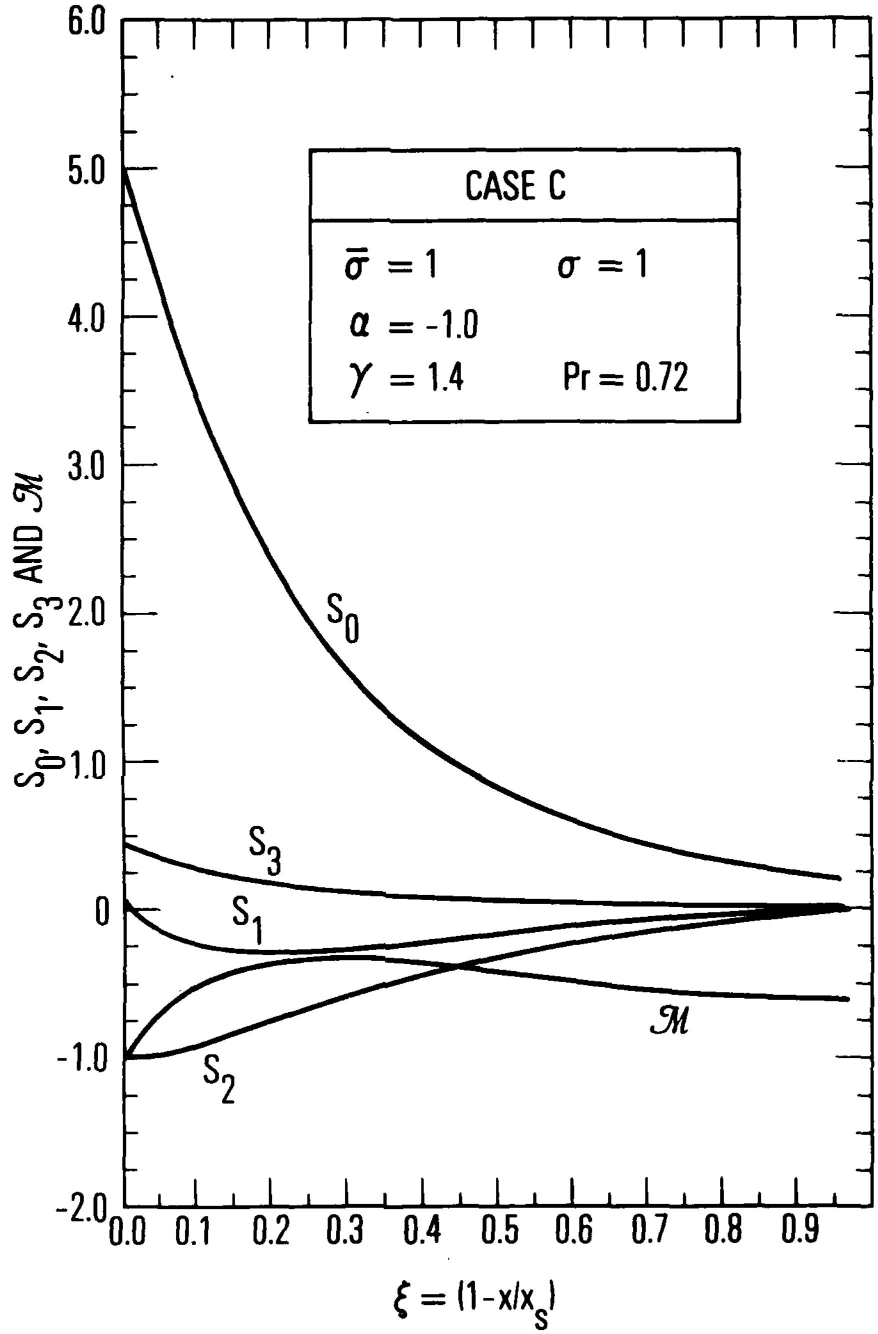

Fig. 13. Integral lengths and lateral mass flux, Case C

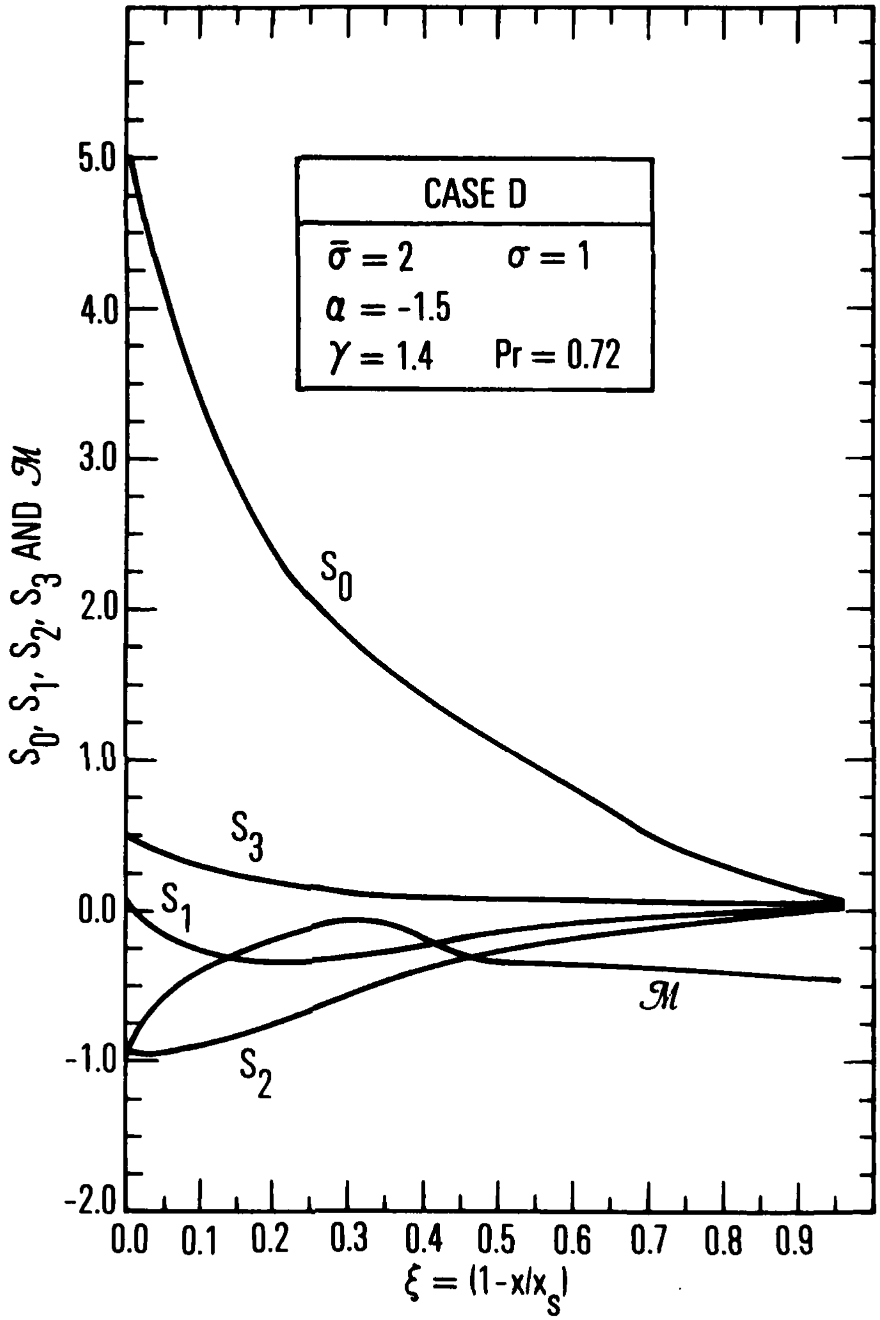

Fig. 13. Integral lengths and lateral mass flux, Case D

Table 5A. Boundary-layer functions for Case A

CASE A $\bar{\sigma} = 0.0$, $\sigma = 0.0$, $\gamma = 1.4$, Pr = 0.72

ξ	$f_{\eta\eta}(\xi, 0)$	$g_\eta(\xi, 0)$	S_0	S_1	S_2	S_3	$\mathscr{M}$
0.00	.661981	.898636	5.0249	.0628	-.9750	.4531	-1.0274
.10	.786964	.794417	4.0363	-.1667	-1.0087	.3579	-.6299
.20	.925999	.726410	3.2793	-.2751	-.9707	.2892	-.4623
.30	1.078690	.684236	2.7069	-.3302	-.9131	.2372	-.3975
.40	1.245440	.666328	2.3162	-.3552	-.8488	.1963	-.3865
.50	1.424570	.675090	2.0642	-.3580	-.7809	.1641	-.4057
.60	1.609090	.713830	1.8884	-.3424	-.7116	.1406	-.4532
.70	1.783150	.779053	1.7528	-.3152	-.6472	.1258	-.5101
.80	1.928510	.851701	1.6340	-.2878	-.5960	.1173	-.5638
.90	2.046290	.909773	1.5102	-.2686	-.5598	.1112	-.5983

Table 5B. Boundary-layer functions for Case B

CASE B $\bar{\sigma} = 1.0$, $\sigma = 0.0$, $\gamma = 1.4$, $Pr = 0.72$

ξ	$f_{\eta\eta}(\xi,0)$	$g_{\eta}(\xi,0)$	S_0	S_1	S_2	S_3	$\mathcal{M}$
0.00	.651981	.898636	5.0249	.0628	-.9750	.4531	-1.0274
.10	.836106	.699514	4.0552	-.2908	-1.0748	.3301	-.5528
.20	1.018720	.583187	3.2853	-.4450	-1.0547	.2427	-.3456
.30	1.219840	.512713	2.6570	-.5400	-1.0030	.1621	-.1829
.40	1.454370	.485995	2.2411	-.5745	-.9089	.0831	-.0845
.50	1.722890	.523739	2.0144	-.5119	-.7656	.0408	-.2060
.60	1.970780	.637757	1.8713	-.4101	-.6487	.0532	-.3810
.70	2.126890	.720685	1.7570	-.3724	-.6030	.0587	-.3912
.80	2.267300	.759502	1.6827	-.3541	-.5673	(.5197)	-.4000
.90	2.405150	.807216	1.6260	-.3322	-.5400	(.4973)	-.4260

Table 5C. Boundary-layer functions for Case C

CASE C $\bar{\sigma} = 1.0$, $\sigma = 1.0$, $\gamma = 1.4$, $Pr = 0.72$

ξ	$f_{\eta\eta}(\xi,0)$	$g_{\eta}(\xi,0)$	S_0	S_1	S_2	S_3	$\mathscr{M}$
0.00	.661981	.898536	5.0249	.0628	-.9750	.4531	-1.0274
.10	.945834	.801057	3.4854	-.2307	-.9146	.2853	-.5187
.20	1.315150	.787550	2.3857	-.2845	-.7544	.1885	-.3574
.30	1.810560	.845471	1.6212	-.2717	-.5988	.1253	-.3395
.40	2.503180	1.006040	1.1436	-.2282	-.4564	.0832	-.3515
.50	3.480520	1.327780	.8155	-.1731	-.3345	.0573	-.4296
.60	4.881010	1.883540	.5870	-.1224	-.2380	.0413	-.5102
.70	7.069370	2.777460	.4365	-.0831	-.1635	.0290	-.5474
.80	11.338800	4.469330	.3233	-.0515	-.1017	.0181	-.5824
.90	23.999900	9.462470	.2371	-.0240	-.0479	.0087	-.6139

Table 5D. Boundary-layer functions for Case D

CASE D $\bar{\sigma} = 2.0$, $\sigma = 1.0$, $\gamma = 1.4$, Pr = 0.72

ξ	$f_{\eta\eta}(\xi, 0)$	$g_\eta(\xi, 0)$	S_0	S_1	S_2	S_3	$\mathcal{M}$
0.00	.661981	.898635	5.0249	.0628	-.9750	.4531	-1.0274
.10	.995978	.713260	3.3624	-.3165	-.9576	.2643	-.4516
.20	1.421550	.650611	2.3499	-.3895	-.8001	.1529	-.2531
.30	2.016990	.679150	1.7593	-.3701	-.6207	.0713	-.1153
.40	2.881340	.865368	1.3850	-.2758	-.4350	.0327	-.2387
.50	4.030960	1.294200	1.0654	-.1836	-.3045	.0314	-.4014
.60	5.521770	1.829020	.7715	-.1333	-.2235	.0247	-.4077
.70	7.941190	2.614960	.4945	-.0931	-.1555	.0167	-.4276
.80	12.736900	4.195700	.2731	-.0580	-.0969	.0105	-.4689
.90	27.230900	9.023530	.1047	-.0269	-.0453	(.0504)	-.5043

IV. CONCLUDING REMARKS

The results of this study provide the first exact solutions of the laminar boundary layer behind power-law shocks that cover the entire terrain swept by a blast wave, with the exception of a small area near the center of the blast where the inviscid and viscid equations are singular. Upon increase in ξ, the results depart significantly from the previous solutions[1] for $\xi^2 \ll 1$. In particular, in all four cases, Case A through Case D, the normalized heat transfer showed a minimum before $\xi = 0.5$. For the axisymmetric boundary layers ($\sigma = 1$, Case C and D) both wall shear and heat transfer increase at much faster rates with increase in ξ than were indicated by the solutions for $\xi^2 \ll 1$.

Boundary-layer transition is discussed in Appendix B. The present results are applicable only in that portion of the flow field where the boundary layer remains laminar. For strong shocks in air or argon, the boundary layer is laminar for $p_\infty x_s \le 0\,(10^{-3} - 10^{-2})$ atm-ft. For larger values of $p_\infty x_\infty$, the fraction of the disturbed field that remains laminar is $\xi_t = 0(10^{-3} - 10^{-2})/p_\infty x_s$, where $p_\infty x_s$ is in units of atm-ft. Therefore, the results presented here are of primary interest for low pressure test facilities and, possibly, for studies of the interaction of pulsed laser induced blast waves with ambient surfaces.

APPENDIX A

BLAST-WAVE STRENGTH

The variation of blast-wave radius x_s with time t is discussed herein. For blast waves with constant energy E the variation of shock radius with time can be expressed[4]

$$x_s = \left(\frac{E}{\bar{\alpha}\rho_\infty}\right)^{\frac{1}{\bar{\sigma}+3}} t^{\frac{2}{\bar{\sigma}+3}} \tag{A-1}$$

where $\bar{\alpha}$ is a nondimensional constant that depends on γ and $\bar{\sigma}$. Numerical estimates for $\bar{\alpha}$ are obtained from[4,5]

$$\bar{\alpha} = \Delta\left(\frac{2}{\bar{\sigma}+3}\right)^2 \int_0^1 \left(\frac{F}{\gamma-1} + \frac{\varphi^2 R}{2}\right) \xi^{\bar{\sigma}} d\xi \tag{A-2}$$

where $\Delta = 2$, 2π, and 4π for $\bar{\sigma} = 0$, 1, and 2, respectively. The choice $\Delta = 2$ for $\bar{\sigma} = 0$ indicates that the latter corresponds to a symmetric blast (i.e., $-1 \le \xi \le 1$). The units of E in Eq. (A-1) are energy/area, energy/length, and energy for $\bar{\sigma} = 0$, 1, and 2, respectively. Numerical estimates for $\bar{\alpha}$ are provided in Table A-1.

Table A-1. Blast-wave strength parameter. Data obtained from Ref. 5 ($\bar{\sigma} = 0, 1$) and H. Bagwell ($\bar{\sigma} = 2$) Values for $\bar{\sigma} = 0$ correspond to symmetric blasts, $-1 \leq \xi \leq 1$.

$\bar{\sigma}$	$\bar{\alpha}$		
	$\gamma = 1.15$	$\gamma = 1.4$	$\gamma = 5/3$
0	2.999	1.078	0.606
1	2.674	0.984	0.551
2		0.851	0.493

APPENDIX B

BOUNDARY-LAYER TRANSITION

The boundary layer is laminar directly behind the shock, but it may undergo transition to a turbulent boundary layer at some distance behind the shock. The location of the transition point defines the extent of the laminar boundary layer and, therefore, the region of validity of the present theory. The latter is discussed herein.

Assume that local Reynolds number Re can be characterized by flow conditions directly behind the shock. An appropriate Reynolds number (based on distance a freestream particle has traveled relative to the wall) is[6]

$$\begin{aligned} Re &\equiv \frac{u_e (x_s - x)}{\nu_e} \left[\frac{u_e}{u_s - u_e}\right] \\ &= \frac{\xi x_s u_s}{\nu_e} \left[\frac{[R(0) - 1]^2}{R(0)}\right] \end{aligned} \tag{B-1}$$

where R(0) is the density ratio across the shock and $\nu_e = \mu_e / \rho_e$ is evaluated at $\xi = 0$. For an ideal gas, a strong shock ($M_s^{-2} \ll 1$) and $\mu \sim T^{\omega}$, Eq. (B-1) becomes

$$\frac{Re}{\xi x_s} = \left(\frac{2}{\gamma-1}\right)^2 \left[\frac{(\gamma+1)^2}{2\gamma(\gamma-1)}\right]^{\omega} M_s^{1-2\omega} \frac{\rho_\infty a_\infty}{\mu_\infty} \tag{B-2}$$

For most gases, $\omega \doteq 1/2$. Thus the dependence of Eq. (B-2) on shock Mach number M_s is weak. Taking $\omega = 1/2$ in Eq. (B-2) yields

$$\frac{Re}{\xi\, x_s} = \frac{4(\gamma+1)}{[2\gamma(\gamma-1)^5]^{1/2}} \frac{\rho_\infty a_\infty}{\mu_\infty} \tag{B-3}$$

Let ξ_t and Re_t denote the transition location and the transition Reynolds number, respectively. For air and argon, Eq. (B-3) can be expressed in the form

$$p_\infty x_s\, \xi_t \left[\frac{10^6}{Re_t} \; \frac{522°R}{T_\infty}\right] = 2.5 \times 10^{-3} \text{ atm-ft} \qquad \text{(air)} \tag{B-4a}$$

$$= 8.4 \times 10^{-3} \text{ atm-ft} \qquad \text{(argon)} \tag{B-4b}$$

where $x_s\, \xi_t = x_s - x_t$ denotes the distance behind the shock at which transition occurs and ξ_t is a direct measure of the fraction of the flow field which is laminar. The bracketed term on the left-hand side of Eq. (B-4) is of order one. Hence, the boundary layer is laminar in the entire disturbed flow region [i.e., $\xi_t = 0(1)$] for $p_\infty x_s \leq 0\ (10^{-3} - 10^{-2})$ atm-ft. The latter regime occurs primarily in test facilities (e.g., blast-wave-driven low pressure shock tubes) but may also be of interest in connection with the study of pulsed laser induced blast waves. With increase in $p_\infty x_s$ above values of the order of 10^{-2} atm-ft, the fraction of the disturbed flow that is laminar is reduced (i.e., $\xi_t \rightarrow 0$). For $\xi_t < 1$ and a given ambient gas, $x_s - x_t$ depends only on p_∞ and is independent of blast energy and shock radius.

REFERENCES

1. H. Mirels and J. Hamman, Phys. Fluids 5 (1), a1-6 (1962).

2. C. J. Chen and L. M. Chang, "Unsteady Compressible Laminar Boundary Layer Flow Behind a Plan Blast Wave," Paper presented 11th AIAA Thermophysics Conference, San Diego, California, July 1976.

3. F. G. Blottner, "Finite Difference Method of Solution of the Boundary Equations," AIAA Journal 8 (2), 193-205 (February 1970).

4. L. I. Sedov, Similarity and Dimensional Methods in Mechanics (English translation), Academic Press, New York (1959), p. 222.

5. H. Mirels, "Similarity Solutions for Inviscid Hypersonic Flow Over Slender Power and Related Bodies," Advances in Applied Mechanics, Vol. VII, Academic Press, New York (1962).

6. H. Mirels, "Boundary Layer Effects in Shock Tubes," Shock Tube Research, Proceedings of the Eighth International Shock Tube Symposium, ed. J. L. Hollery, A. G. Gaydon, and P. R. Owen, Chapman and Hall, London (1971), p. 6-1.

LABORATORY OPERATIONS

The Laboratory Operations of The Aerospace Corporation is conducting experimental and theoretical investigations necessary for the evaluation and application of scientific advances to new military concepts and systems. Versatility and flexibility have been developed to a high degree by the laboratory personnel in dealing with the many problems encountered in the nation's rapidly developing space and missile systems. Expertise in the latest scientific developments is vital to the accomplishment of tasks related to these problems. The laboratories that contribute to this research are:

Aerophysics Laboratory: Launch and reentry aerodynamics, heat transfer, reentry physics, chemical kinetics, structural mechanics, flight dynamics, atmospheric pollution, and high-power gas lasers.

Chemistry and Physics Laboratory: Atmospheric reactions and atmospheric optics, chemical reactions in polluted atmospheres, chemical reactions of excited species in rocket plumes, chemical thermodynamics, plasma and laser-induced reactions, laser chemistry, propulsion chemistry, space vacuum and radiation effects on materials, lubrication and surface phenomena, photosensitive materials and sensors, high precision laser ranging, and the application of physics and chemistry to problems of law enforcement and biomedicine.

Electronics Research Laboratory: Electromagnetic theory, devices, and propagation phenomena, including plasma electromagnetics; quantum electronics, lasers, and electro-optics; communication sciences, applied electronics, semiconducting, superconducting, and crystal device physics, optical and acoustical imaging; atmospheric pollution; millimeter wave and far-infrared technology.

Materials Sciences Laboratory: Development of new materials; metal matrix composites and new forms of carbon; test and evaluation of graphite and ceramics in reentry; spacecraft materials and electronic components in nuclear weapons environment; application of fracture mechanics to stress corrosion and fatigue-induced fractures in structural metals.

Space Sciences Laboratory: Atmospheric and ionospheric physics, radiation from the atmosphere, density and composition of the atmosphere, aurorae and airglow; magnetospheric physics, cosmic rays, generation and propagation of plasma waves in the magnetosphere; solar physics, studies of solar magnetic fields; space astronomy, x-ray astronomy; the effects of nuclear explosions, magnetic storms, and solar activity on the earth's atmosphere, ionosphere, and magnetosphere; the effects of optical, electromagnetic, and particulate radiations in space on space systems.

THE AEROSPACE CORPORATION
El Segundo, California